To my wife and parents ...

CORRIGENDA

p 13 line 23 read Peeters[20]

p 20 line 9 read For an inviscid gas

p 38 line 19 read Examination of Fig. 2.8 shows

p 40 line 13 read (see Fig. 2.9 in CO_2)

p 42 line 9 read not directly relevant to flames

p 44 line 4 read $\gamma = 1.16$

p 44 line 13 read across the diaphragm

p 69 line 27 read type of system[1]

p 76 line 10 read the Nusselt and

p 93 line 6 read of nitrogen absorbing electron energy[66].

p 97 line 18 read $= 4\pi(n_{i+} - n_{i-})e$ 4.2

p 99 line 28 read convection being negligible.

p100 line 13 read $j = enX(k_+ + k_-) =$

p114 line 18 read $= \dfrac{k_e V}{2y}$

p116 for a read d/2

p117 line 1 read $= \dfrac{n_e e k_e V}{2y}$

p117 line 4 read $= \dfrac{-2k_3 n_A}{k_e V}\, y\, dy$

p117 line 5 read $\exp(k_3 n_A x^2 / k_e V)$

p143 interchange I_{bt} and I_{tp} on curve labels.

p147 line 2 read production of ions varies

p150 line 1 read 9.2×10^{-3} $cm^2 s^{-1} V^{-1}$

p183 Ref. 20 read Comb. Inst. European Symp.

ELECTRICAL CONTROL OF FLAME CARBON

by

Roger John Bowser GradRIC

October 1974

A thesis submitted for the degree of Doctor of Philosophy of the University of London

Department of Chemical Engineering
and Chemical Technology,
Imperial College of Science
and Technology,
London, S.W.7.

ABSTRACT

The primary objective of the research has been to investigate methods for the electrical control of flame carbon in practical systems. It is shown that methods used previously of applying a field to produce unipolar clouds of charge and forcing these to attach to carbon particles cannot be extended to large distances from the flame. Such methods also proved inapplicable in the product region downstream of the flame at smaller electrode separations, even in the presence of a small field applied to the reaction zone to cause an initial separation of charge. It proved possible to transfer carbon to an inert carrier stream and then to collect it downstream of the flame but this method would be inconvenient in most systems. The principle of using charge generated by the flame was abandoned in favour of charging the particles subsequently. Various methods for charging the particles are discussed and a precipitator is described which uses plates heated by the flame products as a source of ions for charging soot particles which may then be manipulated by electric fields.

Secondary objectives concerned the extension to pyrolysing systems, in the absence of oxygen, and an investigation to ensure that the effects of fields are not caused by changes in flame propagation rate. These are discussed first.

The pyrolysis of ethylene by hot surfaces and in a shock tube was investigated. In each case charged particles are produced which could be utilised for electrical control. Ion formation is discussed and a mechanism is proposed for

the formation of $C_3H_3^+$ in the absence of oxygen.

The effect of DC and AC fields on the burning velocity of hydrocarbon-air mixtures was investigated. It was found to be less than 4% and 10% for sooting and non-sooting flames respectively. An unsuccessful attempt was made to change the burning velocity of hydrogen/oxygen/argon mixtures using fast electrons.

The effect of electrons om soot formation in diffusion flames was investigated and a mechanism proposed which may account for the role of ionising additives.

The work led to two methods for controlling flame carbon. They are very similar in that both utilise metal surfaces, coated and maintained hot by the flame, to which a field is applied though entirely different in principle.

ACKNOWLEDGEMENT

I am grateful to my supervisor Professor F. J. Weinberg for his invaluable help, advice and encouragement in the pursuit of this research. I wish to thank Professor A.R. Ubbelohde, F.R.S. for the interest he has shown in this work and I am indebted to Dr. A.R. Jones for his help and useful discussions.

My thanks to Esso Petroleum Co. Ltd. for their financial support, and all the technical staff of the Department for their assistance.

CONTENTS

CHAPTER 1

1.1 OBJECTIVES AND PURPOSE OF RESEARCH

Concern about pollution has been mounting in the last few decades and legislation is gradually being introduced requiring lower levels of pollution. This concern coupled with the escalating cost of fuel and the real possibility of it becoming scarce has led to the redesign of burner systems to utilise leaner mixtures, burning less fuel and producing fewer particulate pollutants than conventional systems. There are, however, many systems where this optimisation may not be successful especially where economics dictate the use of poor fuels such as waste plastic material; then ways must be sought to control the pollution from the flame by external means.

The type of pollution generated depends on the fuel burnt and on the conditions of combustion. Most industrial uses for fuel employ diffusion flames often quenched on cooler surfaces. These flames tend to generate relatively little nitric oxide but a large amount of particulate pollutants of the type C_xH_y- flame carbon. They also generate sulphur oxides depending on the sulphur content of the fuel. Most industrial chemical plant has a stack where excess chemicals are burnt off as a diffusion flame producing similar pollutants.

The more familiar consumers of fuel - internal combustion engines also produce their particular pollutants. A well adjusted diesel engine produces little oxides of nitrogen and carbon monoxide with small amounts of unburnt hydrocarbons

and particulates; a poor engine, however, produces large amounts of these. A petrol engine produces similar pollutants, oxides of nitrogen are higher and hydrocarbon pollutants may be lower but in this case fuel additives such as lead tetra-ethyl and barium compounds appear in the exhaust as particulates too.

Pollutants from flames fall into three categories:

a) stoichiometric products - e.g. sulphur trioxide and lead as its sulphate. No change in flame conditions will affect these.

b) high temperature pollutants - nitric oxide.

c) the result of incomplete combustion - soot. This can always be burnt off if the system is adjusted but this conflicts with minimising nitric oxide production.

A diffusion flame produces a lot of each; the stoichiometric zone gives nitric oxide and the pyrolysis zone generates soot. The trend to cooler flames may produce more of the latter pollutant.

Various methods have been tried to reduce these pollutant levels. Lead and barium are best controlled by not adding them to the fuel; this, however, creates problems in engine design. Pollutant levels have been successfully reduced by novel engine design and a lot of work has been done on recirculating the products and on using a catalyst bed in the exhaust line. This has been fairly successful and reactions such as

$$2CO + 2NO \longrightarrow 2CO_2 + N_2$$

have been exploited.

This does, however, leave a problem with particulate pollutants, especially in the case of industrial flames. Considering the increasing cost of fuel in relation to electricity it does not seem too unreasonable to investigate the use of electrical methods for the control of particulates. This involves more elaborate burner systems but is a trend anyway in the search for more efficient ways to use fuel.

A lot of work has been carried out on minimising soot formation electrically but using academic systems involving flanking the flame with electrodes. There are many systems where this is not possible, e.g. turbulent flames in furnaces and internal combustion engines; the problem is to utilise these electrical methods in awkward practical situations.

1.2 PREVIOUS WORK

1.2.1 ION PRODUCTION IN FLAMES

Calcote[32] reviewed early work and discussed the various proposed mechanisms for ion production in flames. These were, thermal ionisation of impurities, equilibrium and non-equilibrium species and carbon particles, ionisation via translational energy, cumulative exitation and chemi-ionisation. He considered that the most probable mechanism for ion formation was cumulative exitation or chemi-ionisation.

Using Langmuir probe techniques he measured ion profiles and recombination coefficients in flames[24] and deduced ion formation rates. These results were interpreted in terms of chemi-ionisation and possible chemi-ionisation reactions were proposed.

Deckers and van Tiggelen[33] as well as Knewstubb and Sugden[34] applied a mass spectrometer to ion identification in hydrocarbon flames. The dominant ion was found to be H_3O^+ with smaller concentrations of CHO^+ and $C_3H_3^+$. The presence of H_3O^+ can be explained by assuming that CHO^+ is the primary ion[24,26]

$$CH + O \longrightarrow CHO^+ + e^-$$

$$CHO^+ + H_2O \longrightarrow CO + H_3O^+ \qquad \Delta H = 24 \text{kcal mole}^{-1}.$$

The work of Calcote was continued with a further Langmuir probe study on flame ionisation[27]. He obtained positive ion and electron concentrations and electron temperatures. The positive ion concentrations were greater than the electron concentrations indicating the formation of negative ions.

Typical concentrations were n_+ 1·42 x 10^{10} cm^{-3} and n_e 2·42 x 10^9 cm^{-3}. Electron temperatures exceeded the gas temperature and did not decay as rapidly as might be expected.

A mass spectrometric technique for obtaining ion profiles of good spatial resolution was outlined and detailed profiles were presented for an acetylene-oxygen flame at 2·5mm Hg. The ion CHO^+ peaks ahead of $C_3H_3^+$ which precedes H_3O^+. Many other ions are observed to peak at about the same position in the flame as $C_3H_3^+$. In a later study[28] Calcote discusses mechanisms for the formation of secondary ions. These are considered to be produced by charge exchange reactions from the primary ion CHO^+ and stable neutral combustion intermediates. It is also concluded that $C_3H_3^+$ is a primary flame ion and the mechanism proposed for its formation is[31],

$$CH^* + C_2H_2 \longrightarrow C_3H_3^+ + e^-.$$

Peeters and van Tiggelen[25] measured the kinetics of chemi-ionisation reactions and obtained a value of $7 \pm 1{\cdot}5 \times 10^{-9}$ $cm^2 ion^{-1} sec^{-1}$ as the rate constant for

$$CHO^+ + H_2O \longrightarrow CO + H_3O^+$$

using saturation current densities[1,35] to measure ion concentrations.

Matsuda and Gutman[29,30] measured the expotential growth of CH^* emission and chemi-ion production simultaneously behind reflected shock waves during the induction period of the acetylene-oxygen reaction. CH^* emission was measured by an end-on technique and ion concentrations were measured using

saturation current. The expotential growth rate for chemi-ion production was found to be twice that for CH^* emission and the results established that chemi-ionisation is second order with respect to reaction intermediates. This rules out the reaction

$$CH^* + C_2H_2 \longrightarrow C_3H_3^+ + e^-$$

and is consistent with the reaction

$$CH + O \longrightarrow CHO^+ + e^-$$

being the major chemi-ionisation reaction during the early stages of ion formation. The presence of $C_3H_3^+$ during the induction period is explained by an ion-molecule reaction consistent with the data obtained.

$$CH + O \longrightarrow CHO^+ + e^-$$

$$CHO^+ + C_2H_2 \longrightarrow C_2H_3^+ + CO$$

$$C_2H_3^+ + O_2 \longrightarrow CH_3O^+ + CO \longrightarrow C_2H_3O^+ + O$$

$$CH_3O^+ + C_2H_2 \longrightarrow C_3H_3^+ + H_2O$$

$$C_2H_3O^+ + C_2H_2 \longrightarrow C_3H_3^+ + CO + H_2$$

Kinbara and Noda in a series of experiments[21-3] measured radical emissions and ion concentrations during the flash photolysis of C_2H_2-O_2-NO_2 mixtures and found evidence to support the reaction

$$CH + O \longrightarrow CHO^+ + e^-.$$

Peeters[21] measured radical concentrations and ion concentrations in several CH_4-O_2-Ar and C_2H_4-O_2-Ar flames at 16·5 torr finding a linear relationship between total ion production and the integral

$S\int_0^\infty [CH][O]\ dz$ - S the flame area, z distance from burner

Hence providing experimental proof for the reaction

$$CH + O \longrightarrow CHO^+ + e^-.$$

No evidence was found for the reaction

$$CH^* + C_2H_2 \longrightarrow C_3H_3^+ + e^-$$

even though $[CH^*]$ and $[C_2H_2]$ were large in some of the flames studied.

1.2.2 CARBON FORMATION IN FLAMES

Homann and Wagner discussed the chemistry of carbon formation in flames in a series of papers[9-11,17]. Carbon formation is not exclusively determinded by flame chemistry. The curvature of the flame front also influences carbon formation - the higher the curvature, the greater the carbon formation; this effect is attributed to the back diffusion of hydrogen into the reactants from the products. Regarding the formation and growth of soot particles, analysis in and downstream of the reaction zone of low pressure C_2H_2/O_2 flames gave the following results. The main reaction products are CO, H_2, H_2O, CO_2 and C_2H_2 the concentrations of H_2O and CO_2 pass through a maximum close to the end of the oxidation zone, see Fig. 1.1a. Polyacetylenes ($C_{2n}H_2$) also show maxima here with their concentrations remaining constant in the products, these profiles are shown in Fig. 1.1b. Other hydrocarbons are found in the oxidation zone such as propylene, methyl acetylene, dimethyl acetylene, vinyl acetylene, benzene, methane and others. They all reach a concentration maximum inside the oxidation zone and have practically disappeared when oxygen is consumed.

Several stable radicals have also been detected in the

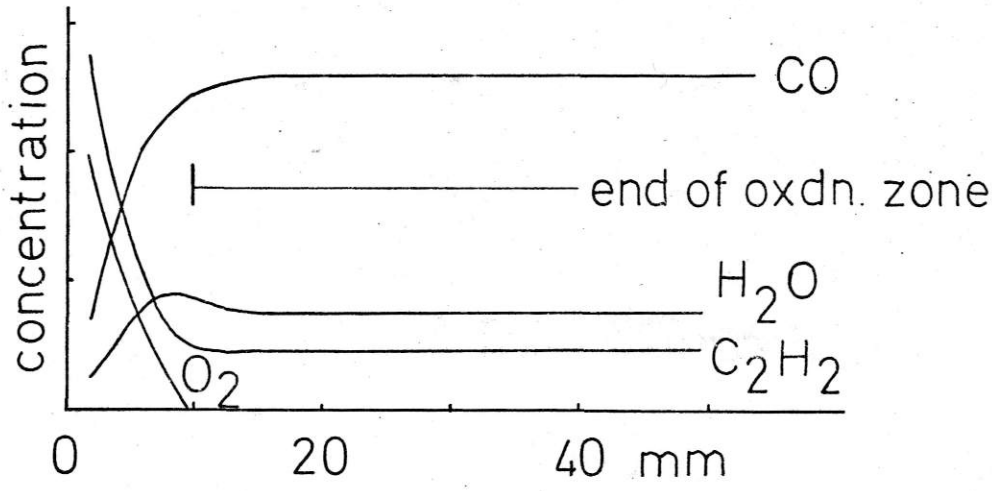

a) profiles of main components

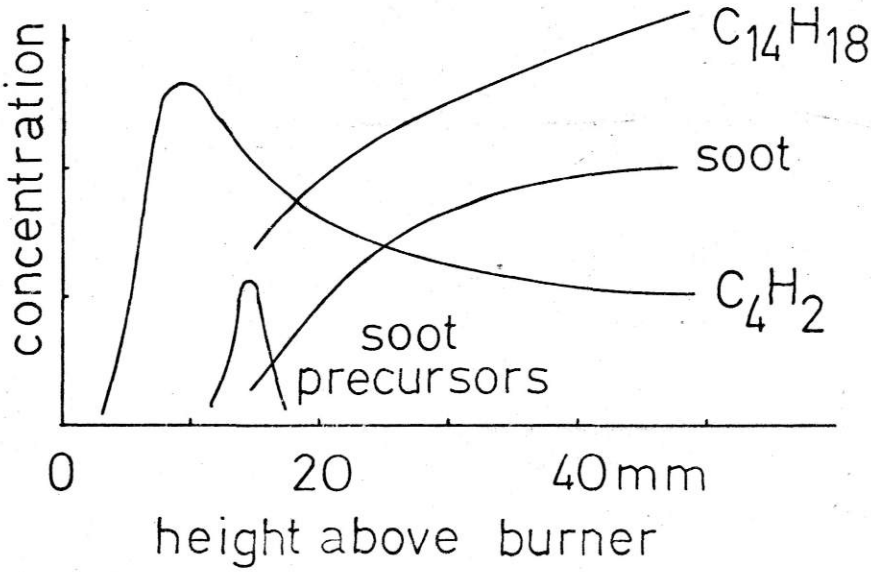

b) profiles of various products

Fig. 1.1 Profiles for a flat C_2H_2-O_2 flame at 20mm Hg.

reaction zone of the acetylene flame eg. C_2H_3, C_2H, C_2, CH, H, O and OH.

Other hydrocarbon species are present in the reaction zone; one characteristic group is the polycyclic aromatic hydrocarbons such as napthalene, phenanthrene, pyrene, 3-4 benz-pyrene and coranene. The concentration profile of $C_{14}H_8$ is shown in Fig. 1.1b. These species start to appear at the end of the oxidation zone and their concentrations increase steadily into the burnt gas.

Another characteristic group of hydrocarbons were detected in the gas phase, see Fig. 1.1b. They have molecular weights of between 250 and 550 (the upper limit of the mass spectrometer) and in contrast to the polycyclic aromatic hydrocarbons their concentrations show a maximum 12-14 mm above the burner and they disappear again within the zone where the carbon particles grow. Their individual concentrations are 10^{-7} on average and the compounds contain 16-40 carbon atoms. Their relative hydrogen concentration is larger than for condensed aromatic species of the same number of carbon atoms. With increasing height in the flame the relative concentration maximum within this group of substances is shifted to higher molecular masses, while their absolute concentrations decrease steadily. Their peak concentration depends on the C/O ratio and follows a similar level to the number of 'young' carbon particles. They are considered to be important intermediates during the formation of solid particles. Agglomeration and growth of particles continues up to 5cm above the burner, with the size and total mass of the particles increasing

and their total number decreasing.

A physical model for carbon formation in flames has been developed by Howard[8]. Positive ions are assumed to serve as nuclei and the particles remain ionised during growth and agglomeration. The analysis considers the effects exerted during growth and agglomeration by the electrostatic forces between particles and predicts the chained structure of carbon particles collected from flames and the uniform size and crystallite structure of the spherical chain units. The predicted size of the crystallites is similar to the experimentally observed value of 20-30 A^{o}.

The formation and growth of pyrolytic carbon films and soot particles has been discussed by Tesner[12]. The work is based on experimental investigations of their formation rates and both are considered to two stage processes involving nucleation and growth of nuclei. He concludes that the formation of pyrolytic carbon from methane at temperatures below 1300^{o}K is a molecular process with activation energies for formation and growth of nuclei 80 and 50 kcal $mole^{-1}$ respectively. It is suggested that the formation of soot particles takes place in two different ways each differing in the nature of the nuclei and in the structure of the soot particles obtained. The nuclei may be complex unsaturated polymer molecules or simple radicals. The molecular nucleus, obtained from reactions including condensation, aromatisation and dehydrogenation, continues to grow by virtue of the same reactions and produces a soot particle having an indefinite structure and containing a considerable amount of volatiles.

A 'radical nucleus' produces soot particles with a compact, regular structure. The nucleus is converted first into one having a physical surface then growth occurs by a branched chain molecular process taking place on the surface direct from the gas phase building the carbon atoms into a planar graphite lattice.

Howard et al[13] have measured the size distribution, number concentrations and fraction charged of carbon particles at successive stages of formation in a low pressure flat flame using molecular beam sampling. They observed cluster-type structures within roughly spherical particles and decreasing particle number concentration following rapid nucleation. They concluded that coagulation occurs during growth. Calculations indicated that first nucleated particles grow predominantly by surface growth to a mean diameter of 100 A^{o} and that the number of primary particles per spherical unit within the final chainlike clusters is of the order of ten.

1.2.3 THE EFFECT OF ADDITIVES ON CARBON FORMATION

Addecott and Nutt[14] measured the effect of metal compounds on carbon formation in diffusion flames in order to attempt to relate their activities to their electronic properties. The results demonstrate that for elements within each of the groups I and IIA of the periodic table, their smoke reducing efficiency increases in order of increasing ease of ionisation as measured by the magnitude of the ionisation potential. However, this relationship does not hold across groups, though this could be attributed to the ionisation mechanism.

Measurements were also carried out on flame ion concentrations and it was found that the lower the ionisation potential of the additive the lower the observed concentration of flame ions. Similar effects concerning production and inhibition of soot formation were observed by Feugier[16].

Salooja[15,19] has continued this work using additives held on quartz loops in the flame. He found two effects, an increase in the amount of soot formed when the loop was held in the upper part of the flame and a decrease when the loop was held in the lower part of the flame. In each case the size of the soot particles was increased and the smaller the ionisation potential the larger the effect. The effects were ascribed to electrons released by the additives, the antismoke effect due to the destruction of carbon bearing flame ions by the electrons and the prosmoke effect to the electrons reducing the positive charge on some of the carbon particles making agglomeration easier.

Cotton et al[18] examined soot reduction by metal additives in a propane diffusion flame and proposed a semiquantitative mechanism for the alkaline earth metals, its basis being that these metals undergo a homogenous gas phase reaction with flame gases to produce hydroxyl radicals which rapidly remove soot or soot precursors. Soot removal by most other metals is thought to involve another mechanism and possibilities are discussed.

1.2.4 ELECTRICAL PROPERTIES WITH RESPECT TO PARTICULATES AND WIND EFFECTS

Lawton and Weinberg[1] showed that maxima limiting all practical effects of the movement of flame ions in electric fields depend on the current density available. The theory of the electric field and space charge distributions inside and outside the flame was developed, checked experimentally and used to deduce such maxima.

For an invicid gas flowing unimpeded through a gauze electrode the velocity at the electrode is given by

$$v = \pm \left[ja/k_{\pm}\rho\right]^{\cdot 5}$$

The current density is limited by the rate of ion generation per unit flame area or the space charge induced breakdown at the electrodes. The latter is ultimately limiting, because it is generally possible to increase the former, and is given by

$$j = \frac{X_b^2 k}{8\pi a} \quad \text{esu}$$

The maximum practical effects may be calculated from this. For H_3O^+ ions with a ·5cm electrode spacing the limiting current in air becomes ·25 mA cm^{-2}. This corresponds to 2 g min^{-1} of soot from a 100 cm^2 flame assuming 10^4 atoms of carbon per charge. Also the maximum static pressure due to the ionic wind, the maximum wind velocity and the maximum force/unit volume respectively are given by:-

$$P_{ib} = X_b^2/8\pi \quad = 400 \text{ dyne cm}^{-2}$$

$$v_b = X_b/2\sqrt{2\pi\rho} \quad = 550 \text{ cm s}^{-1}$$

$$F_b = X_b^2/8\pi a \quad = 800 \text{ dyne cm}^{-3}$$

It has been shown that[3-6] carbon particles in sooting flames are charged, or at least can all be caused to acquire a desired charge in the presence of an applied field, and can thus be manipulated by means of such fields. This applies not only to fully grown particles which can by this means be caused to deposit in specified places, in varying forms of aggregate but also during their period of growth in the pyrolysis zone. By varying the residence time in the reaction zone, particle size and hence the total amount of carbon formed can be varied greatly, see Fig. 1.2. Thus by rapidly removing the carbon surface on which further growth normally occurs, it has proved possible to reduce the total amount of carbon formed by over 90% with corresponding reductions in particle size and flame luminosity. Conversely, by using fields so as to hold particles almost stationary against the gas flow within the pyrolysis zone, macroscopically large aggregate could be grown.

Mayo and Weinberg[2] measured particle mobility and carried out detailed size analysis. It was found that the particles accounting for the mass deposited have mobilities ranging from 10^{-3} to 3×10^{-2} $cm^2 s^{-1} V^{-1}$ depending on the applied potential. This allowed their field trajectories to be calculated and showed, when taken together with size measurements from electron micrographs, that each carries unit charge over practically the entire experimental range. It was also concluded that both growth of carbon on flame ions and initially neutral growth followed by attachment charging do occur, charging by thermionic emission being unimportant under most conditions.

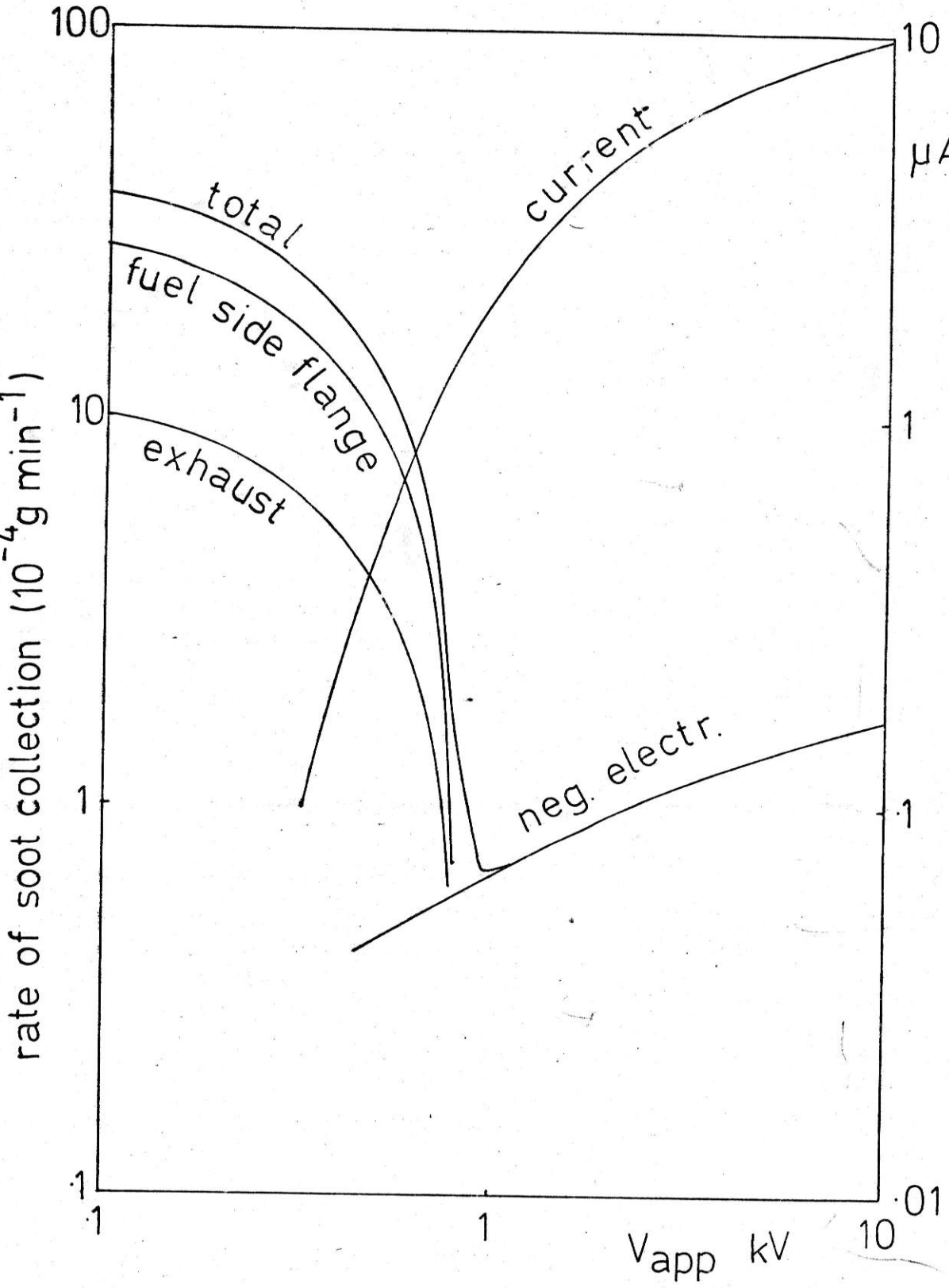

Fig. 1·2 Rate of soot collection / Applied voltage

This work has been extended[7] to particulate pollutants from flames in general. Examples chosen were silica and lead oxide from tetra-ethyl lead. In the latter case difficulties arose because the lead oxide is a vapour in the region where charges usually attach and an alternative method of charging was developed using a secondary flame as an ion source in a cooler part of the product stream. Optimum charging conditions were investigated and the theory of charge acquisition was generalised.

These investigations have been carried out on flames between electrodes; the work to be described extends this to more practical systems.

1.3 PLAN OF WORK

The ultimate objective of this work is to control flame carbon or soot under conditions when a field cannot be applied directly to a flame. This includes most industrial applications where combustion is carried out in a combustion chamber or in the cylinder of an engine. Even in the case of furnace flames where a field could be applied to the flame it would be far more convenient to treat the products separately in an exhaust flue.

Two side issues arise from this work. Do the methods developed depend on a flame with its chemi-ionisation zone or could the methods be applied to pyrolysing systems - eg. gaseous fuels in hot pipes? This is dealt with in Chapter 2 during studies on the pyrolysis of ethylene.

The second side issue is; to what extents are the effects produced due to interaction with the flame process itself? There is a background of conflicting information as to whether electrical effects are important to propagation reactions. In assuming that the manipulation of flame carbon is simply moving charged particles to alter a parameter concerning the particles themselves, eg. residence time or site of deposition, it is presupposed that the carbon forming reaction is not related to the main propagation reaction. This cannot be completely true for by altering the particulate concentration in the pyrolysis zone, hence altering the surface area on which carbon can form, the fuel consumption rate in the pyrolysis zone will be altered. The central question is whether this reaction affects the

main propagation reaction and the heat release rate. The most direct way of resolving this is to measure the effect of electric fields on the burning velocity of sooting flames. In order to establish a datum work was carried out on non-sooting flames first. Another question arises from this work, can the soot formation in flames be controlled by altering the electron concentration in the flame? Here again a datum was established by work on non-sooting flames. This work is presented in Chapter 3.

Chapter 4 deals with the electrical control of flame carbon using large fields, high voltages producing low currents, applied to the flame and its product region.

Additives are discussed in Chapter 5 and an entirely new method for controlling soot formation is presented using low field strengths and correspondingly low currents produced by hot electron emitting surfaces within the flame.

The conclusions and recommendations for further work are contained in Chapter 6.

CHAPTER 2

ETHYLENE PYROLYSIS IN THE ABSENCE OF OXYGEN

2.1 IN THE PRESENCE OF SOLID SURFACES

The first step was to investigate the pyrolysis of ethylene in the absence of oxygen to determine a) whether pyrolysis occured, b) charged particles were produced and hence c) the contribution of the charged particles from the pyrolysis zone of a flame to the total current. The apparatus envisaged consisted of a burner producing a uniform flow impinging on a heated flat plate, the whole being enclosed in an inert atmosphere, see Fig. 2.1. The plate was to be made of carbon and heated by a radiant cavity, see Weinberg and Wilson[77].

Some preliminary experiments were carried out whilst waiting for this apparatus to be completed. These were on the lines of the above experiment, but using simpler apparatus. The apparatus consisted of a pyrex tube having a perforated graphite end plate. Ethylene was passed in from the other end of the tube, the excess being burnt at the holes or carried away by an exhaust system. The ethylene was pyrolysed on an electrically heated tungsten wire, see Fig. 2.2. Burning waste ethylene above the plate made no difference to the results obtained. No current was detected due to this flame. The heater current was about 18A giving a temperature of around 1100^{o}K and the ethylene flow rate was around 1 lmin^{-1}. Current voltage characteristics were recorded for various conditions.

1) During pyrolysis filament negative
2) During pyrolysis filament positive

} see Fig. 2.3

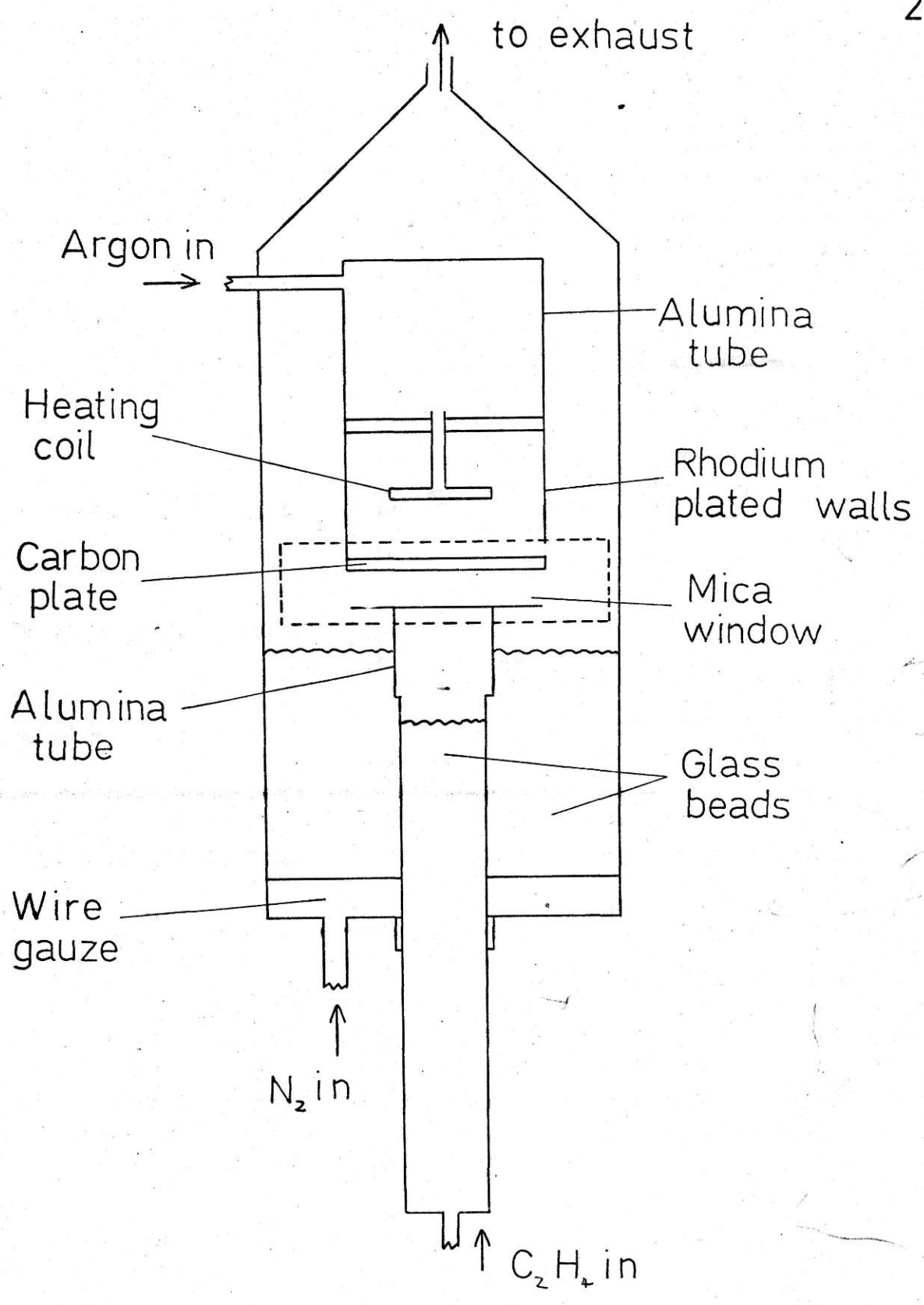

Fig. 2-1 Diagram of hot plate apparatus

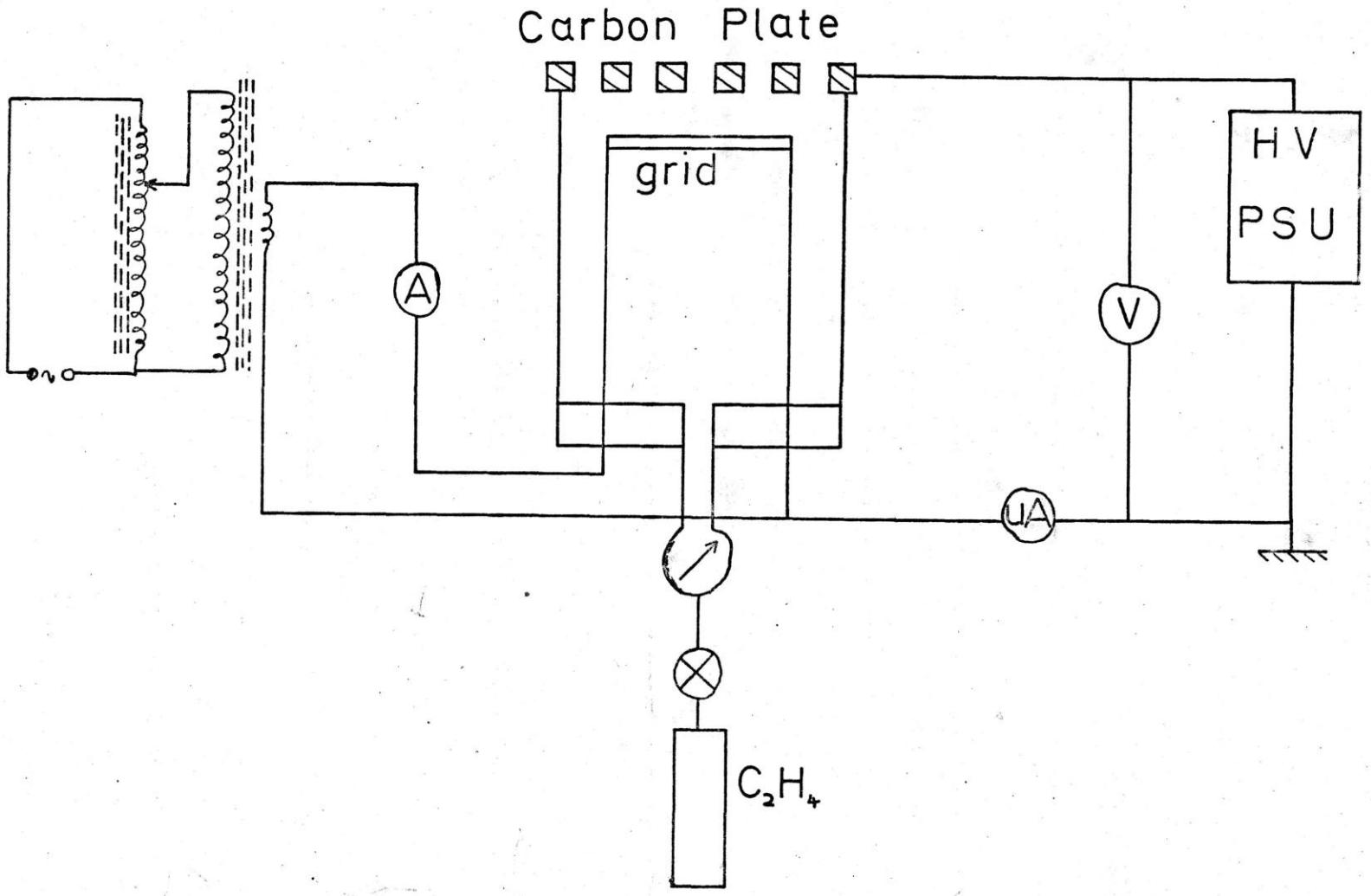

Fig. 2·2 Apparatus for C_2H_4 pyrolysis on solid surfaces

Tungsten filament in ethylene at 1100°K

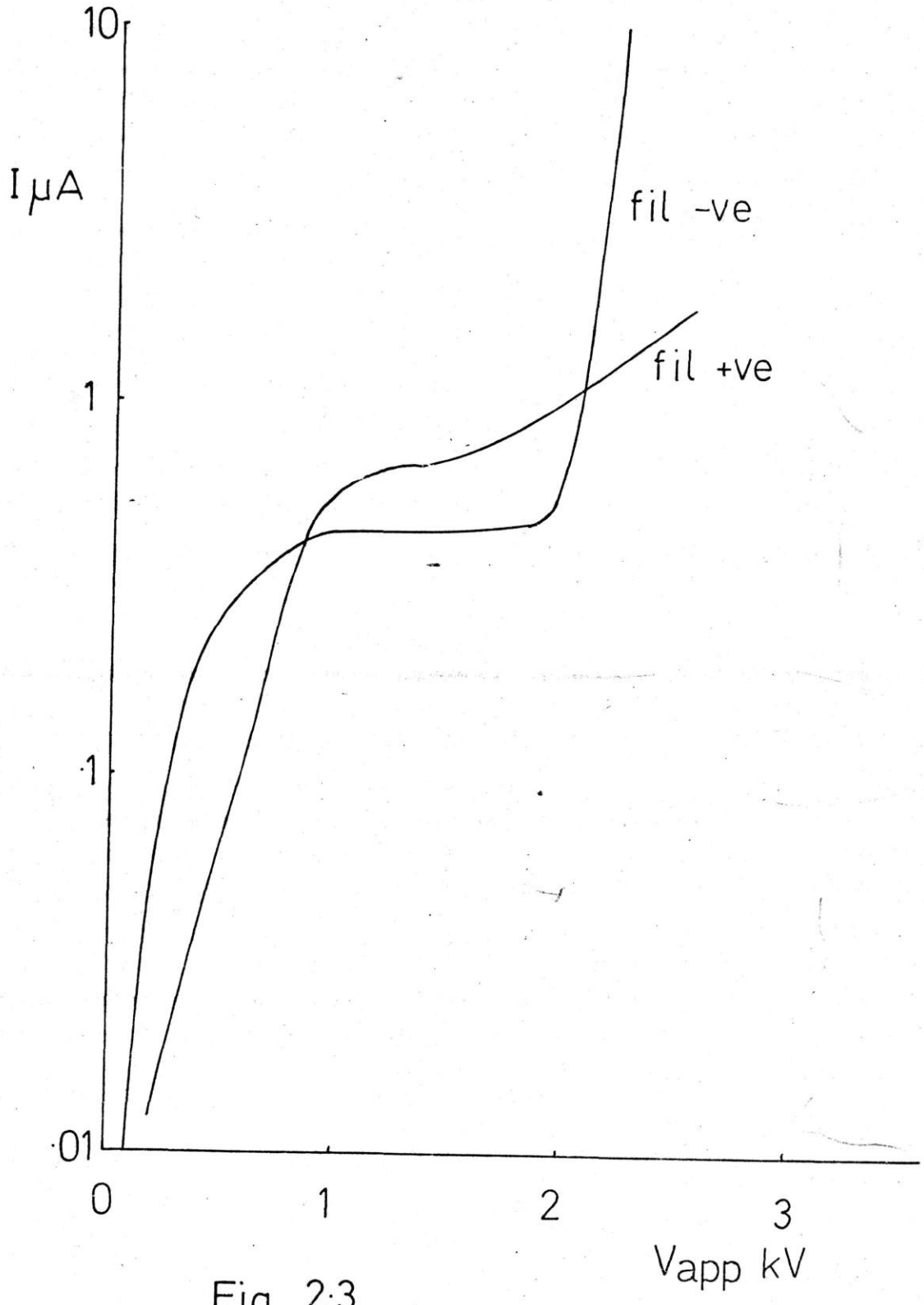

Fig. 2·3

3) Hot filament in nitrogen just after pyrolysis filament negative
4) Hot filament in nitrogen some time after pyrolysis filament negative

} see Fig. 2.4

5) Hot filament in nitrogen just after pyrolysis filament positive
6) Hot filament in nitrogen some time after pyrolysis filament positive

} see Fig. 2.5

7) Plot of current versus time in N_2 filament negative just after pyrolysis at constant voltage of 2kV. see Fig. 2.6

During pyrolysis, carbon filaments streamed from the top of the tube. These gradually disappeared as the potential was increased starting at 1kV and disappearing by 2kV. All the carbon formed collected on the negative electrode. It had a light fluffy appearance and collected on lines of force between the electrodes. The appearance of the filament changed during pyrolysis. Its diameter increased by up to twice and the surface became porous.

Carbon particles formed during the pyrolysis of ethylene on a tungsten wire bear a positive charge. Figure 2.3 shows that the particles are charged and that saturation currents are obtained. Carbon is always deposited on the negative electrode; hence the particles are positively charged.

Examination of Figs. 2.4,2.5 and 2.6 together with observations on the physical state of the filament before and after pyrolysis suggest that surface reactions are involved.

Tungsten filament in nitrogen at 1100°K

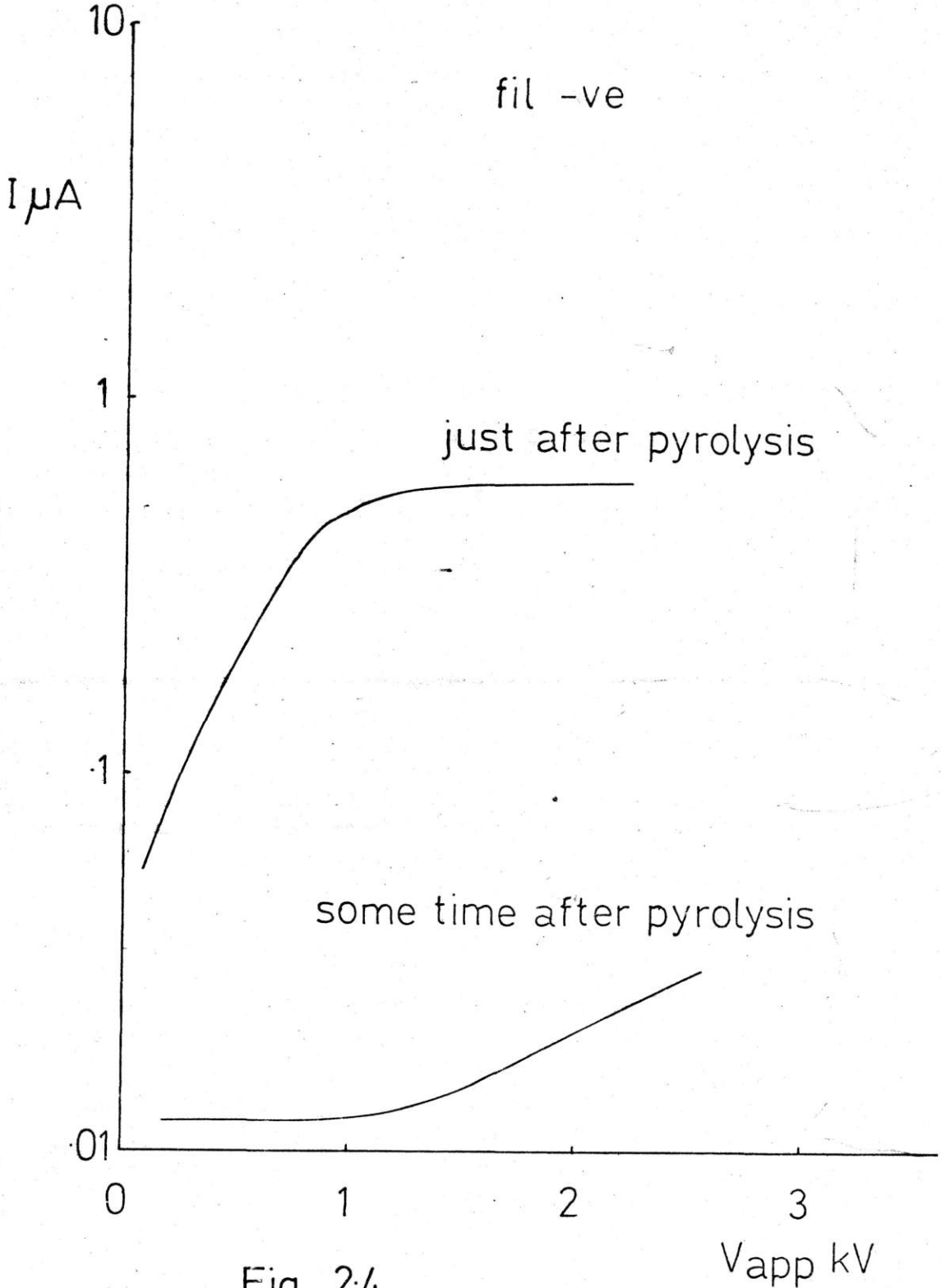

Fig. 2·4

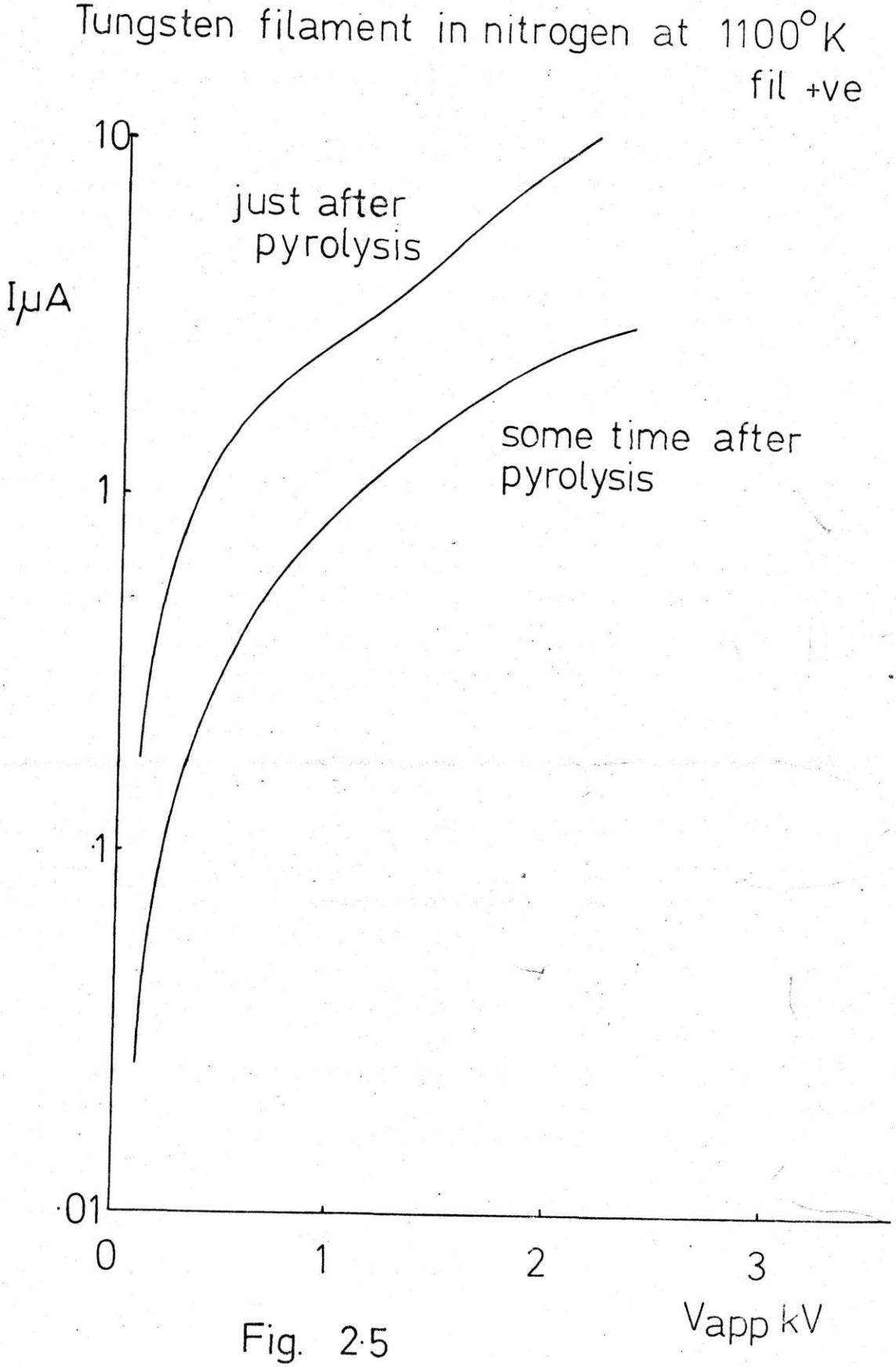
Tungsten filament in nitrogen at 1100°K
fil +ve
10
1
·1
·01
IμA
just after pyrolysis
some time after pyrolysis
0
1
2
3
Vapp kV

Fig. 2·5

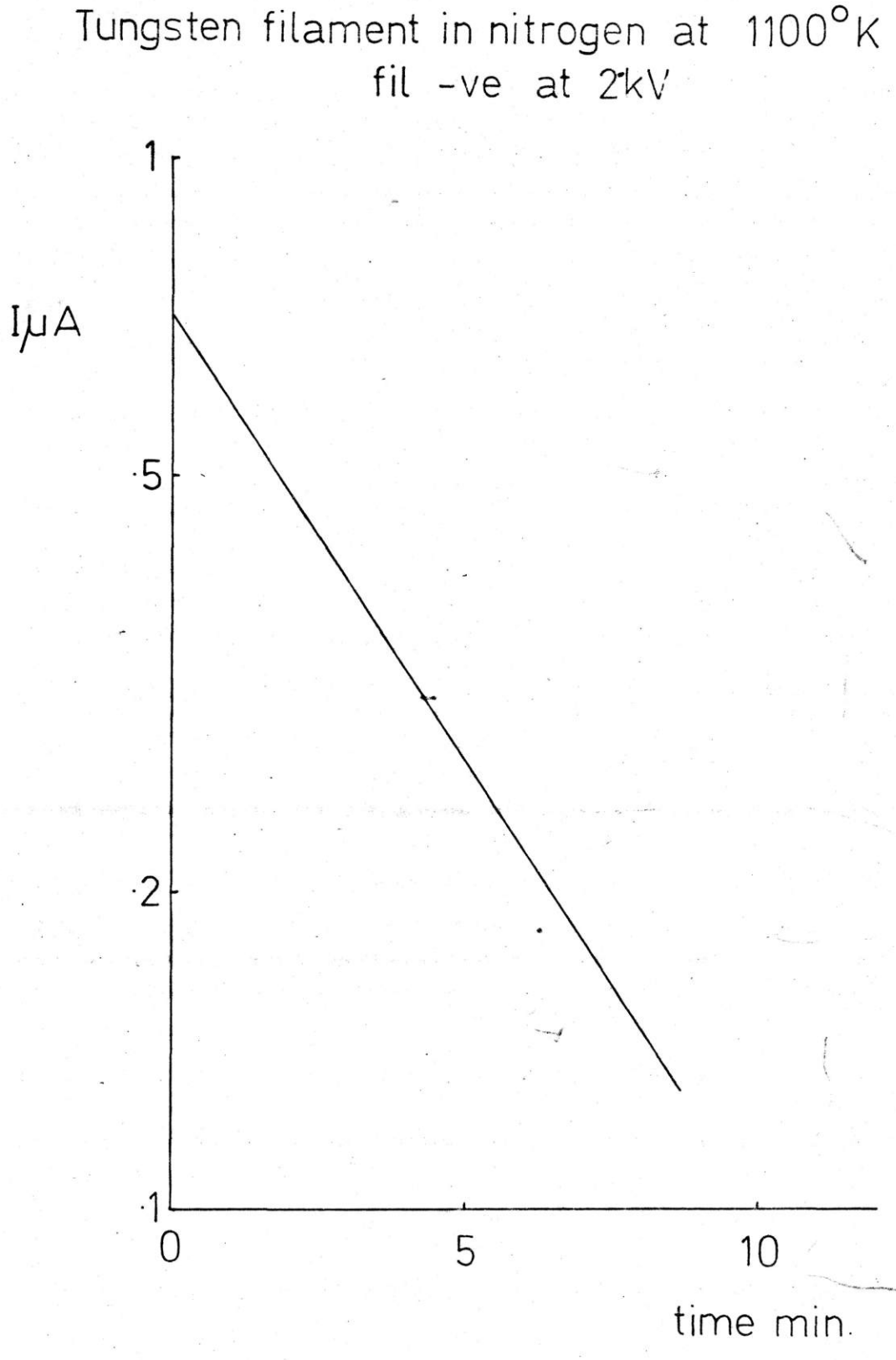

Fig. 2·6 Current / time after pyrolysis

It was deduced that immediately after pyrolysis the filament has adsorped ethylene on the surface, since on heating the filament in nitrogen, this gives a current which falls off expotentially with time, see Figs. 2.4 and 2.6. Chemisorped ethylene on the filament surface changes its structure, making it porous. This suggests that catalysis could occur on the filament surface, explaining the formation of ions at temperatures where conditions for radical reactions are thermodynamically more favourable.

The apparatus was modified to overcome two difficulties.

1) The tube was enlarged to 3" internal diameter to prevent corona type discharge to the walls and also to allow the use of a larger filament.
2) The filament material was changed to carbon in an attempt to eliminate catalysis, since any effect due to a carbon surface would also occur in a flame.

The conditions were as before, ie. filament temperature 1100°K at a current of 50A. The ethylene flow rate was 1 $lmin^{-1}$. The following series of current voltage characteristics were taken:

1) During pyrolysis filament negative
2) During pyrolysis filament positive

} see Fig. 2.7

3) In N_2 filament negative
4) In N_2 filament positive
5) In C_2H_4 filament positive no pyrolysis

} see Fig. 2.8

6) In Ar filament positive
7) In He filament positive
8) In CO_2 filament positive

} see Fig. 2.9

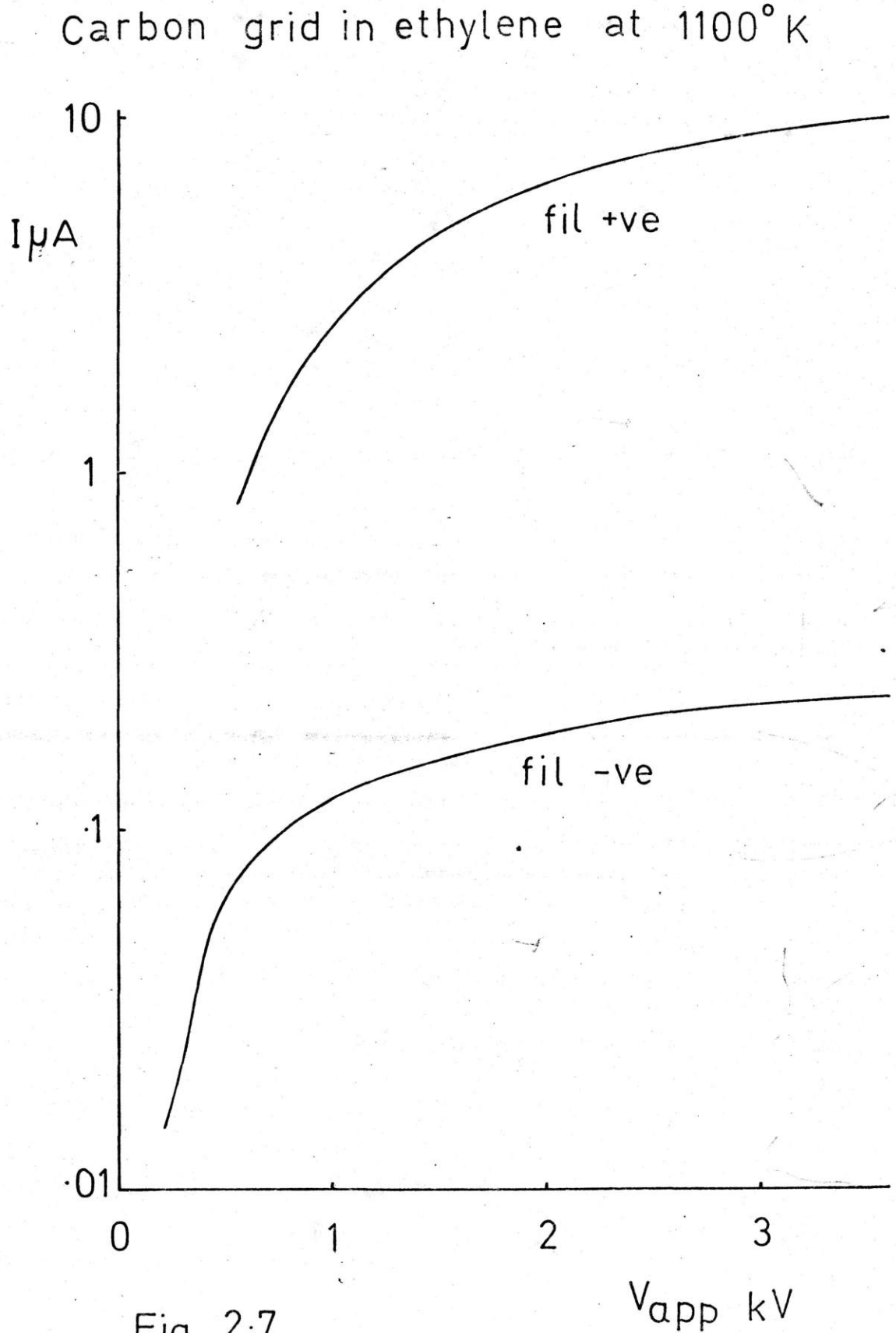
Carbon grid in ethylene at 1100°K
10
IμA
1
·1
·01
fil +ve
fil -ve
0
1
2
3
Vapp kV

Fig. 2·7

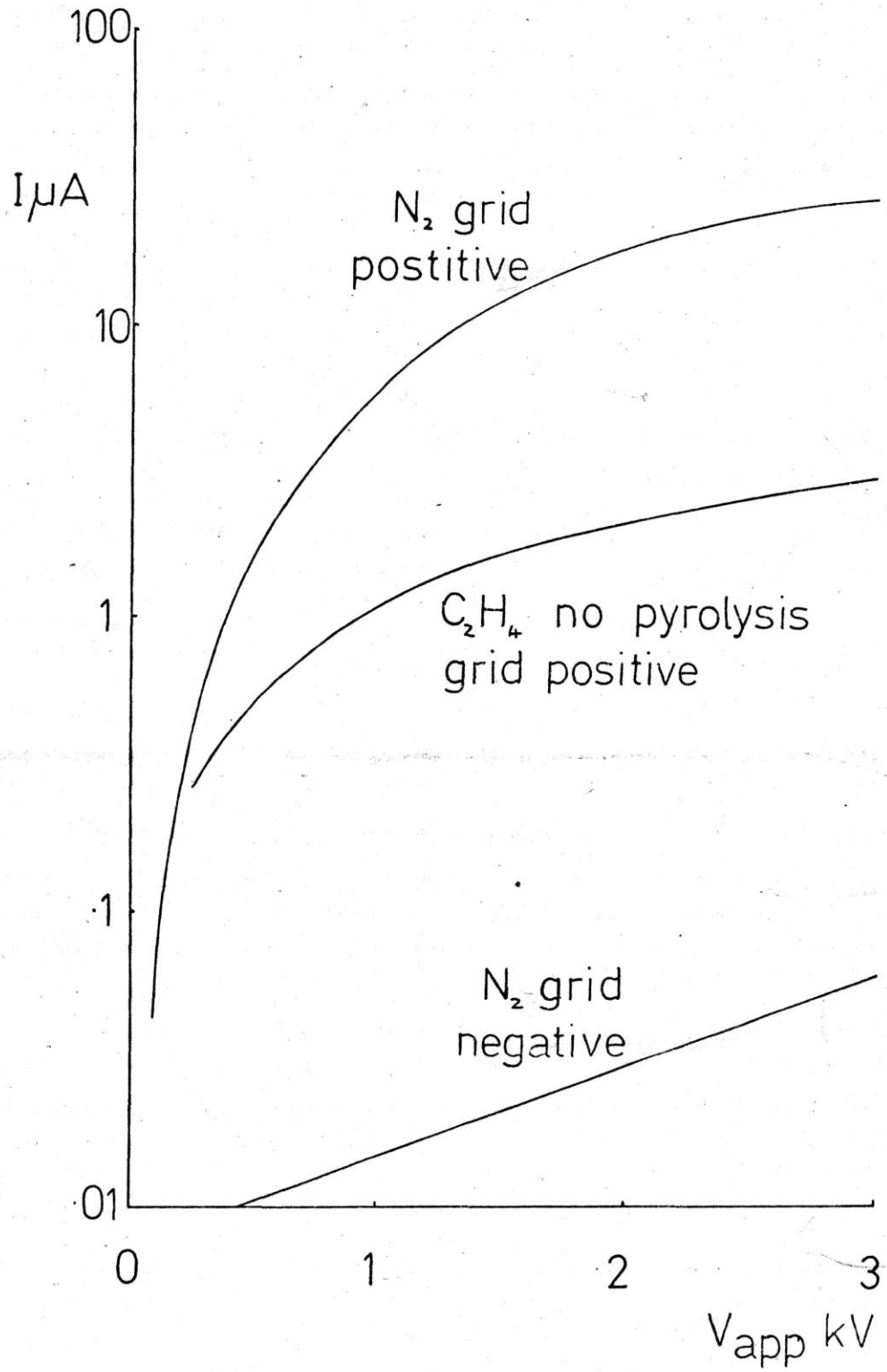
Carbon grid at 1100°K
100
IμA
10
1
·1
·01
N₂ grid
postitive
C₂H₄ no pyrolysis
grid positive
N₂ grid
negative
0
1
2
3
Vapp kV

Fig. 2·8

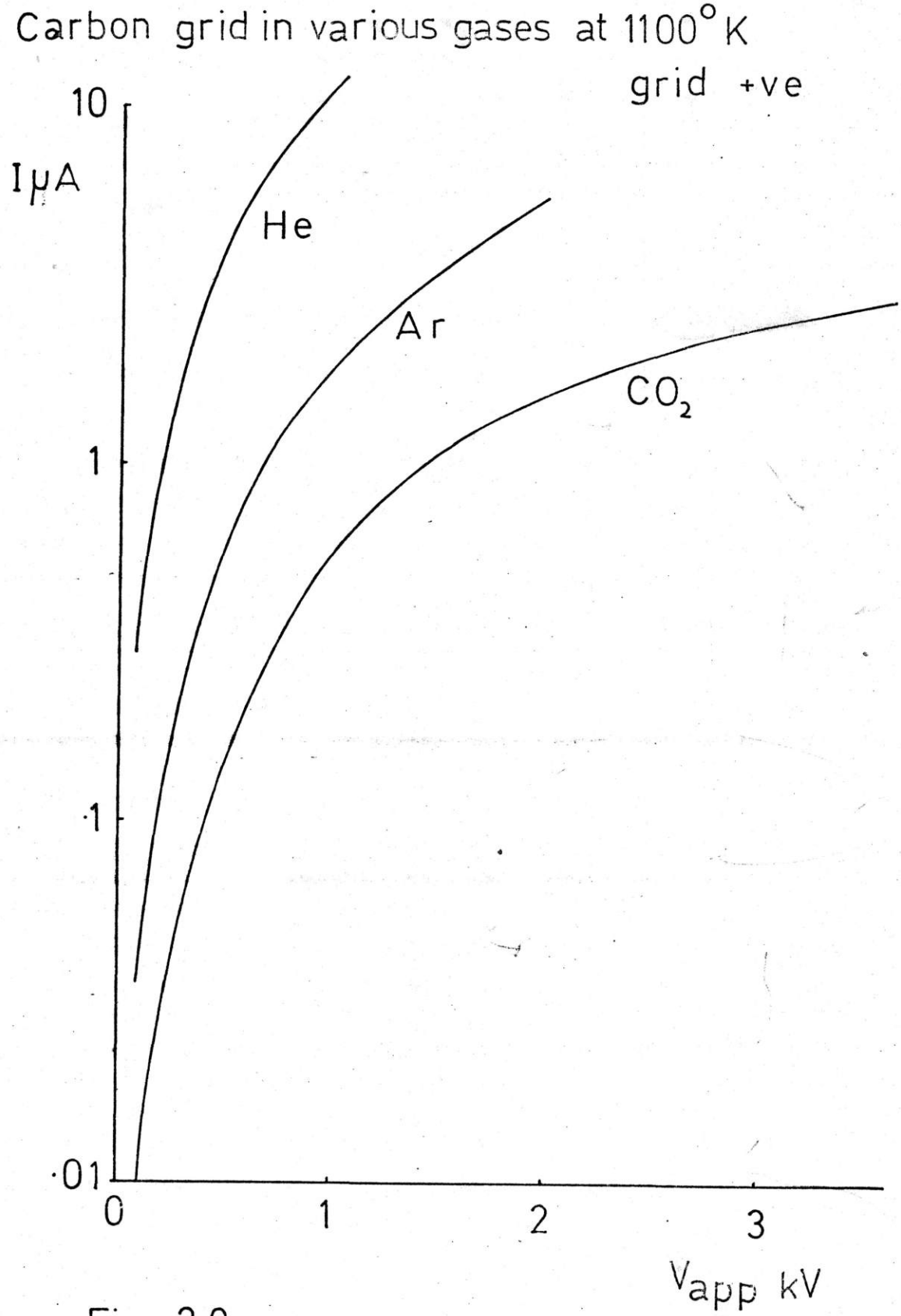
Carbon grid in various gases at 1100° K
grid +ve
10
IμA
1
·1
·01
He
Ar
CO_2
0
1
2
3
V_{app} kV

Fig. 2·9

9) Plot of current versus time in N_2

filament positive at 2kV. see Fig. 2.10

Pyrolysis occured and the carbon particles behaved as before. The filament increaed in diameter with time but this appeared to be due to carbon baking on the filament surface. Examination of the results show that the carbon particles formed during pyrolysis on a carbon filament bear a positive charge. With the filament negative, see Fig. 2.7, a plateau occurs, giving a saturation current of about 0·2 μA on a filament area of about 1 cm^2. Comparing this with a flame saturation current of 1·2 μAcm^{-2} shows that current from charged particles formed in the flame pyrolysis zone is not an insignificant contribution to the total flame current.

Formation of charged carbon particles directly from the gas phase is thermodynamically improbable, but formation of ions by catalysis on the first-formed uncharged carbon particles would be possible. Ie. if nucleation in the pyrolysis zone gives uncharged particles, growth may still give charged carbon.

Examination of Fig. 2.10 shows a very low current, almost unmeasureable when the filament is negative in N_2. This fits in well with theory, from von Engel[36]:-

Maximum thermionic emission current from a solid surface in a vacuum

$$j = BT^2 \exp\left(\frac{-eG}{k_z T}\right) \quad Acm^{-2} \qquad \ldots\ldots\ldots\ldots 2.1$$

For carbon B = 48 G = 4.4 eV

Hence at 1100°K $j = 3{\cdot}9 \times 10^{-7}$ μAcm^{-2}

This current is negligible.

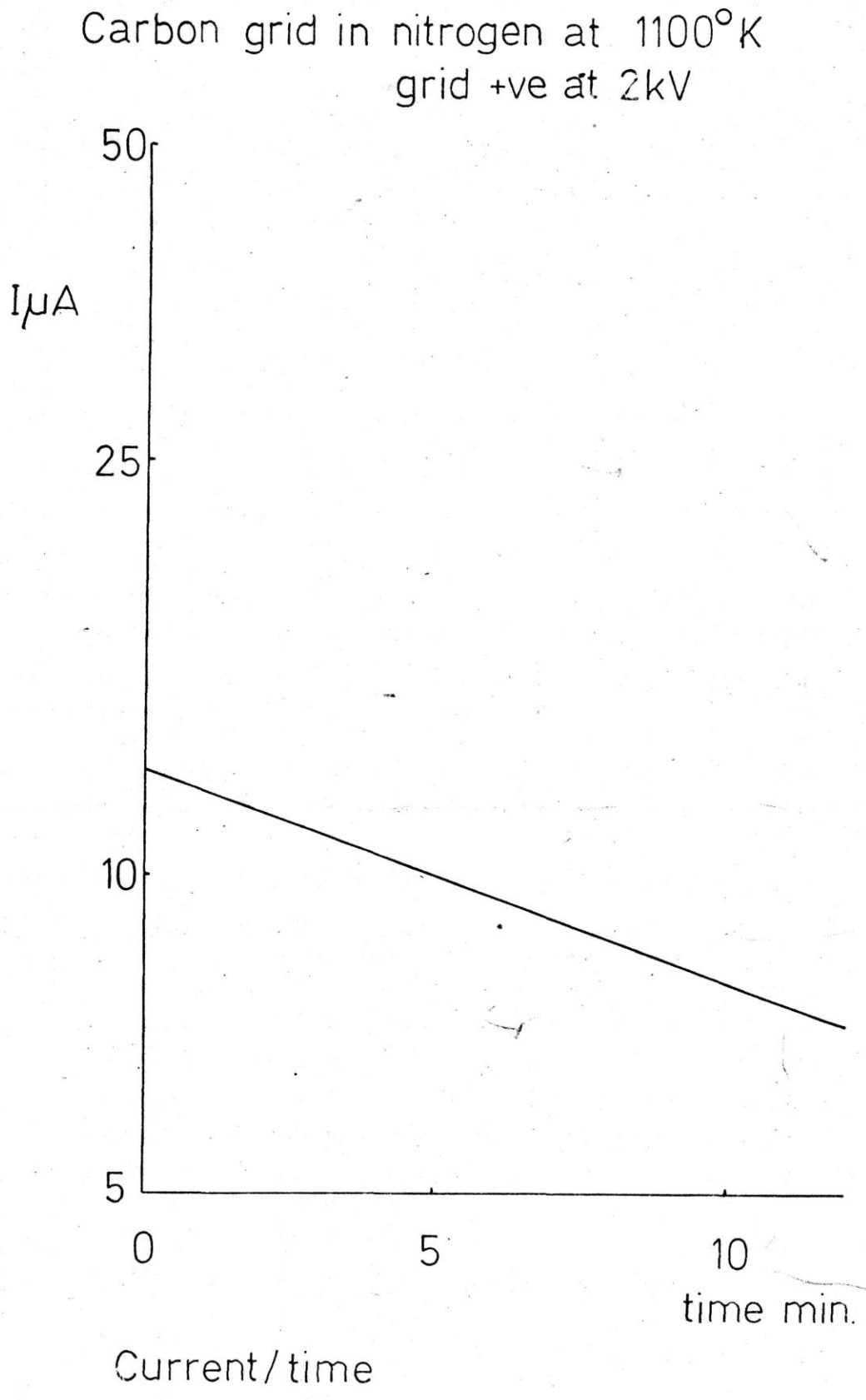

Current/time

Fig. 2·10

Examination of the curves with the filament positive show that they all have the same form. Hence apart from minor variations the curve obtained is a function of the filament itself rather than the gas. This is probably due to emission of positive ions from the filament, either carbon ions or alkali metal impurity ions in the filament. The curve from the tungsten wire, see Fig. 2.5, could be due to tungsten ions (1st IP 8·1eV) or carbon ions (1st IP 11·2eV) from reactants and/or products adsorped on the filament. For positive ion emission the current voltage characteristics are of the form:-

$$j = \frac{9kV^2}{32\pi d^3} \quad \text{- from von Engel}^{37}. \qquad \ldots\ldots\ldots \; 2.2$$

Taking a typical case $j = 3\ \mu A cm^{-2}$ at 3·6 kV (see Fig. 2.10 in CO_2) gives $k = 2{\cdot}59 \times 10^{-12}$ A cm V^{-2}. Using this data a theoretical current-voltage curve was calculated, see Fig. 2.11.

The curve shape obtained was very similar to the experimental one. Hence the filament acts as an ion source. Using the above formula and assuming $d \sim 1$cm and filament area was $\sim 1 cm^2$ the mobility k was calculated as

$$k = 2{\cdot}34\ cm^2\ sec^{-1}\ V^{-1}.$$

This is of the correct order for small ions at atmospheric pressure.

Comparing the calculated values of current-voltage for a carbon filament from Fig. 2.11 with results during pyrolysis and a negative filament (see Fig. 2.7) a close correlation is shown up to the plateau level.

V kV	$I_{calc.}$ μA	$I_{meas.}$ μA
·2	·0095	·0106
·3	·0215	·023

Calculated characteristic for carbon grid

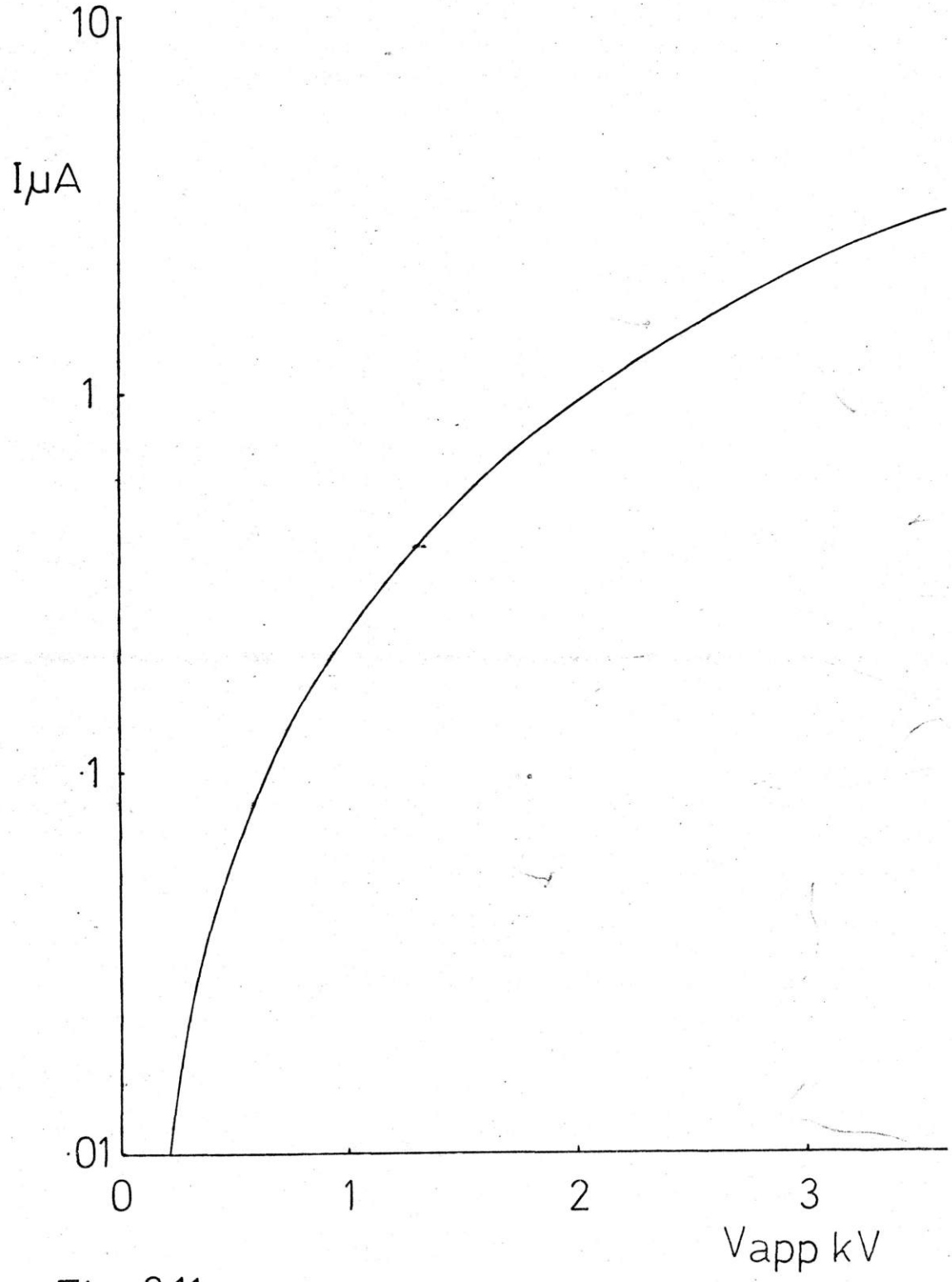

Fig. 2·11

V kV	$I_{calc.}$ μA	$I_{meas.}$ μA
·4	·038	·043
·5	·059	·065
·6	·085	·081

Hence the ions causing a large current with the filament positive have the same mobility as carbon ions from pyrolysis.

The conclusions are that pyrolysis in ethylene occurs at temperatures as low as 1100°K though this may be a surface reaction not directly relvant to flames. The carbon particles produced are all positively charged in the presence of a field. Any practical system would have hot surfaces and under these conditions carbon particles would become positively charged and hence would be amenable to electrical control.

Hot surfaces emit charge in an electric field due to at least two mechanisms in addition to the expected small thermionic emission and corona current. They are: negative charge for some time after exposure to ethylene, which may be due to the same mechanism that charges carbon positively on the surface, and the emission of positive charges that hot surfaces emit continuously, which has been accounted for theoretically in terms of ion emission.

These results suggest that the planned experiments would have been less useful than anticipated, partly because they have already answered several of the questions asked. With the hot plate negative, pyrolysing carbon goes to the carbon surface and bakes on, making collection and examination of the carbon difficult. When the hot plate is positive copious ion emission swamps the contribution from carbon particles.

2.2 ETHYLENE PYROLYSIS IN A HOMOGENOUS GAS SYSTEM

The mechanism of ion formation during the pyrolysis of ethylene in the presence of solid surfaces is unclear from 2.1. Ions could be formed by a gas phase reaction or by a surface reaction. In order to eliminate the possibility of surfaces contributing a study of ethylene pyrolysis was carried out in a shock tube.

It was decided to study the pyrolysis in the reflected shock, this has the advantages that the gas remains stationary with respect to the tube for the duration of each experiment so that observation is carried out on the same gas molecules. Also a low incident Mach No. can be used and the design of the test chamber is simplified.

2.2.1 THE CALCULATION OF SHOCK PARAMETERS

In order to simulate the conditions used in section 2.1 calculations were done assuming the following final state for the gas:-

100% ethylene heated to 1100°K at no more than a few atmospheres pressure. Now the relationship between temperature behind the reflected shock, initial temperature and incident Mach No. in an ideal gas is given by[38]:-

$$\frac{T_5}{T_1} = \frac{\left[2(\gamma-1)M_1^2 + (3-\gamma)\right]\left[(3\gamma-1)M_1^2 - 2(\gamma-1)\right]}{(\gamma+1)^2 M_1^2} \quad \ldots\ldots 2.3$$

γ for ethylene at 298°K is 1·24[39] falling to 1·09 at 1100°K. The mean value of 1·16 was considered sufficiently accurate

to predict the initial conditions required; the actual temperature reached being calculated from the measured shock speeds.

Using $T_5 = 1100^oK$ and $T_1 = 298^oK$ and $\gamma = 1{\cdot}16$ the required incident Mach No. M_1 was found to be 4·0. To allow for real gas effects 10% was added to this giving a required M_1 of 4·4. From this value the required initial pressure P_1 was calculated[38].

$$\frac{P_5}{P_1} = \left[\frac{2\gamma M_1^2 - (\gamma-1)}{\gamma+1}\right]\left[\frac{(3\gamma-1)M_1^2 - 2(\gamma-1)}{(\gamma-1)M_1^2 + 2}\right] \quad \ldots\ldots\ldots 2.4$$

This gives $\frac{P_5}{P_1} = 194$, hence the required starting pressure is of the order of 10 mm Hg for an experimental pressure close to atmospheric.

The pressure ratio across the diaphram P_4/P_1 is given by[38]:

$$\frac{P_4}{P_1} = \frac{2\gamma_1 M_1^2 - (\gamma_1-1)}{\gamma_1+1}\left[1 - \left(\frac{\gamma_4-1}{\gamma_1+1}\right)\frac{f_1}{f_4}\left(M_1 - \frac{1}{M_1}\right)\right]^{-\left(\frac{2\gamma_4}{\gamma_4-1}\right)} \quad \ldots 2.5$$

giving a value of 91 using hydrogen as the driver gas.

In order to facilitate relatively speedy operation of the tube at the pumping speed available a moderate value of initial pressure was chosen at about 20mm Hg.

Hence P_4 was of the order of 1800mm Hg or about 36psi. The radius of the diaphram was 2" so that a 50 μ Mylar diaphram was suitable, bursting at 47 psi across the diaphram.

2.2.2 DESCRIPTION OF TUBE AND TEST CHAMBER

A diagram of the shock tube system is shown in Fig. 2.12. The tube was made from 2" diameter stainless steel with a 3 m driver section and a 4 m test section. The diaphram was separated from the main body of the driver section by a 2" Klinger valve, A. The tube was operated by flushing out the test section and the driver section between the diaphram and valve with ethylene and then filling at the correct pressure. The main body of the driver section was filled with hydrogen at 60 psi and the tube operated by opening valve A. This method of operation ensured uniform conditions from one run to the next and overcame any slight leakage problems around the diaphram.

Shock speeds were measured using two resistance detectors, see Fig. 2.13, placed just before the test section. The waveforms were differentiated, amplified and displayed on an oscilloscope. The test chamber was constructed by blocking off the end of the tube with a perspex plate carrying an axial electrode protruding a few mm back into the tube. A field was applied between this and the wall of the tube - the current being monitored by an oscilloscope triggered by the first resistivity detector.

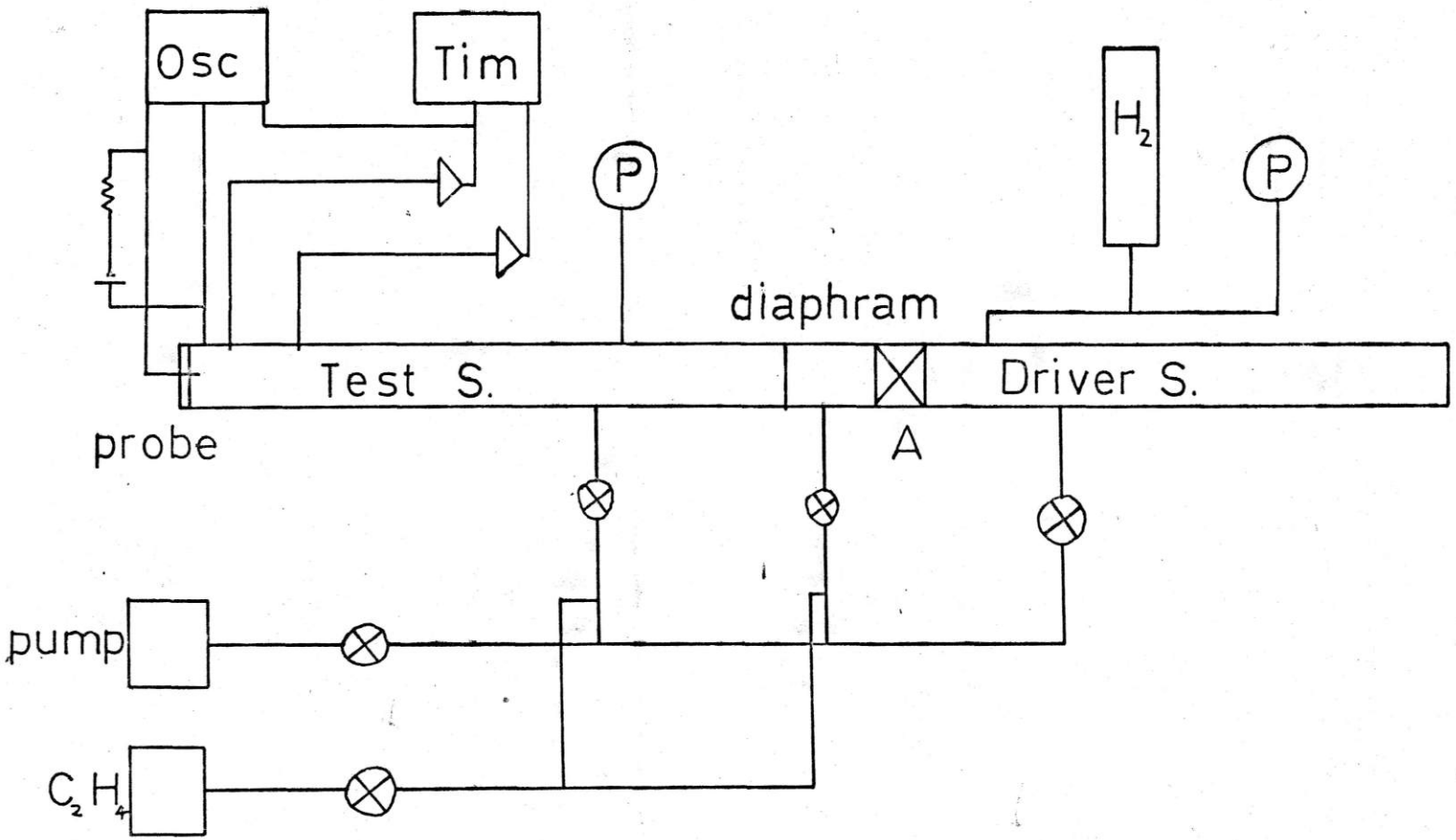

Fig. 2·12 Shock tube system for ethylene pyrolysis

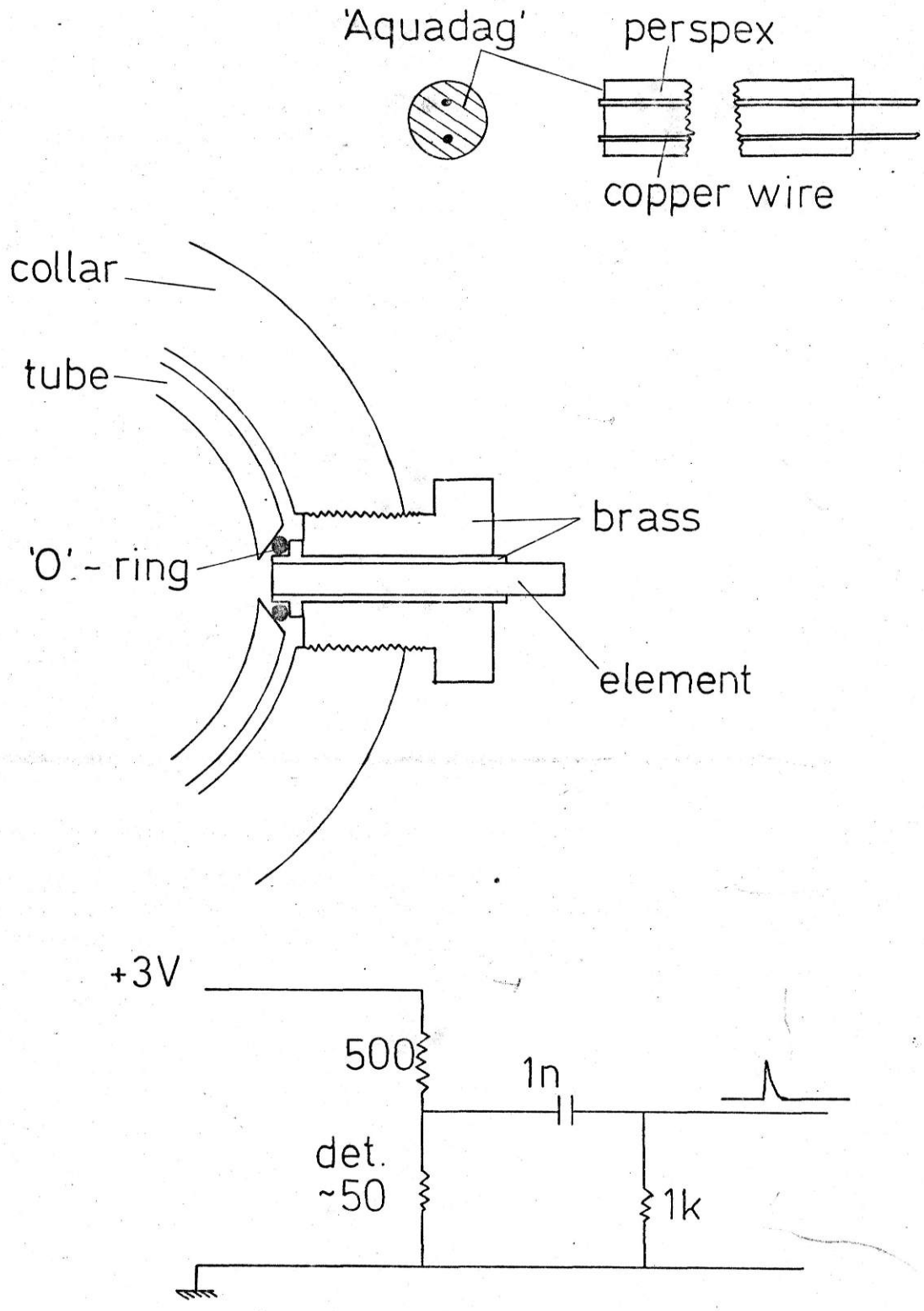

Fig. 2·13 Resistance detector for shock front

2.2.3 RESULTS

It was found experimentally that a starting pressure P_1 of 6 mm gave a measured initial shock speed, M_1, of Mach 4·0. A series of experiments were carried out over a range of starting pressures from 5 mm to 20 mm giving measured incident shock speeds of between Mach 6 and 2 and temperatures calculated from 2.3 from 2400°K to 500°K. The probe circuit used for these experiments is shown in Fig. 2.14 and typical oscillograms in Fig. 2.15.

At all experimental temperatures current of the order of a few micro-amperes was registered by the probe. Two types of oscillogram were observed depending on the temperature reached, see Fig. 2.15. At low temperatures the current rose to a peak and fell off. At moderate temperatures the current rose suddenly to a peak, as the reflected shock formed and remained at the same value until the rarefaction wave arrived. At higher temperatures this was accompanied by a bright yellow flash from the end of the tube. No current was observed during the passage of the incident shock.

The current measured at higher temperatures is undoubtedly caused by ionisation in the pyrolysing ethylene. There is, however, another possibility at lower temperatures. The test chamber is a capacitor charged up by the probe voltage. When the temperature and pressure change in this capacitor the dielectric constant will change and hence the voltage across the plates will alter. This could explain the observed signal. To test this a simple calculation was

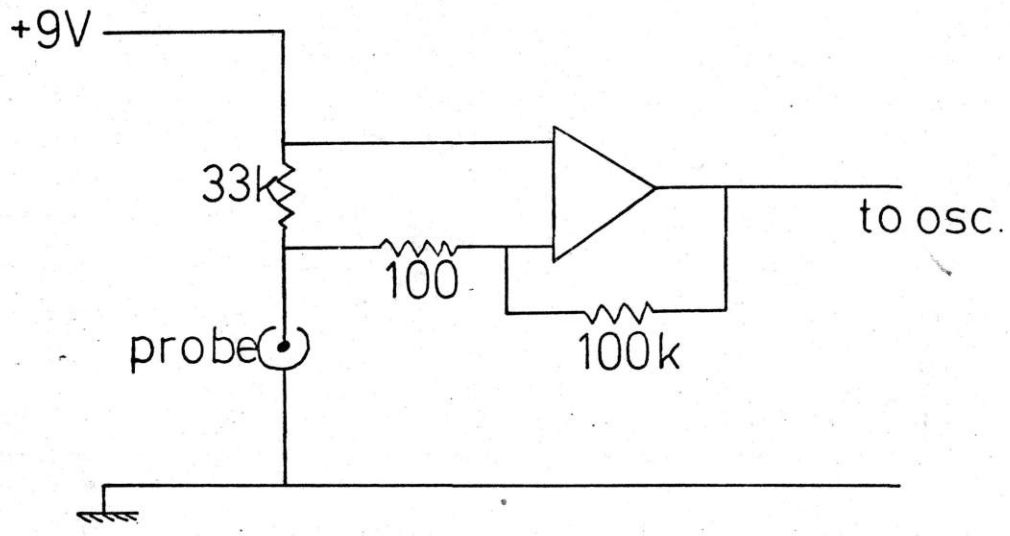

Fig. 2·14 Probe circuit for current measurements

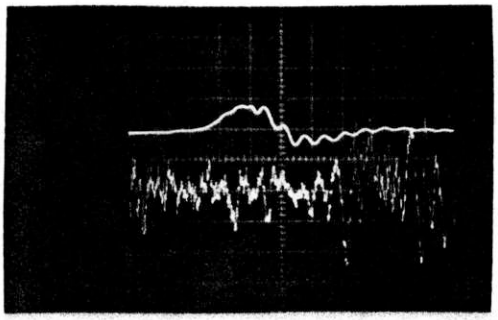

a) at low temperatures

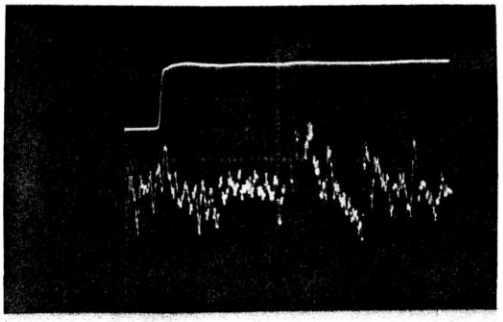

b) at high temperatures

Fig. 2.15 Current - voltage characteristics of probe during low and high temperature pyrolyses of ethylene, (upper traces). Lower traces, timing signals from resistivity detectors.

performed.

The capacity for a cylindrical capacitor is given by[40]:

$$C = \frac{2\,lk_{r\,o}}{\ln r_2/r_1}$$

giving a capacity for the probe of ·24pF.
Charge is given by $q = CV = 2 \times 10^{-12}$ coulombs.
Hence the maximum output would be 2 μA for 1 μs. This is several orders of magnitude lower than observed experimentally. The current must then be caused by ionisation.

A second series of experiments were carried out using a circuit to measure saturation current, see Fig. 2.16. A ramp voltage derived from the oscilloscope timebase was applied to the probe, current being measured as before. Temperatures ranged from 900 to 1800°K a typical trace is shown in Fig. 2.17.

2.2.4 DISCUSSION

The peaks in probe current recorded at lower temperatures, Fig. 2.15a are almost certainly caused by initial ionisation followed by recombination; the field strength of 2V cm^{-1} being insufficient to prevent this. At higher temperatures the rate of ionisation is very fast and a plasma is formed as the recombination rate is relatively slow.

A plot of log saturation current against 1/T is shown in Fig. 2.18 for the second series of experiments. Field strengths used here were also fairly low, up to 50 V cm^{-1},

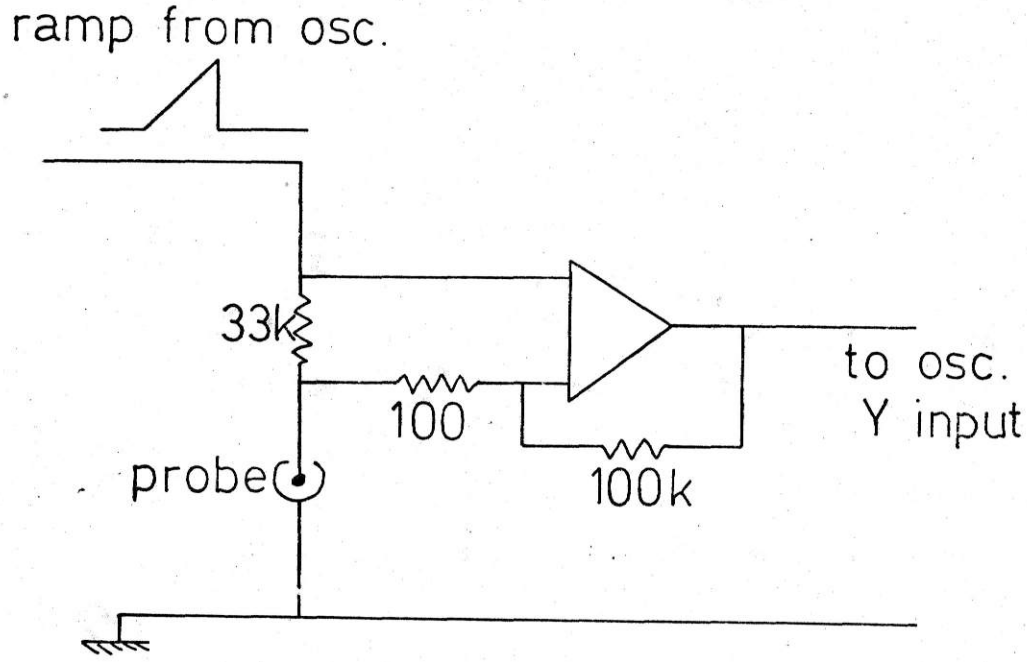

Fig. 2·16 Probe circuit for saturation current measurements

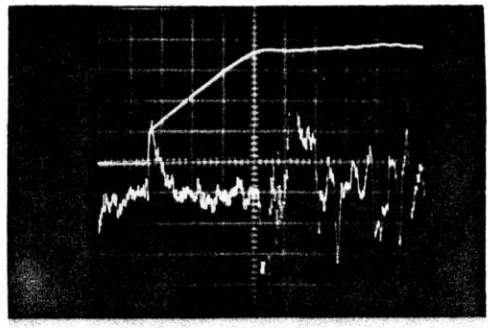

Fig. 2.17 Current - voltage characteristic of probe using a ramp voltage during the pyrolysis of ethylene, (upper trace). Lower trace, timing signals from resistivity detectors.

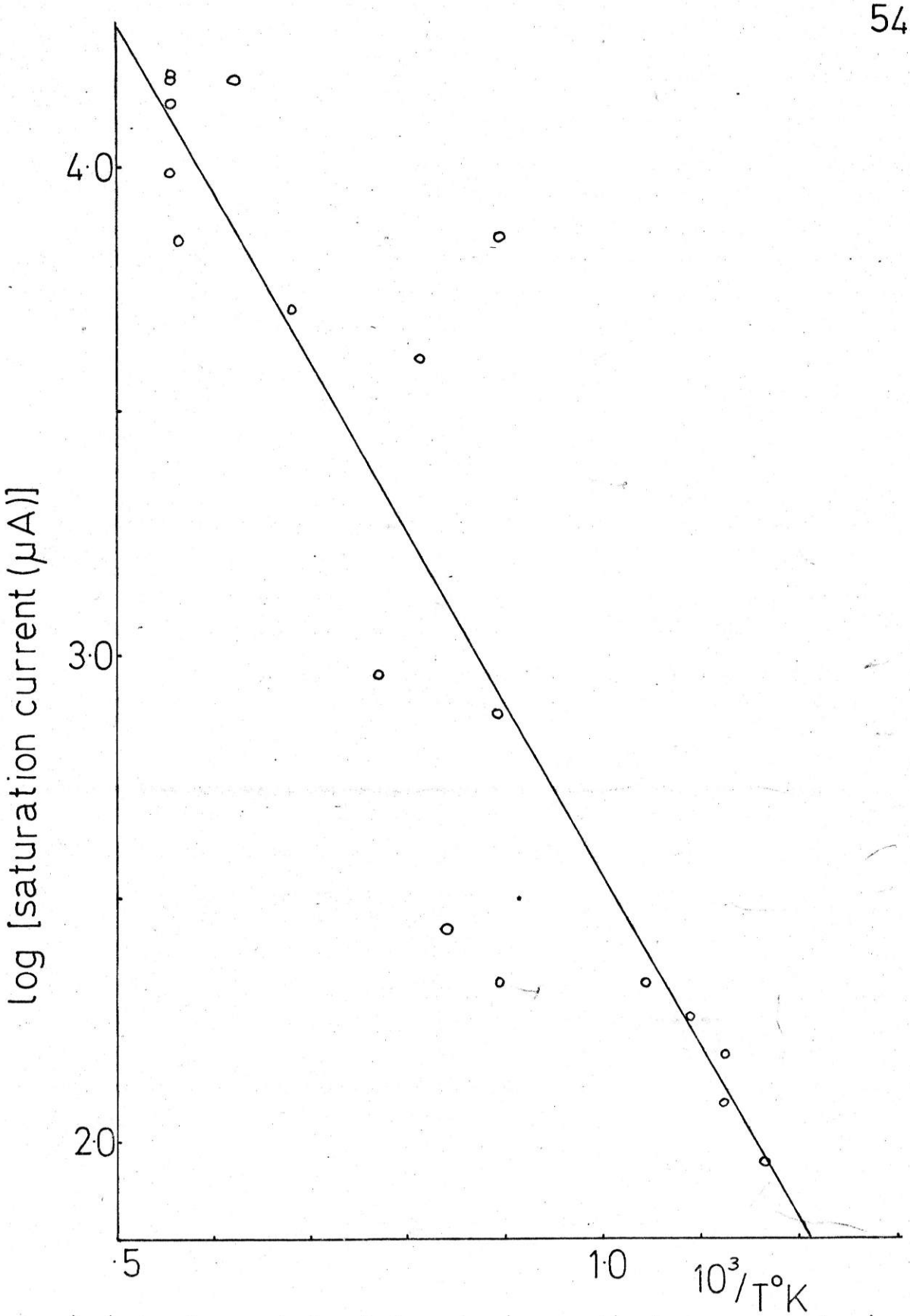

Fig. 2·18 Arhennius plot of I_S during ethylene pyrolysis

and the current may not have reached saturation especially at high ion concentrations.

In order to overcome this difficulty an attempt was made to compute ion concentrations in the test chamber from experimental voltage and current values.

Using the relationship:-

$$j = \frac{e(k_+ + k_-)^2 V^2}{2\alpha d^3} \left\{ \left(1 + \frac{4d^4 (\frac{dN}{dt}) \alpha}{(k_+ + k_-)^2 V^2} \right)^{\frac{1}{2}} - 1 \right\}$$

equation 4.29 from Chapter 4.2, and rearranging to give,

$$\frac{dN}{dt} = \frac{\alpha d^2 j^2}{e^2 (k_+ + k_-)^2 V^2} + \frac{j}{ed} \quad \ldots\ldots\ldots\ldots \quad 2.6$$

rates of ion generation may be calculated for values of V and j. The current values were read off from the oscillograms at a time corresponding to 150 μs after the formation of the reflected shock. The applied voltage, V, at this time, was deduced from the ramp characteristic.

α, the recombination coefficient, is temperature dependent and the relationship[41]

$$\alpha = \frac{B}{T^3}$$ was used for correlation.

An initial value for α was taken from Chapter 4.2 as $5{\cdot}3 \times 10^{-5}$ $cm^3 s^{-1}$ at 300°K, though the exact value is unimportant in this treatment of the data.

For an ion producing reaction of order n in ethylene we have,

$$\frac{dN}{dt} = k_n \left[C_2H_4\right]^n = \frac{k_n'}{T^n} = \frac{A' e^{-E/RT}}{T^n}$$

Plots of this data for first and second order reactions are shown in Fig. 2.19 with activation energies of 47·6 and 45·2 kcal mole^{-1} and correlation coefficients of -·88 and -·89 respectively.

Induction time data was also taken from the oscillograms, this was taken as the time interval between the reflected shock forming and the appearance of current at the probe. The equation used for correlation is[78,79]:-

$$\rho^n \Delta t = A' e^{-E/RT}$$

This was plotted as log $\Delta t/T^n$ against $10^3/T$ for first and second order reactions, see Fig. 2.20 with activation energies of 6·9 and 10 kcal mole^{-1} and correlation coefficients of ·53 and ·50 respectively.

The points are rather scattered - this may be caused by uncertainties in the measured parameters as these were read off from oscillograms. Also errors due to real gas effects were ignored during the calculation. However, the results are good enough to indicate an approximate activation energy and to demomstrate that ions are formed during the pyrolysis of ethylene with number concentrations of between 10^{11} and 10^{15} cm^{-3}, not insignificant in terms of electrical effects.

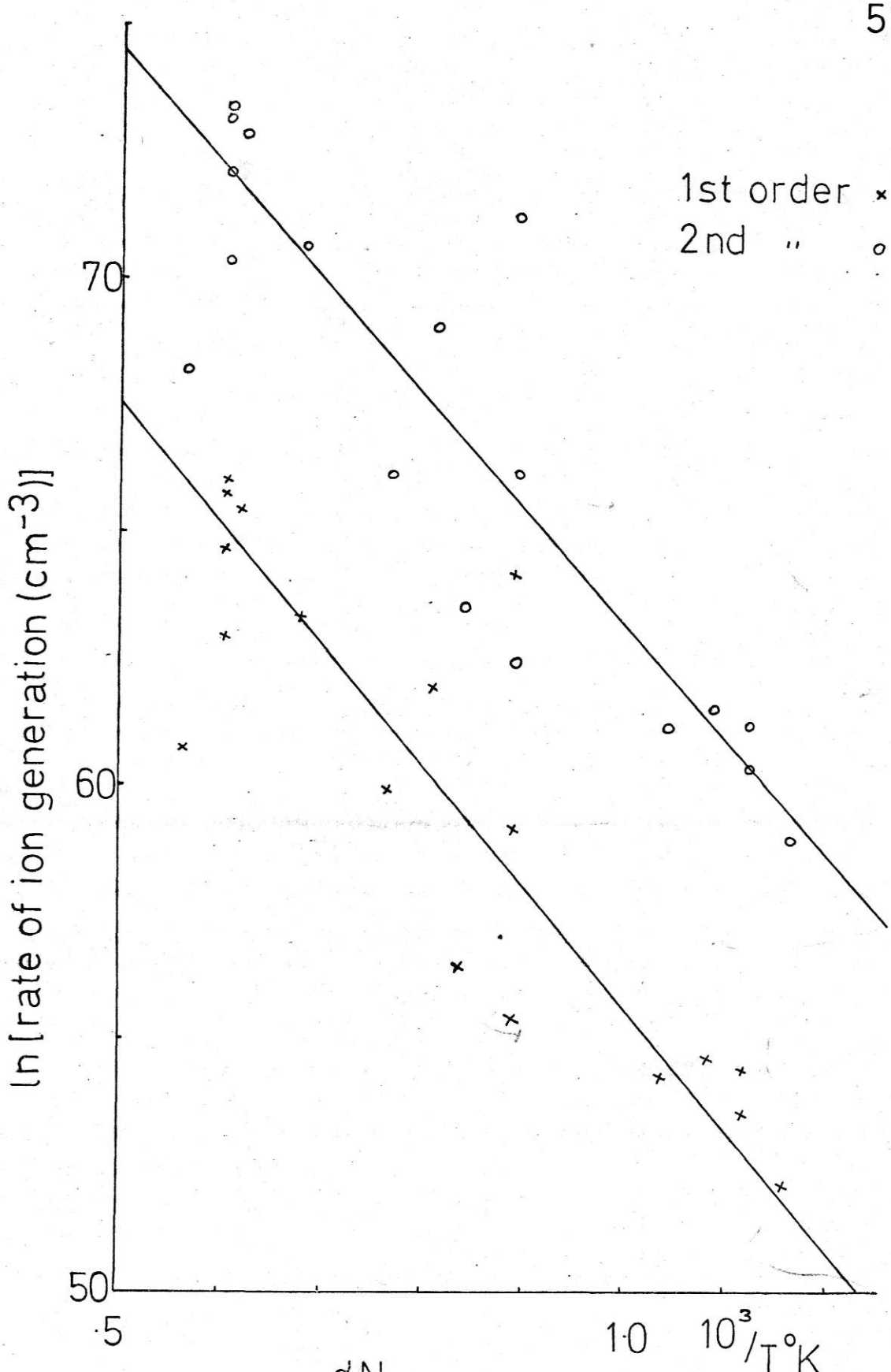

Fig. 2·19 Arhennius plot of $(\frac{dN}{dt})$ during ethylene pyrolysis

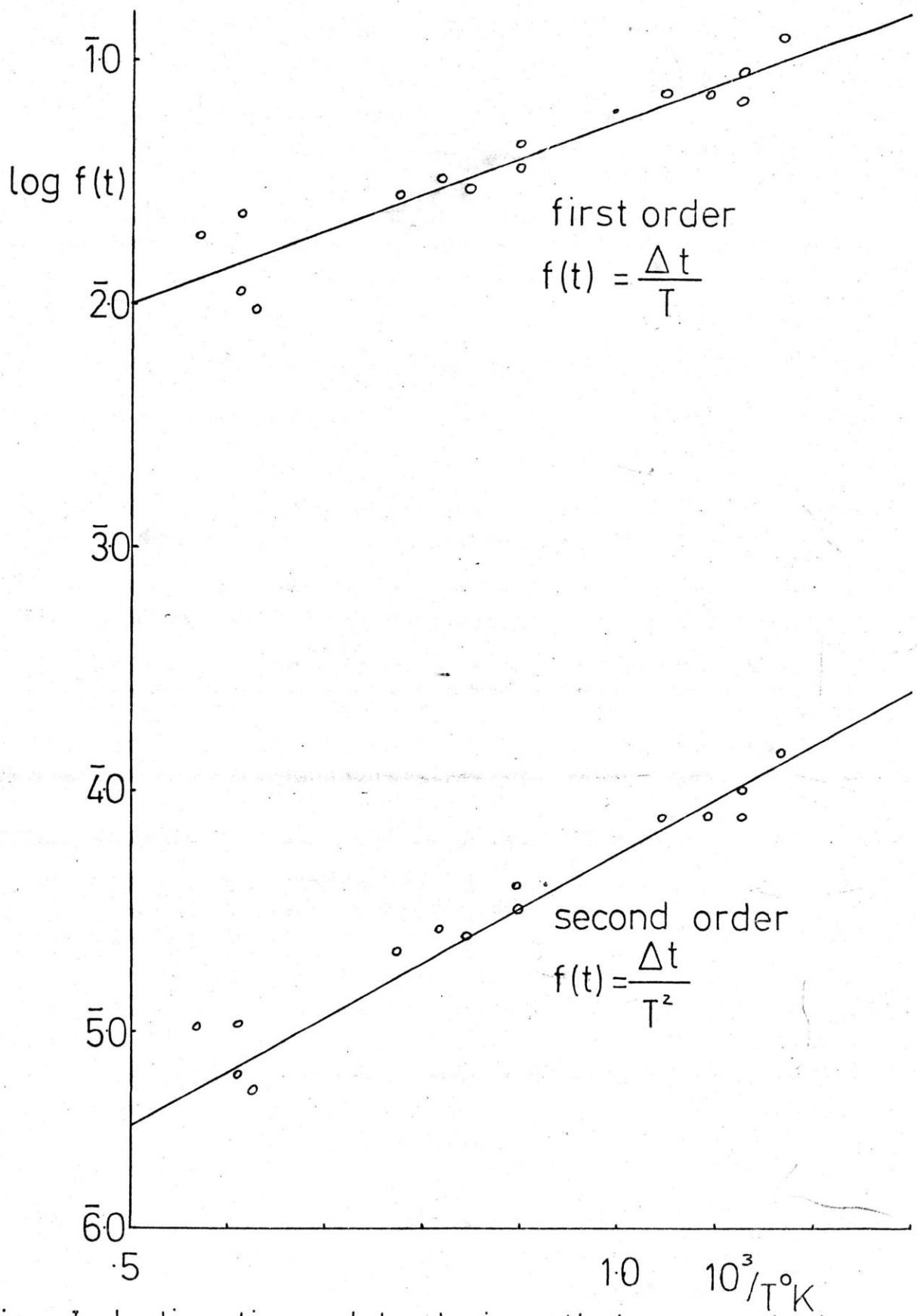

Fig. 2·20 Induction time plots during ethylene pyrolysis

It is therefore necessary to consider possible mechanisms by which this ion formation could occur. There are two broad possibilities, ion formation in the presence and absence of oxygen. The ethylene was not purified before use so that oxygen could have taken part in the reaction. The ethylene used was 99·85% minimum purity the main impurities being hydrocarbons so that the oxygen concentration was unlikely to have exceeded 10^{16} molecules cm^{-3}. In view of the fact that the ion concentration observed here is similar to those observed in flames containing much higher oxygen concentrations it seems unlikely that the majority of the ions were produced by a reaction involving oxygen.

In the absence of oxygen the reactions most likely to produce ions are:-

$$CH^{*} + C_2H_2 \longrightarrow C_3H_3^{+} + e^{-} \quad \Delta H \ -7 \text{ kcal mole}^{-1}$$ [31],

and

$$CH + C_2 \longrightarrow C_3H^{+} + e^{-} \quad \Delta H \ 50 \text{ kcal mole}^{-1}$$ [80].

However all published mechanisms for the production of CH involve oxygen, eg.,

$$C_2 + OH \longrightarrow CO + CH$$ [42]

C_2 being produced by[43]:-

$$C_4H_2 + H \longrightarrow H_2 + C_4H$$

$$C_4H + O_2 \longrightarrow CO + C_2 + CHO \quad \Delta H \ -22 \text{ kcal mole}^{-1}.$$

It has been observed that[42] in some very rich flames there is CH emission below the region of C_2 emission - hence CH is formed before C_2. There are also some flames giving weak CH emission with no C_2 emission examples being $HCHO/O_2$ and rich C_3H_8/O_2 in preignition. Hence there must be other

reactions leading to CH formation especially in the preflame region or pyrolysis zone. The reaction most commonly proposed for ion formation in the presence of oxygen is:-

$$CH + O \longrightarrow CHO^+ + e^- \qquad \Delta H = 20 \text{ kcal mole}^{-1}\ ^{26}.$$

During work on the pyrolysis of 99·9% pure ethylene[81] and 'pure' acetylene[82] in shock tubes using spectroscopic techniques C_2 was detected but CH was not. Thus it is improbable that the ion forming reactions involve CH. The activation energy for the formation of C_2 from ethylene was found to be 50 kcal mole^{-1} [81].

The only fragment, that has been detected, and is energetic enough to be a possible ion precursor is C_2, though the mechanism for its production in the absence of oxygen is unclear. Direct formation from acetylene seems unlikely because of the low activation energy reported by Tsang et al[81]. They suggest the following mechanism for its formation from ethylene.

	ΔH kcal mole^{-1}
$C_2H_4 + X \longrightarrow C_2H_4^* + X \longrightarrow C_2H_2 + H_2$	39·8
$C_2H_2 + C_2H_2 \longrightarrow C_4H_2 + H_2$	2·7
$C_2H_2 + C_2H_2 \longrightarrow C_2H_3 + C_2H$	74
$C_4H_2 + C_2H_2 \longrightarrow C_4H_3 + C_2H$	54
$C_4H_2 + C_2H_2 \longrightarrow C_4H + C_2H_3$	58
$C_4H_3 + C_2H_2 \longrightarrow C_4H_2 + C_2H_3$	21
$C_2H_3 + C_2H_2 \longrightarrow C_2H_4 + C_2H$	10
$C_4H_2 + C_2H \longrightarrow C_4H_3 + \boxed{C_2}$	72·5
$C_2H + C_2H \longrightarrow C_2H_2 + \boxed{C_2}$	19
$C_4H + C_2H \longrightarrow C_4H_2 + \boxed{C_2}$	35

			ΔH kcal mole^{-1}
$C_4H + C_2H$	$\longrightarrow$	$C_2H_2 + C_4$	22
$C_4H + C_4H$	$\longrightarrow$	$C_4H_2 + C_4$	42
$C_4H + C_2H$	$\longrightarrow$	C_6H_2	-102

This mechanism suggests that no C-C bond fission occurs, being energetically unfavourable. However, it has been reported that scrambling of carbon atoms occurs during the formation of C_2 from acetylene flames[83] and during acetylene pyrolysis[84] using $^{12}C_2H_2$ and $^{13}C_2H_2$. One possibility for this is the following rearrangement, possibly between excited states.

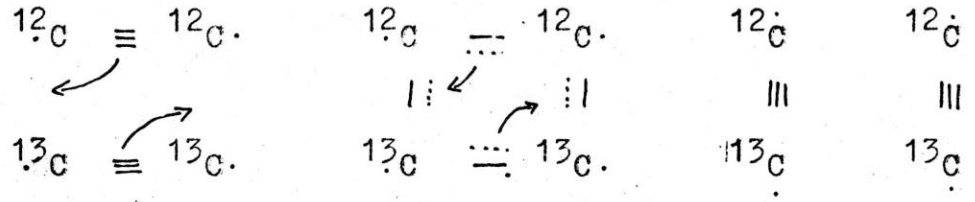

The first order activation energy obtained for ionisation of 48 kcal mole^{-1} compares favourably with the value for the formation of C_2 during the pyrolysis of ethylene[81]. The value obtained from the induction time data compares well with the activation energy of 10 kcal mole^{-1} obtained by Hooker[79], from induction time data, during the pyrolysis of acetylene, though it is not clear whether the induction time refers to C_2 formation or to carbon formation. However, the values are sufficiently close to suggest that ion formation may occur via C_2.

The following reaction for ion production from C_2 is suggested:

$$C_2 + CH_3 \longrightarrow C_3H_3^+ + e^- \qquad \Delta H = 39 \text{ kcal mole}^{-1}$$

The ion formed initially would be $^+C \equiv C - CH_3$ but this

rearranges to give the cyclopropenyl ion 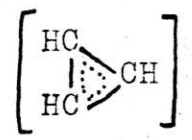 85.

The reaction with ground state C_2 would be endothermic but excited C_2 is formed during the pyrolysis of ethylene, the excitation energy to produce Swan spectra being 55 kcal mole^{-1} [84], so that the reaction

$$C_2^* + CH_3 \longrightarrow C_3H_3^+ + e^-$$

may even be exothermic.

CH_3 is formed by the following reaction scheme[44],

			Δ H kcal mole^{-1}
$2C_2H_4$	$\longrightarrow$	$C_2H_3 + C_2H_5$	63
$C_2H_5 + C_2H_4$	$\longrightarrow$	$C_2H_6 + C_2H_3$	-5
C_2H_6	$\longrightarrow$	$2CH_3$	83

In order to elucidate the reaction mechanism further experimental work would be useful. Suggested experiments would be following C_2 and investigating CH concentrations during pyrolysis together with ion yields. On line mass spectrometry could also be used to determine species concentrations. The effect of oxygen could also be determinded.

Despite the uncertainty about the mechanism of ionisation during pyrolysis the fact remains that in a practical flame system ionisation would occur during pyrolysis and thus electrical control of the carbon products would be possible.

CHAPTER 3

DIRECT CONTROL OF COMBUSTION REACTIONS

3.1 LITERATURE SURVEY

The role of electrons and ions in combustion has been discussed for many years. The discussion has centred on whether they play an important part in the combustion process or whether they are an incidental factor. As early as 1910 J.J. Thomson[45] suggested that combustion is concerned with electrons. Many workers have since drawn conclusions from the physical effects of electric fields on flames.

Malinowski[46] studied the effects of an electric field on the propagation of benzene/air mixtures and found that a field arrested flame propagation. He concluded that ions may play an active role in the combustion process. Lewis[47] studied the effect of an electric field on hydrocarbon/air flames. The field was parallel to the flow direction. He found that the flame moved in the direction of positive ion flow and with appropiate field strengths and directions the flame could be extinguished. He concluded that the positive ion plays an important role in the maintenance of flames. Calcote and Pease[48] studied the effects of longitudinal electric fields on the blow off limits, dead space and flame pressure of Bunsen burner flames. They found that the electric field has a strong influence on flame stability, the direction depending on the field polarity. A model based on ionic wind explained most of their results. They concluded that the large number of ions present, $10^{13} cm^{-3}$, cannot be accounted for thermodynamically and must be due to

chemi-ionisation, though the ions did not appear to play a significant role in the combustion process.

Fox[49] found that a continuous glow discharge could increase the blow off velocity of premixed flames. However, no change in burning velocity could be detected on a porous plug burner using propane/air fuel.

Heinsohn et al[50] have found that the extinction limits of an opposed jet diffusion flame are considerably extended by a DC field. They concluded that probable ways in which an electric field can influence a flame are (i) ionic wind, (ii) as a consequence of (i) the concentration of neutral reacting species changes altering the combustion chemistry and (iii) the combustion chemistry may be influenced by the initiation of new reactions.

Guenault and Wheeler[51] and more recently Weinberg et al[1,3] studied the effects of electric fields on flames and concluded that the effects observed were caused by mechanical processes and that the flame chemistry was not altered.

Other workers have studied the effect of electric fields on chemical species in the flame. Nakamura[52] found that electric fields affect the CH, C_2 and OH spectra of diffusion flames. They concluded that the field did not affect the flame propagation, the concentration changes being caused by mechanical effects, but that ionisation and carbon formation are connected.

Popov and Shelkin[53] carried out a spectroscopic investigation of a flat methane/air flame in an electric field. They analysed for C_2 and CH and found that the concentration profile for each species was independent of field. They observed some macroscopic changes in flame structure but concluded that these could all be attributed to the ionic wind effect.

These papers lead to the conclusion that radicals, the species involved in the flame propagation reaction, are not affected by the electric field, by other than mechanical means, although the ion concentrations are. Hence the ions play little or no part in any propagation or chain branching reactions.

Heinsohn et al[54] studied the temperature distribution in a propane/air counterflow diffusion flame subjected to an electric field. They found that the temperature profile shifted towards the cathode on applying the field - in accordance with the wind effect. They also deduced that the flame volume increased but did not draw any conclusions about any changes in concentration in combustion species.

However, many workers have concluded from their experimental results and theoretical calculations that an electric field has a marked effect on burning velocity and hence flame chemistry. Bone et al[55] found that flame speeds were affected by electric fields. They concluded that both mechanical and chemical effects were responsible for this. Calcote[56] experimented with transverse electric fields on burner stabilised flames and observed mechanical effects.

He also deduced changes in the burning velocity across the flame; an increase near the positive electrode and a decrease near the negative electrode. He considered this was caused by changes in positive ion concentration caused by the field.

Fowler and Corrigan[57] measured flame speeds in tubes under the influence of transverse DC and AC electric fields. They found considerable increases in flame speed 50% for 60Hz AC fields and 100% for DC fields. They concluded that the field affected the electron temperature and hence the reaction rate. Becker[58] suggested that from calculations on one dimensional flames the burning velocity of methane/air should increase by 20% on application of a field. Jaggers and von Engel[59] studied effects of DC, AC and HF electric fields on flames in tubes and on floating flames. Fuels used were methane/air and ethylene/air. They deduced appreciable increases in burning velocity up to 20% in the case of methane/air; this was attributed to an increase in the electron temperature caused by the field.

In the case of sooting flames the chemistry of carbon formation is altered, though this is caused by a mechanical effect on the particles rather than being caused by electrons. No conclusions have been drawn about the effect on the flame propagation reactions. Place and Weinberg[5] found that application of fields to sooting flames on a counterflow diffusion burner can markedly affect the growth of carbon in the pyrolysis zone. More recently Mayo and Weinberg[2] extended this to showing that the effect is a mechanical one. Results can be explained by postulating that the field either

removes or traps the particles in the pyrolysis zone hence affecting their growth there.

Many of the early workers supposed that the striking effects that electric fields exert on flames were caused by chemical changes induced by transposing the charge carriers, particularly electrons. Some reactions involving large charge carriers are known to be so affected. Thus the effect on flame carbon formation of moving the charged soot particles by applied fields is well documented. However, the influences of transposing small charge carriers are less easy to investigate.

Many of the effects of fields on flames are known to be due to ionic winds, this was suggested already by Guenault and Wheeler[51]. It is strictly to be expected, since gas velocities produced in this way can attain values as high as 550 cm s^{-1} under ideal conditions [1,41], more in ducted[64] and in multi-stage[87] systems, and are usually several times greater than burning velocities of hydrocarbon/air mixtures, even under far from ideal conditions. Such gas flows are accompanied by entrainment which, in particular systems, can lead to appreciable changes in mixture composition. It is also not symmetrical as regards polarity, if charge carriers of different mobilities are involved in the two electrode spaces, eg. electrons - ions, ions - charged particles. The theory of these processes has been fully analysed[41], the behaviour of practical systems being quantitatively predictable in the case of simple geometries and approximately so for less tractable conditions. This has made it possible to explain effects which had previously been suspected to be chemical

in origin in terms of the fluid-mechanical consequences of forces acting on charge carriers. Thus effects observed[88] only when the flame exhibited a well defined Swan, C_2, spectrum, or showed the onset of sooting, could be explained[41] in terms of the above mentioned asymmetry of the wind effect occasioned by positively charged carbon particles.
Similarly a variety of intricate observations regarding flame stability[48] could be described[41] in terms of electron-ion asymmetries modified by electron attachment over appreciable path lengths in cold gas. None of this of course proves the absence of chemical effects nor does the smallness of the proportion of molecules ionised in flames do so.
At best it has been shown that the ion-driven fluid-mechanical effects, which are inevitably present and quantitatively calculable, account for experimental observations in many cases.

It was decided to measure burning velocities of sooting flames to try to determine whether the reaction leading to to carbon formation was separate from the propagation reactions. Because of the conflicting background to work on non-sooting premixed flames it was decided to carry out some burning velocity measurements on these first.

3.2 EFFECT OF ELECTRIC FIELDS ON THE BURNING VELOCITY OF NON-SOOTING FLAMES

3.2.1 EXPERIMENTAL

It was considered essential to obtain a direct measure of burning velocity rather than attempt to deduce it from any flame speed measurements for it is very difficult to deduce accurate burning velocities from these even in the absence of electric fields. The additional complications produced by an electric field are formidable and perhaps subtle. The changes in flame shape produced by the ionic wind depend strongly[41] on the flame - electrode separation, this may change during the course of the experiment. It also depends on the mobility of the ion which may be different on either side of the flame. Complex circulation, mixing and entrainment patterns can occur close to the electrodes, where the ionic wind velocity is highest[41].

Fortunately it is possible, by combining several recent techniques, to measure burning velocity directly and with great accuracy. The measurements were carried out using a porous plug burner[60]. This was originally designed to measure the burning velocities of freely propagating flat flames as the flow velocity at which the heat loss to the burner would extrapolate to zero. At that point the final flame temperature would reach its adiabatic value - ie. would cease to rise with increasing flow velocity. It became obvious from the very first measurements of saturation current in this type of system[51] that this is probably the most sensitive method available for monitoring flame temperature;

an increase in saturation current density by a factor of 2-4 for an increase of 100°K in final flame temperature being usual for hydrocarbon/air mixtures. This variation has since been considered in greater detail in terms of activation energies for a variety of mixtures, flames and conditions[25,35]. It has been pointed out [61,62] that this type of measurement provides a potentially very accurate method of measuring burning velocity, in principle. The work at Louvain was based on measuring the potential at which saturation set in and plotting this against gas flow velocity, see Fig. 3.1, but the consequences are similar.

Thus saturation current can be used to identify the onset of free flame propagation, when flow velocity becomes equal to burning velocity, with great precision. This provided an ideal method of checking whether field intensity and direction can alter the burning velocity because the saturation current can be attained for a wide range of field intensities in the flame and in both directions, ie. electrons can be confined to traverse reactants only or products only. The accuracy of measuring saturation current and the steepness of its dependence on temperature is such that the accuracy of burning velocity measurement by this method is determinded solely by the errors of flow metering. In view of the very real inaccuracies in the latter there is indeed no important loss in precision when some less sensitive method of monitoring the final flame temperature is used. Thus a thermocouple was used when it was desired to repeat the measurement of burning velocity in the total absence of any field - in order to ensure that no electrical perturbation

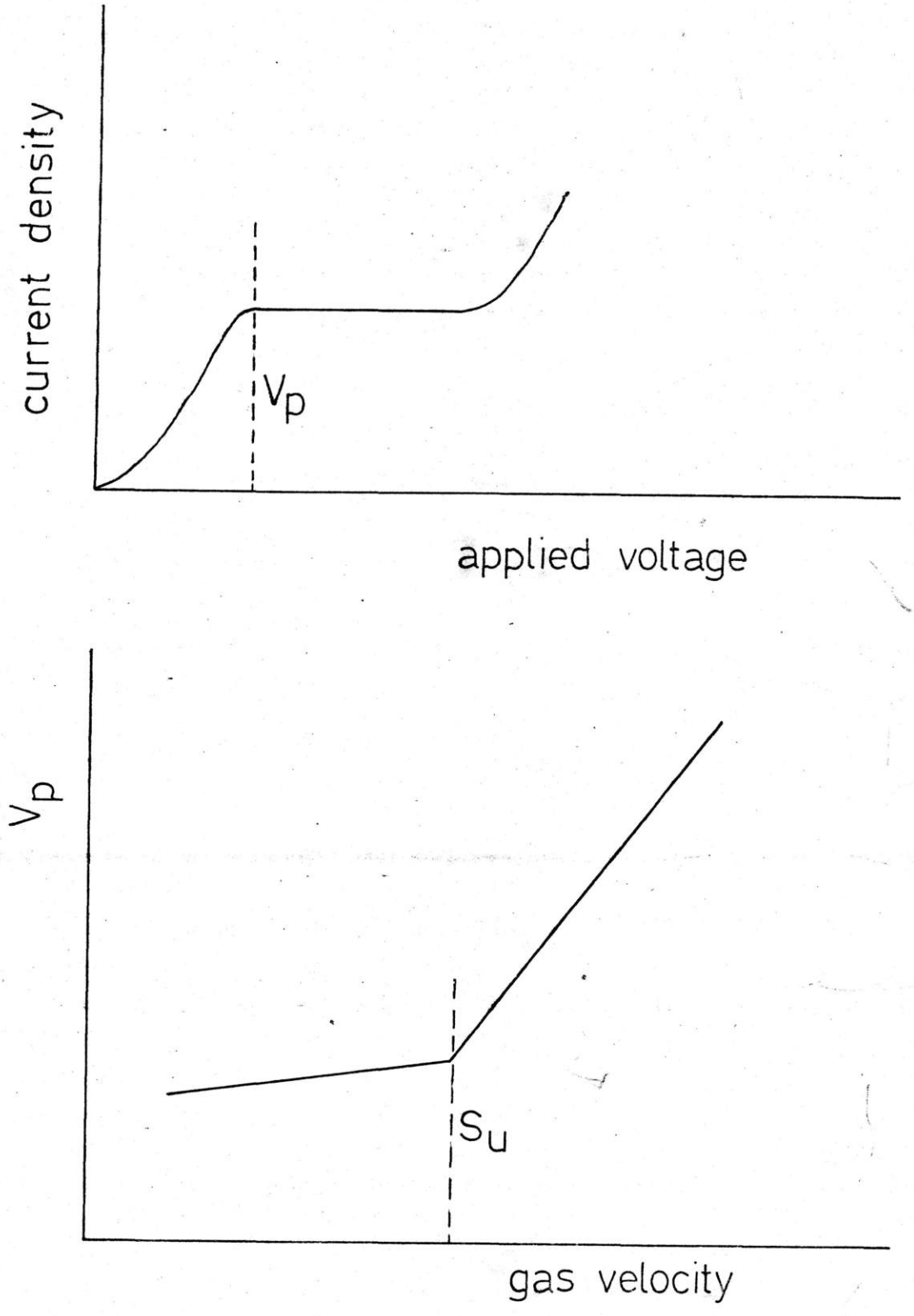

Fig. 3.1 Method for measuring burning velocity used at Louvain

whatsoever could occur. For this purpose the thermocouple was used solely as an 'end-point indicator' which established only the flow velocity at which the flame temperature ceased to increase with flow velocity. Hence no thermocouple calibration, correction for radiation or for convection, etc., is necessary. The only precaution required was to place the junction far enough downstream for it to be unaffected by the temperature distribution within the flame's structure, so that the reading remained unaltered by the small changes in the flame's position as its upstream boundary moved in and out of the porous disc.

The apparatus is illustrated in Fig. 3.2. When using saturation current as the indicator of zero heat loss to the burner, it was found most convenient to plot saturation current against flow velocity, keeping the applied potential high enough to ensure saturation under all experimental conditions, yet not so high as to induce secondary ionisation. This regime is most easily established in advance from current-potential curves such as that shown in Fig. 3.3. This was not possible with some burner-electrode configurations and so an XY plotter was used to obtain current-voltage plots at different flow rates. The circuit used is shown in Fig. 3.4. Once the flame detaches from the porous plug burner and becomes freely stabilised by propagation against the gas stream, at a velocity S_u, the flame temperature becomes constant and the rate of increase of the saturation current suddenly decreases. It does not fall to zero because beyond this point the flame area, S, commences to increase with volume flow, V_f, according to

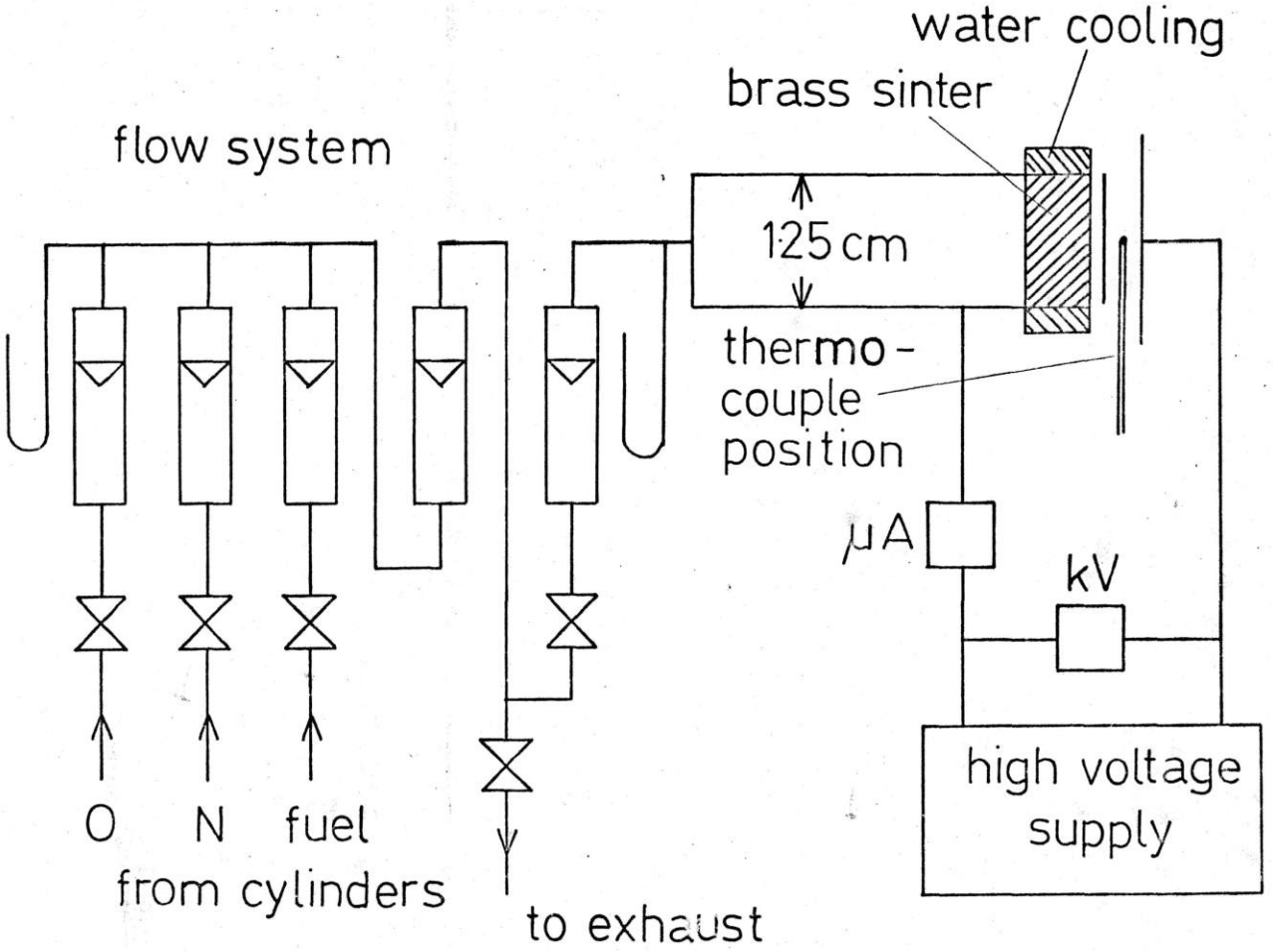

Fig. 3.2 Experimental system for burning velocity measurements

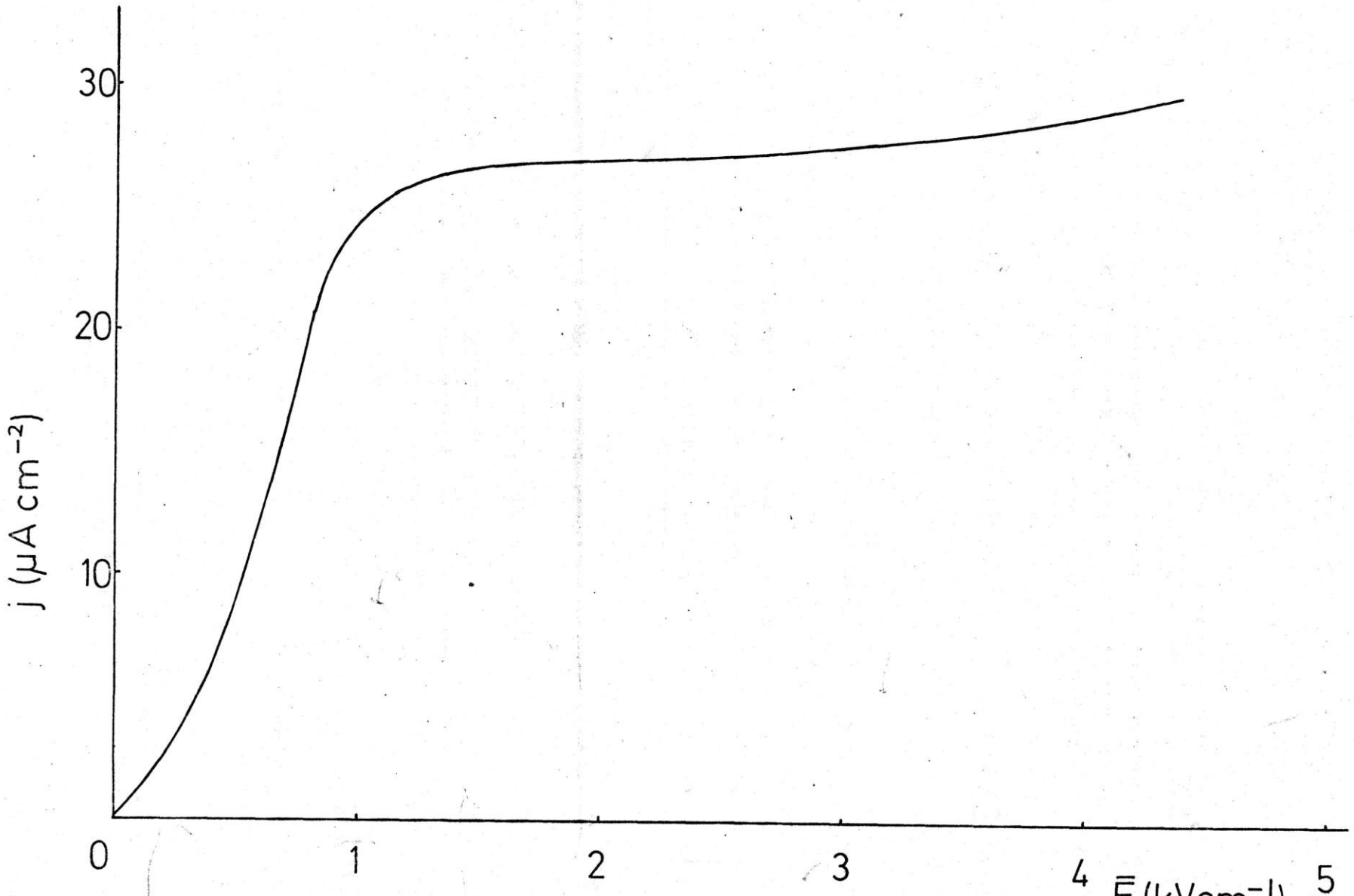

Fig. 3.3 Typical saturation current plot

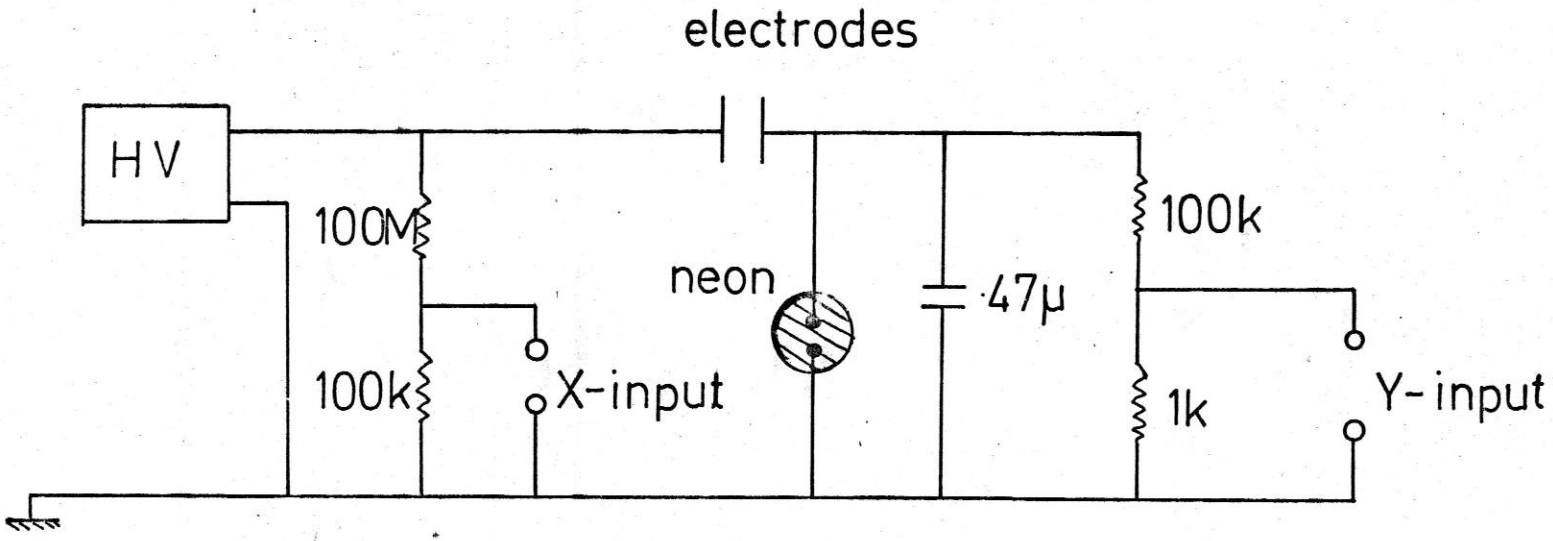

Fig. 3·4 Circuit for using X-Y plotter to draw current-voltage characteristics of flames

$$S = \frac{V_f}{S_u} .$$

This relationship has been fully verified in terms of saturation current[63]. The burning velocity can be read off accurately from the intersection of the two graphs, see Fig. 3.5.

Thermocouple readings also manifest a gradual rise beyond the point of free stabilisation. This is caused by an increase in convective heat transfer to the thermocouple as the flow velocity increases. The relationship between the Nussult and Reynolds numbers was used for interpolation.

$$N_u = \frac{hy}{k_{th}} = DRe^B$$

$$\therefore \quad \frac{hy}{k_{th}} = D\left\{\frac{\rho vy}{\eta}\right\}^B$$

Heat gained by convection = Heat lost by radiation

$$\therefore \quad c\sigma T_s^4 = c_1 h(T_g - T_s)$$

$$\therefore \quad \frac{T_s^4}{T_g - T_s} = \frac{k_{th} c_2}{y\sigma}\left\{\frac{\rho y}{\eta}\right\}^B v^B$$

$$\frac{T_{s'}^4 (T_g - T_{s''})}{T_{s''}^4 (T_g - T_{s'})} = \left\{\frac{v_{'}}{v_{''}}\right\}^B$$

Now $T_{s'} \approx T_{s''}$

$$\frac{T_{s'}}{T_{s''}} = \left\{\frac{v_{'}}{v_{''}}\right\}^{B/4}$$

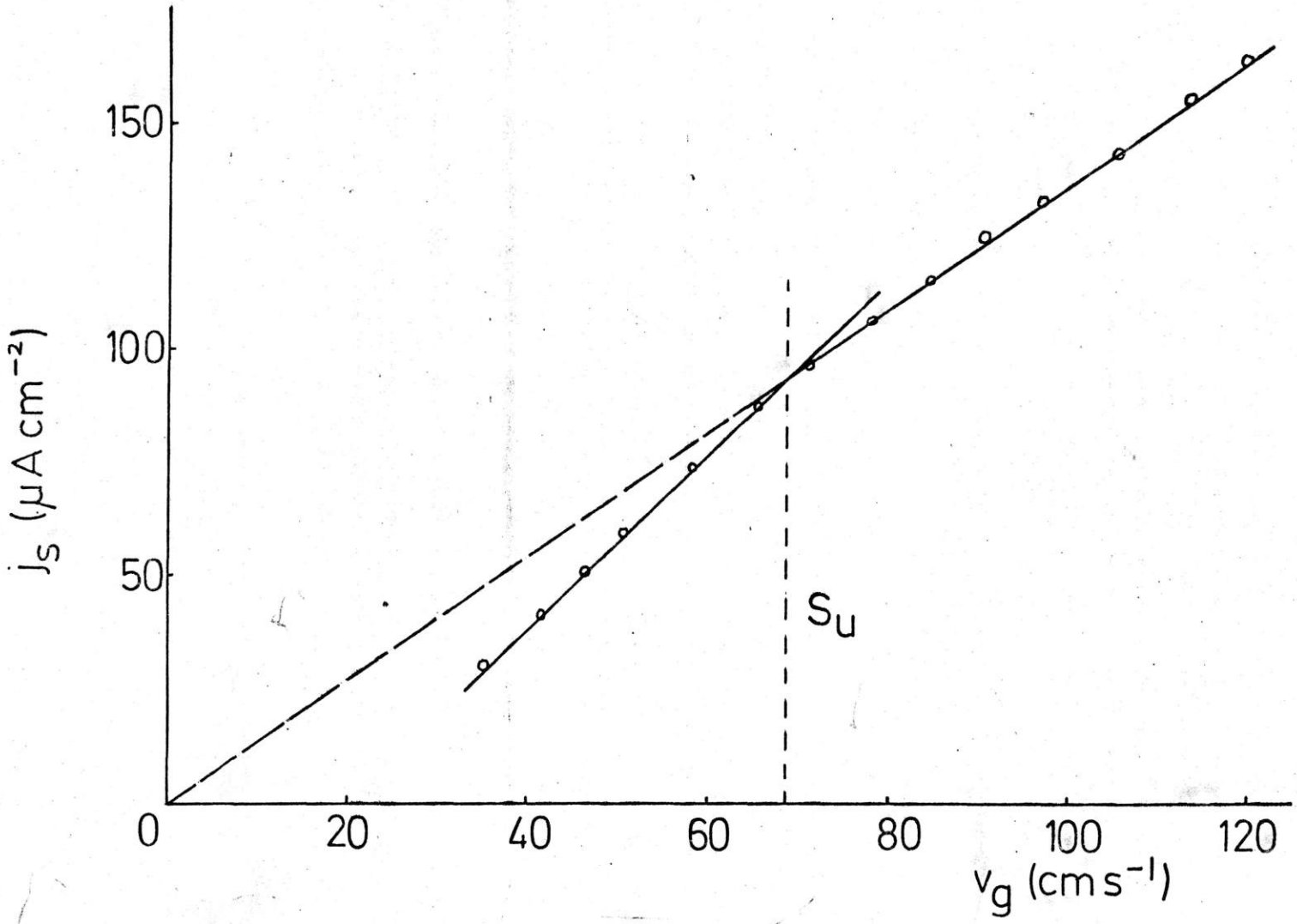

Fig. 3.5 Saturation current density - gas velocity

This relationship was used to extrapolate the gentle temperature rise at high flow velocities to lower velocities below the burning velocity, see Fig. 3.6. The burning velocity was read off as the intersection.

The intensity of the field in the flame was altered by varying the separation between the electrodes, and the field direction reversed by interchanging their polarity. When the burner is positive, the range of saturation potentials is less extensive, due to the earlier onset of breakdown caused by space charge as the more distant electrode collects the larger positive ions on the hot side[64].

The total gas flows used were as follows:-

Ethylene - nitrogen - oxygen flames,

N_2	$101{\cdot}5 \pm {\cdot}5$ cm^3s^{-1}
O_2	$26{\cdot}0 \pm {\cdot}3$
C_2H_4	$8{\cdot}7 \pm {\cdot}1$

Thus stoichiometry defined as $\dfrac{(C_2H_4/O_2)_{actual}}{(C_2H_4/O_2)_{stoich}}$

$= 1{\cdot}01 \pm {\cdot}03$

Ethane - nitrogen - oxygen flames,

N_2	$101{\cdot}5 \pm {\cdot}5$ cm^3s^{-1}
O_2	$26{\cdot}0 \pm {\cdot}3$
C_2H_6	$7{\cdot}8 \pm {\cdot}1$

Giving a $1{\cdot}01 \pm {\cdot}03$ stoichiometric flame.

In each case $\dfrac{[O_2]}{[O_2]+[N_2]}$ was $\cdot 204 \pm \cdot 004$ compared with air at $\cdot 212$.

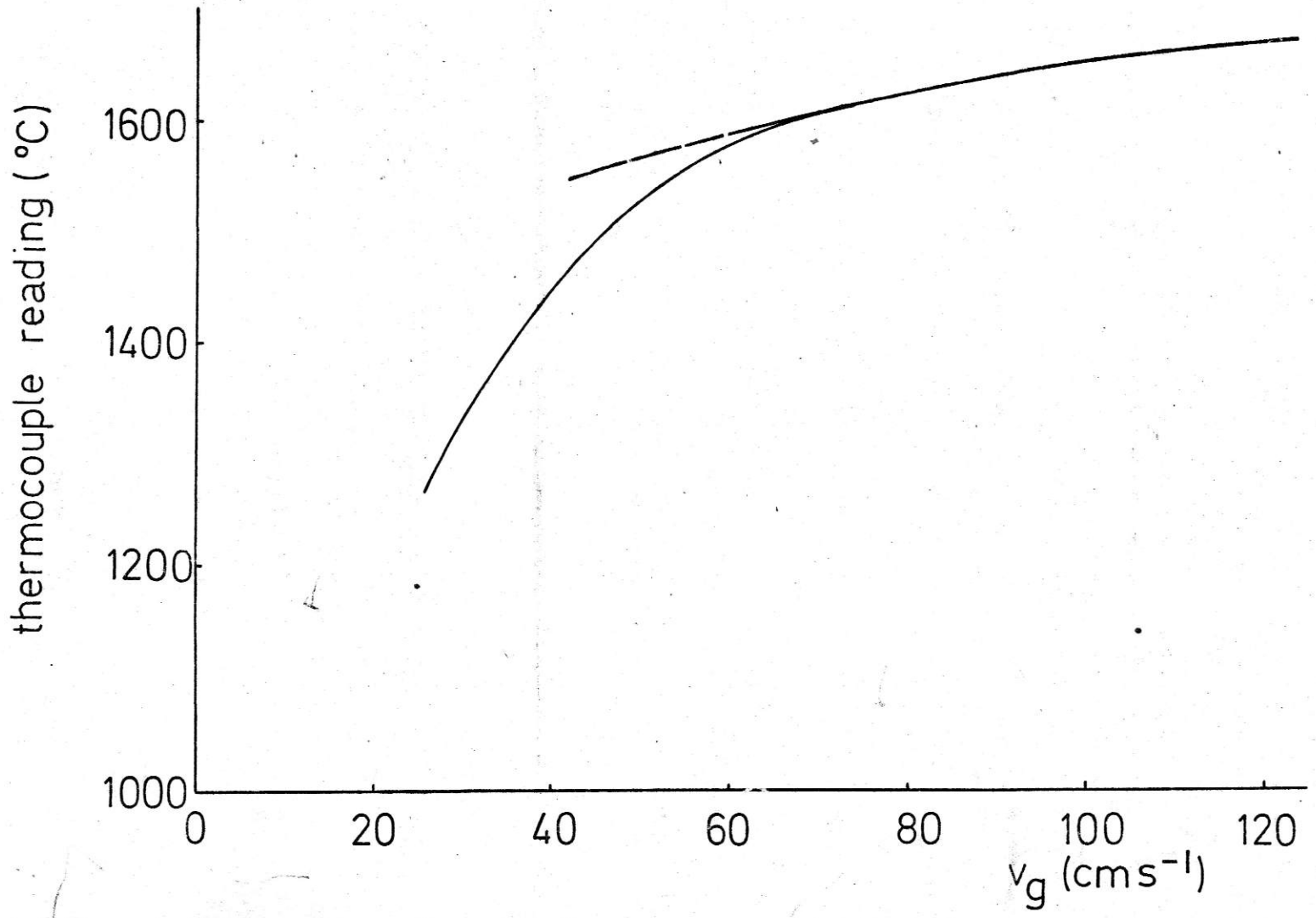

Fig. 3.6 Thermocouple reading - gas velocity

The area of the flame stabilised just below the burning velocity was measured photographically and the value of $1{\cdot}255 \pm {\cdot}025$ cm^2 was used to calculate the burning velocities.

The measured burning velocities of ethylene/air and ethane/air flames plotted against potential are shown in Fig. 3.7. Mean values for ethylene/air are:

burner negative	69·1 cm s^{-1}	rms deviation	2·0
burner positive	66·2		1·5
averaged together	67·9		2·3
no field	67·9		1·6

For ethane/air these are:

burner negative	41·7 cm s^{-1}	rms deviation	2·2
burner positive	41·4		1·0
averaged together	41·6		1·9
no field	41·2		1·7

The error in measurement estimated on the basis of the least change legible on the flow meters is $\pm$ 1·9 cm s^{-1} in each case. To this accuracy, there is no detectable effect on burning velocity of varying the applied potential from 1 to 15kV, under saturation conditions (field intensity 2·2 - 6·0kV cm^{-1}). There may be a slight, 4%, difference between the two field directions for ethylene. Values deduced by thermocouple in the absence of any field fall within 4% of the mean for ethylene and 1% for ethane. If the difference between positive and negative fields in the case of ethylene is real (it is only just above the standard deviation and would not have been noticed, even by this method, had not the two sets of results been averaged

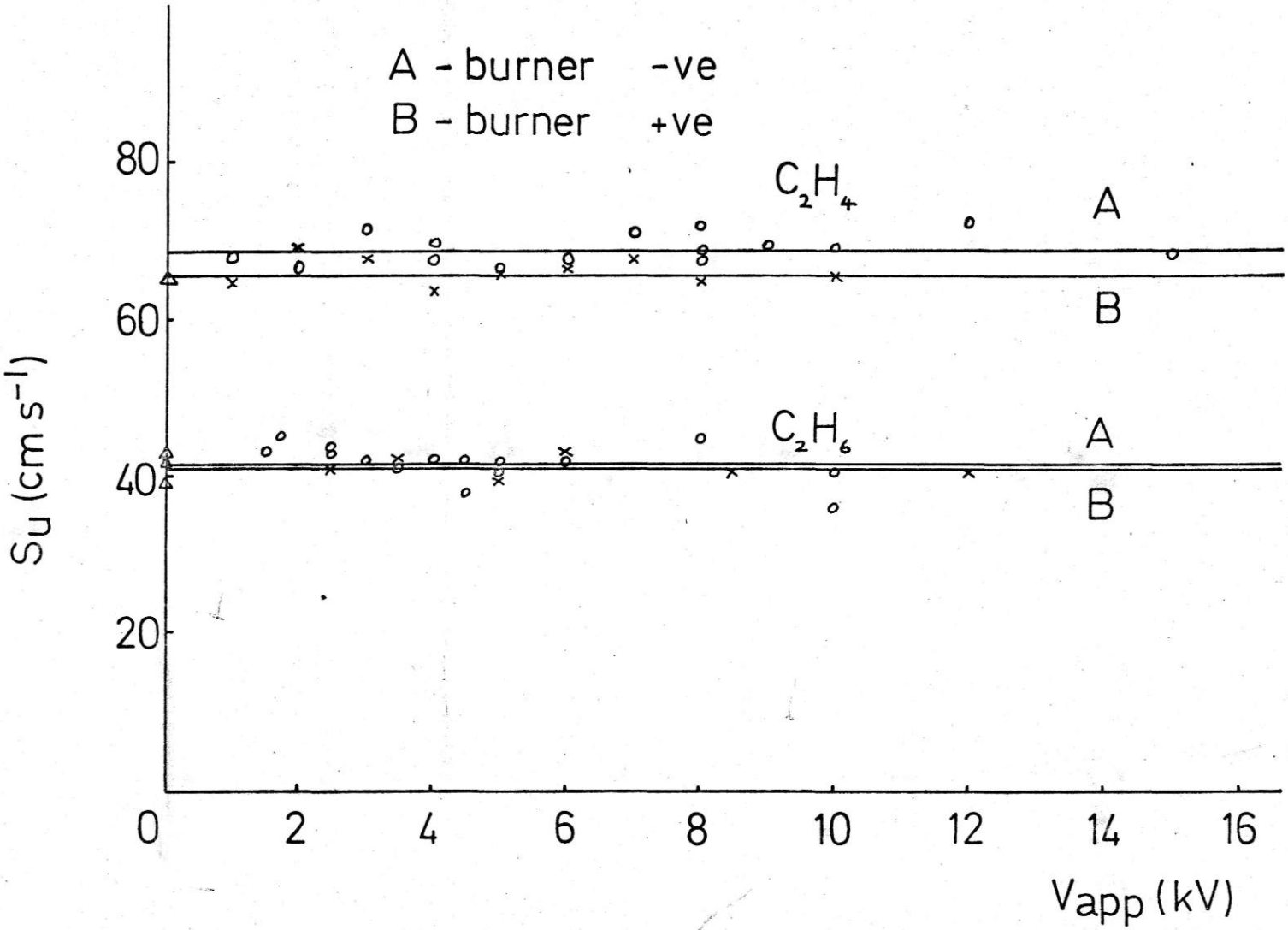

Fig. 3·7 Burning velocities of hydrocarbon / air flames - applied potential

separately) it causes the burning velocity to be greater when electrons are driven into the burnt products and removed from the reaction zone.

Results obtained for methane/air mixtures are similar:

burner negative 30·6 cm s^{-1}

burner positive 29·9

The figures are less accurate than for ethylene or ethane and more difficult to reproduce because of flame instability on the small burner used leading to large current fluctuations.

Burning velocity measurements were also carried out on ethylene/air and ethane/air flames with radio frequency fields applied. The thermocouple method was used for simplicity. The apparatus used is that shown in Fig. 3.2, the high voltage supply was replaced by an RF generator giving a field strength of 1kV rms cm^{-1} at 6MHz.

Values obtained for the ethylene/air and ethane/air mixtures used were as follows:

C_2H_4/air	68·5 cm s^{-1}	rms deviation	·4
C_2H_6/air	42·0		.3

3.2.2 DISCUSSION

It emerges that if there is a real difference between burning velocities under conditions of zero field, fields of the two opposing polarities and AC fields it is very small - less than 4% in the largest case - and could, in all probability, not have been detected by any pre-existing method of

measuring burning velocity. What difference there is, would suggest that a flux through the reactants of positive ions, rather than electrons, is conducive to increasing reaction rate. Under saturation conditions, with the burner negative, no electron could ever reach the cold side.

Allowing for the possibility that mechanical or thermal effects could account for what little difference there is, the most obvious mechanisms which come to mind are divergence of flow-lines due to the 'ionic wind' back pressure and the increased thermal conductivity due to the additional drift velocity of the positive ions. The latter quantity may be calculated:

Number of hot ions drifting back to burner/second

$$= \frac{j}{e} = \frac{j}{Ne} \text{ mole } s^{-1} \text{ hot gas}$$

Heat lost by ions = Heat gained by cold gas

$$\frac{j}{Ne} \overline{c}_p (T_p - T) = \frac{V_f c_p}{22{\cdot}4} (T - T_r)$$

Hence T, the raised temperature of the reactants may be calculated. With a current of 130 μA and assuming a final flame temperature of 2375°K $(T - T_r)/T$ is estimated as 5 ppm. This quantity is clearly negligable. As regards the former, one of the chief merits of this burner system is, of course, that it minimises these wind effects by the small distance (of the order of the quenching distance) between the negative electrode and the ion source, as well as opposing its force directly by the metered gas flow. However, a change in radius of the stream tube of only 2% would suffice to produce

an area change equivalent to that in burning velocity.

This effect was tested for optically, because of the high sensitivity required, double exposure laser interferometry[65] was used, the optical system is shown in Fig. 3.8. The presence of such a small effect is shown in the photographs in Fig. 3.9a,b and c.

Fig. 3.9a is with no applied field and shows isotherms in the plume of hot products. The interferogram, Fig. 3.9b, with burner negative shows a wider plume. This could be a result of increased flame area due to ionic wind resulting in a measured increase in burning velocity. The wider plume also shows that there is increased recirculation at the edge of the burner due to ionic wind. This would have the effect of increasing heat transfer to the burner leading to a small increase in burning velocity. Fig. 3.9c is an interferogram taken with the burner positive. The plume is narrower, possibly caused by a decrease in flame area lowering the measured burning velocity. The narrowing is probably a result of the ionic wind entraining cold air into the flame, cooling the flame and hence lowering the burning velocity.

The conclusions are that any change in burning velocity caused by DC or RF electric fields is less than 4% and can be explained by mechanical and thermal effects. However, this does not rule out any chemical effects; a change in the final flame temperature of only 1% could account for the results.

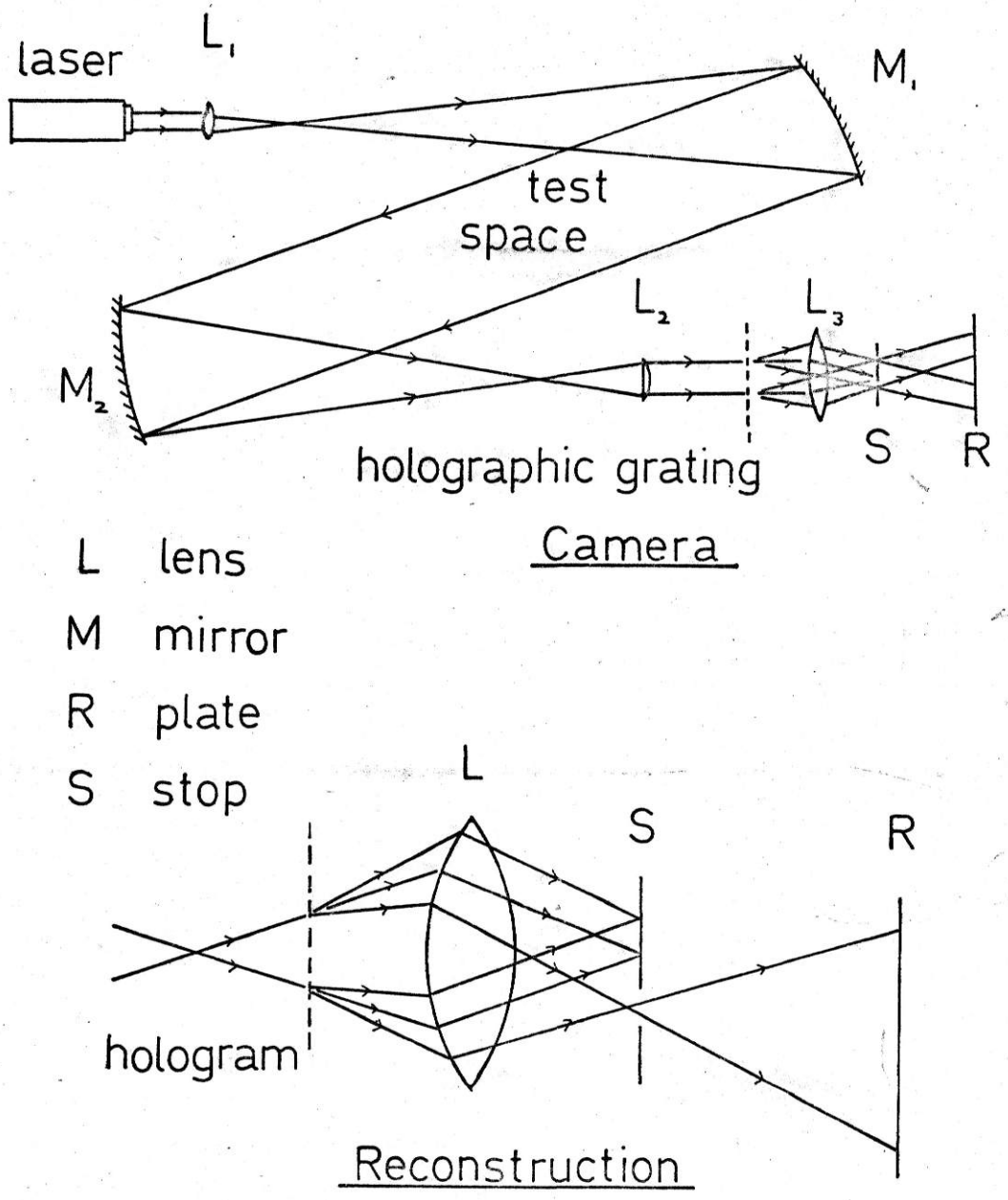

Fig. 3·8 Optical system for making and reconstructing holograms for laser interferometry

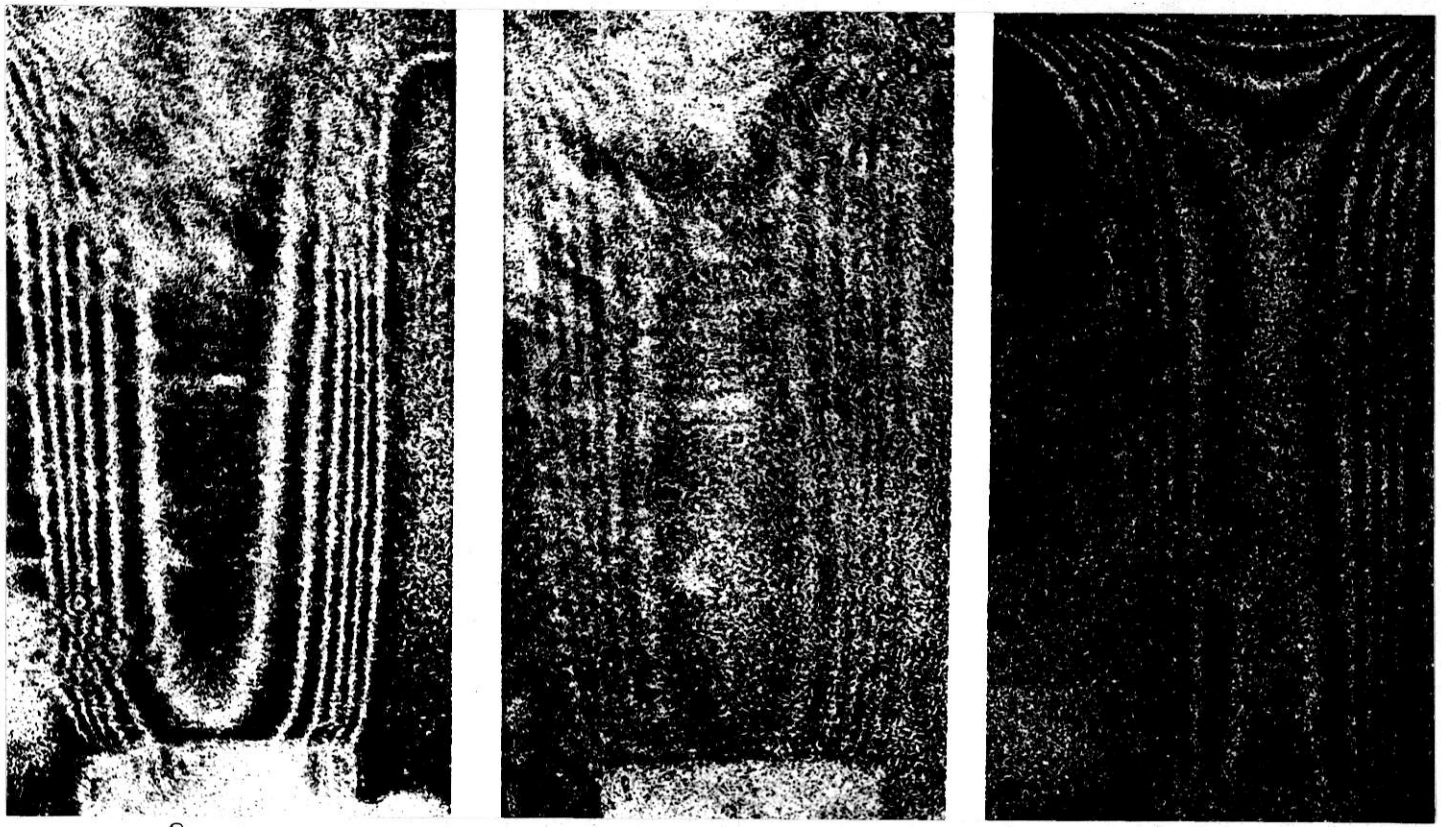

Fig. 3.9 Interferograms of flame a) no field, b) burner negative, c) burner positive.

3.3 EFFECT OF DC ELECTRIC FIELDS ON THE BURNING VELOCITY OF SOOTING FLAMES

3.3.1 EXPERIMENTAL

The apparatus and method described in section 3.2 was used to measure the burning velocity of sooting flames under the influence of DC electric fields and under conditions of zero field. The mixtures used to produce sooting flames were as follows:

Nitrogen	52 cm^3 s^{-1}
Oxygen	16
Benzene	2·2
Ethylene	2·8 - 6·6

Hence $\frac{[O_2]}{[O_2]+[N_2]}$ was ·235 compared with air at ·212.

The partial pressure of ethylene was varied to produce a transition from non-sooting to heavily sooting flames. This gave a change in stoichiometry defined as,

$$\frac{(\text{fuel/oxygen})_{\text{actual}}}{(\text{fuel/oxygen})_{\text{stoich}}}$$

from 1·55 to 2·27. The burner gas velocity was varied by bleeding off different amounts of the above mixtures.

An axial ring electrode was used and the burner was made negative to reduce ionic wind effects; this configuration also gave the maximum effect on non-sooting flames, see section 3.2. An X-Y plotter was used to measure the saturation currents. Evidence of turbulence and aeration, caused by ionic wind, was especially noticeable with heavily sooting flames. This showed as an increase in the saturation

current with voltage and can be seen in Fig. 3.10. Values of saturation current were chosen from the X-Y plotter curves so that saturation had occured with little turbulence. These corresponded to field strengths from ·4 to ·8 kV cm^{-1}, going from sooting to non-sooting flames. The burning velocities obtained are plotted against total ethylene flow rate in Fig. 3.11.

3.3.2 DISCUSSION

As the mixture became fuel rich the burning velocity decreased. This is to be expected and may be compared with the burning velocities of ethylene/air flames for varying stoichiometry as shown in Fig. 3.12[86].

The results with an applied field are more scattered than the thermocouple results, this can be attributed to ionic wind effects which are much greater when particulates are present. The velocities obtained with an applied field may be 10% lower than those without, though this could be explained by scatter in the results.

Hence electric fields have little effect, less than 10%, on the flame propagation reaction in sooting flames and it may be concluded that the fields applied to manipulate flame carbon will not do so by altering the kinetics of propagation.

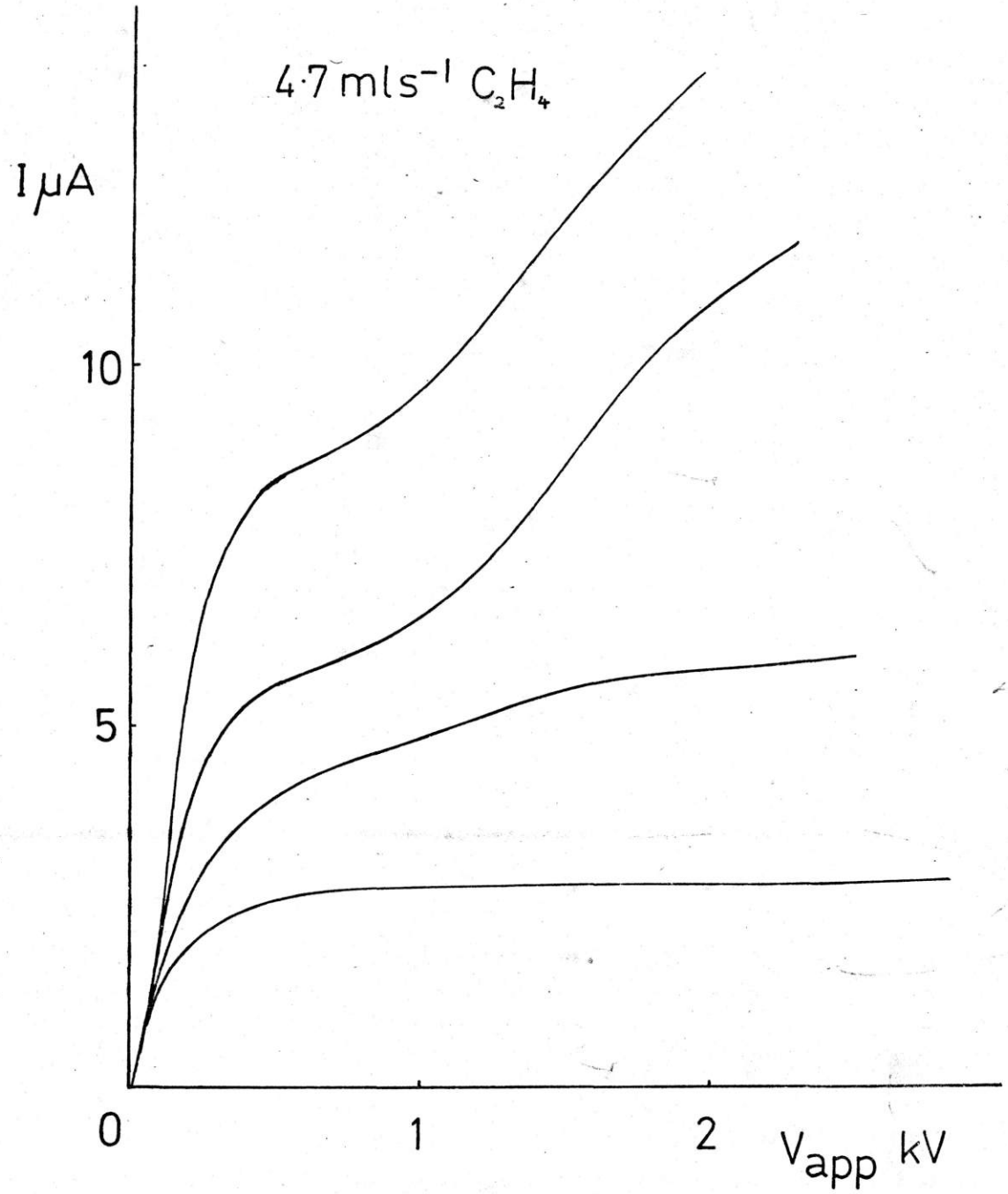

Fig. 3·10 Current-voltage plots for a sooting flame at various flow rates

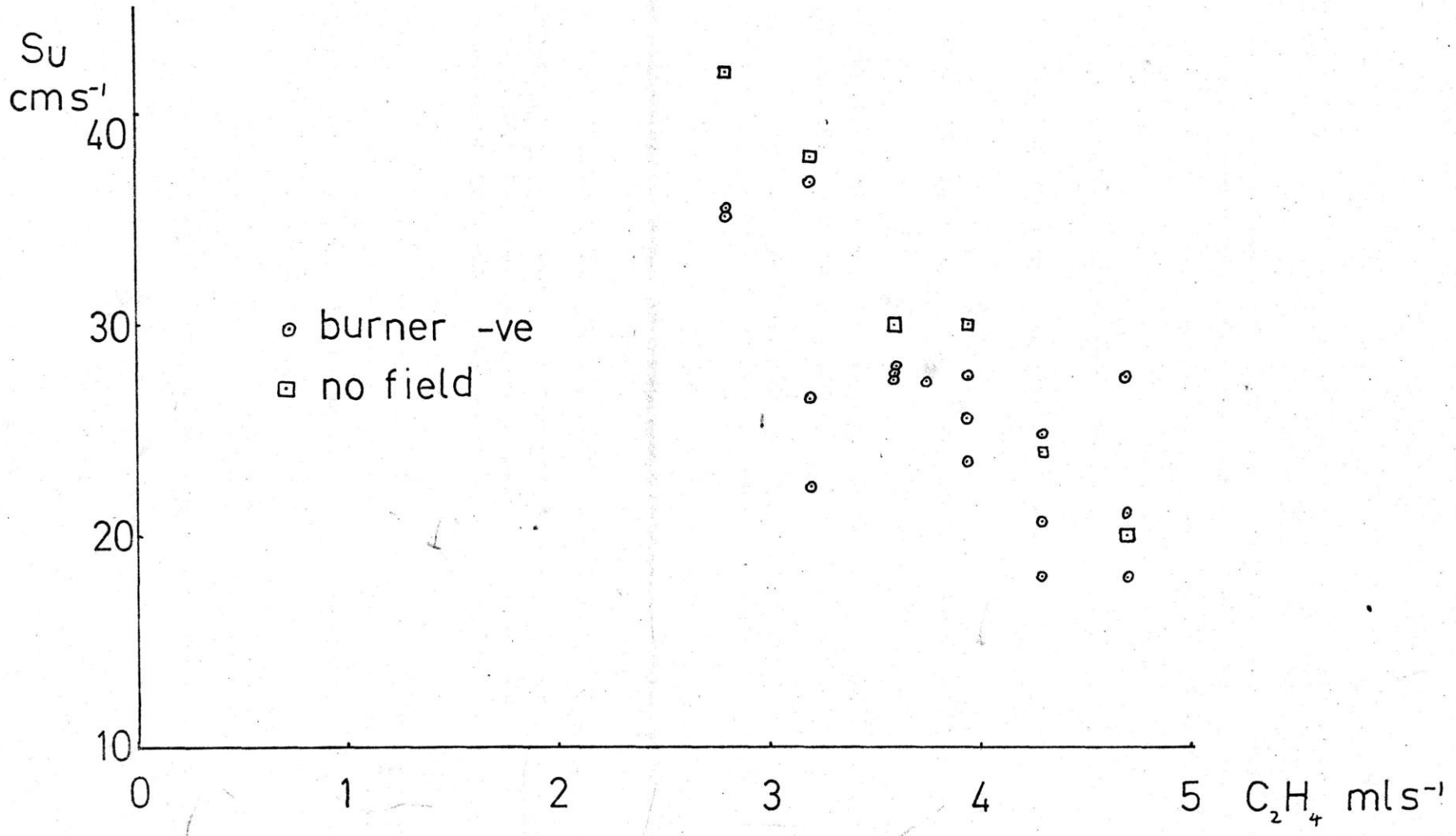

Fig. 3.11 Burning velocities for sooting flames

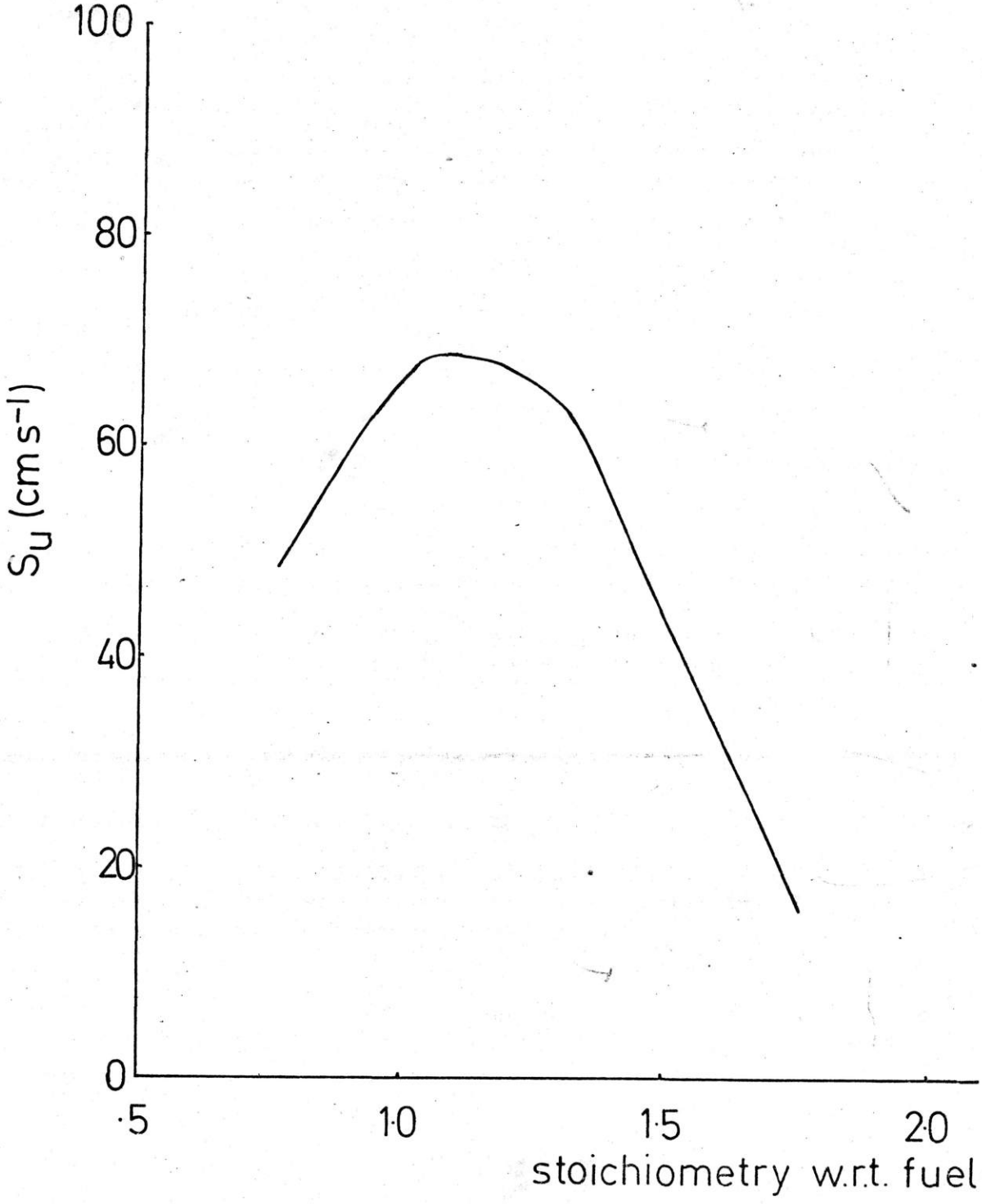

Fig. 3·12 Burning velocities of ethylene/air flames - stoichiometry

3.4 THE EFFECT OF FAST ELECTRONS ON BURNING VELOCITY

The experiments described in section 3.2 may not show any changes in burning velocity caused by fast electrons because of the impossibility of obtaining large fields in an ion source. To overcome this difficulty the experiment was repeated using a flame having a similar propagation reaction to ethylene and ethane but producing no chemi-ions. A separate hydrocarbon flame was used as the source of electrons to be driven into the non-ionising flame. In this way the electrons were able to arrive at a high velocity in an appreciable field.

3.4.1 EXPERIMENTAL

The apparatus and method described in section 3.2 was used to measure the burning velocity of hydrogen/oxygen/argon flames under the influence of DC electric fields. The change in flame temperature was monitored with a thermocouple. A second flame of propane/oxygen/argon was used as a source of electrons.

The gas mixture used was as follows:

Argon	125·7 cm^3 s^{-1}
Oxygen	15·1
Hydrogen	24·7

giving a stoichiometry defined as:

$$\frac{(\text{fuel/oxygen})_{\text{actual}}}{(\text{fuel/oxygen})_{\text{stoich}}}$$

of ·82. The burner gas velocity was varied by bleeding

off different amounts of this mixture.

The apparatus is shown in Fig. 3.13. The hydrogen burner was made positive to drive electrons from the propane flame into the hydrogen flame. Argon was used as a diluent in preference to nitrogen because of the high probability of nitrogen combining with free electrons giving negative ions[66].

Measurements were carried out at zero field and at field strengths of 250, 350 and 500 V cm^{-1}.

3.4.2 DISCUSSION

The results obtained are as follows:-

Field V cm^{-1}	0	250	350	500
S_u cm s^{-1}	72 ± 4	71 ± 4	71 ± 4	$74{\cdot}5\pm4$

Hence within the experimental error fast electrons have no effect on burning velocity in the case considered. This is to be expected as electrons have a high mobility and so their effective concentration would almost be reduced to zero in this case. A more conclusive experiment would be to use an HF AC field with a small DC component superimposed to excite and hold the electrons in the pre-reaction zone of the pre-mixed flame.

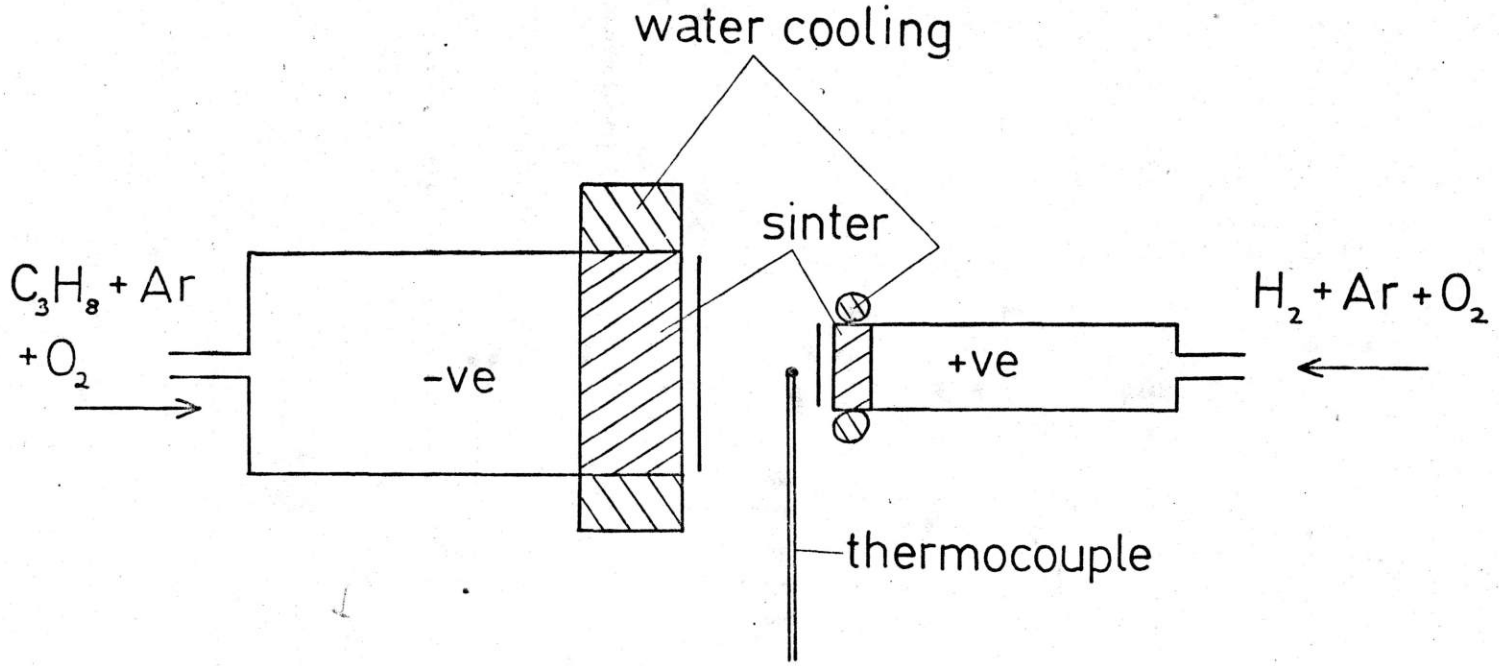

Fig. 3.13 Apparatus to determine the effect of electrons on burning velocity

CHAPTER 4

THE ELECTRICAL CONTROL OF FLAME CARBON IN PRODUCTS

4.1 THE THEORY OF APPLYING A FIELD TO AN ION SOURCE

4.1.1 THE SIGNIFICANCE OF CURRENT DENSITY

The current flowing across unit area parallel to the electrode is by far the most important parameter in calculating the magnitude of all practical effects and, in addition, its measurement provides a valuable tool for the study of the fundamental ionisation processes in the flame. In phenomena involving the transport of ions, knowledge of the ionic mass alone is required to convert maximum current densities into maximum rates of mass deposition or flow.

The current density is given by,

$$j = en_{i\pm}k_{\pm}X \qquad \ldots\ldots\ldots 4.1$$

where k is the ionic mobility and the field does not exceed about 3×10^4 V cm^{-1} times the pressure in atmospheres.

4.1.2 THE FACTORS LIMITING CURRENT DENSITY

Two entirely different limitations apply, either of which could, in principle, determine the absolute maximum. The first occurs in the flame and is due to the finite rate at which charge is generated. The second occurs in the electrode regions, is due to space charge and is largely independent of the nature of the ion source.

In considering the former, it will be convenient to think of a single plane reaction zone situated between parallel

plane electrodes. This model can be reproduced in practice by using a suitable flat flame burner. For usual fuels, excepting pure hydrogen, the rate of ion generation in the reaction zone is so much greater than any thermal ionisation that the latter may be disregarded. In the absence of a field the ion concentration reaches an equilibrium value when the rate of ion generation equals that of recombination. Various methods have been used to determine concentrations (see, for example, Poncelet, Berendsen and van Tiggelen[68]; Kinbara, Nakamura and Ikegami[69]; Padley and Sugden[70]; Bulewicz and Padley[71]). As soon as a field is applied, the equilibrium concentration is modified because charge removal by the field is now added to recombination, whilst the rate of generation, being a flame parameter, remains in each zone a property of the reactant mixture alone.

As the applied field is increased, the ion current rises at the expense of recombination. This trend continues until the current reaches a maximum value characteristic of each particular flame. Further increases in electrode potential produce no further increases in current so long as no secondary ionisation occurs. This maximum current is termed the saturation current and its value per unit area the saturation current density, j_s. In the case of a single thin reaction zone which is plane and parallel to the electrodes, it is obvious that the failure of the current to increase for further large increases in field must imply that charges are being removed so fast that they no longer have time to recombine. Thus j_s is equal to the rate of generation of charge per unit area of flame front - a

fundamental property of the reactant mixture.

The second kind of limitation to current sets in when the field strength becomes so large that ion energies are sufficient to cause secondary ionisation by collision with other species. It differs from the first in that, beyond it, the ion current once more increases with increasing applied potential. This increase, however, is not a useful one within the present frame of reference. The main reason is that the secondary ions do not derive from the flame - the phenomenon acquires the characteristics of an electric discharge and the secondary ions, moreover, tend to neutralise those from the reaction zone in the counterflow regions.

The relevant events now occur in the electrode regions. In the presence of space charge, the field strength X is not uniform. Its variation with y, the co-ordinate perpendicular to the planes of the flame and electrodes, is given by Gauss's law

$$\text{div } X = dX_y/dy = 4\,(n_{i+} - n_{i-})e. \quad \ldots\ldots\ldots 4.2$$

It will be shown below that the solution of this equation with that of charge conservation yields a field distribution of the general form shown in Fig. 4.2, which is such that the field strength rises continuously in going from the flame to either electrode and reaches its maximum value at the electrodes. It follows that breakdown occurs first at the electrode or, in the symmetrical case, at both electrodes. Since the distribution of field strength depends only on the current density and the relevant field strength

at breakdown is solely a property of the gas in contact with the electrode(s), this criterion is largely independent of the properties of the ion source. The limiting current density at breakdown, j_b, is simply that j for which the distribution of space charge causes secondary ionisation in the gas at one or both electrodes. This obviously depends on electrode spacing, since space charge continues to increase X over the extent of these regions, unlike j_s, which is a property of the flame alone.

It transpires that this second criterion is the one that ultimately limits all practical maxima. For flames which are such strong ion sources that $j_b < j_s$ for all reasonable electrode configurations, j_b is obviously limiting. For flames which are weak ion sources, $j_s < j_b$, and with electrodes close to the flame the saturation plateau in the current-potential curve may be quite extensive; ie. the difference between the applied potential at which saturation occurs, and that larger value at which secondary ionisation sets in, may be very large. Under these conditions j_s is limiting.

4.1.3 THIN ION SOURCES IN ELECTRIC FIELDS

The development of the theory of field and space charge distribution is therefore a necessary and sufficient preliminary to predicting practical maxima. It is also a necessary preliminary to the measurement of saturation currents, for the following reason. The mean field between the electrodes is always greatly in excess of that in the flame, because of

the effects of space charge discussed above. If breakdown occurs before j_s is attained, ie. if $j_s > j_b$, no saturation current is, of course, measureable. Since j_b and the fraction (field at the flame)/(field at the electrodes) depend on the separations of the two electrodes from the flame, the theory is necessary to calculate how breakdown may be delayed long enough for saturation to be attained first. Without special precautions, saturation currents are attainable with only the weakest ion sources.

The simplest basis on which a representative theory may be developed is the following model. The flame, consisting of a single, plane and infinite reaction zone is held between two parallel, plane and infinite electrodes. It is of a constant thickness within which the rate of ion generation and the coefficient of ion recombination are constant. The 'reaction zone thickness' is thus defined as the thickness of that slab which combines the above properties with the net rate of ion generation of the real flame. This is a convenient basis for discussion rather than a necessary assumption. In the spaces between the flame and the electrodes no charge is generated and no charge is destroyed (because, when a field is applied, only one kind of charge exists in each space). These electrode spaces are usually vastly greater than the reaction zone thickness and that they can never be made smaller than the quenching distance.

Slow ion removal within the reaction zone.

In the absence of a field only recombination rivals ion generation, the effects of convection being negligable,

and the concentrations of negative and positive charges are equal. Thus

$$\frac{dN}{dt} = \alpha n_+ n_- = \alpha n^2 \qquad \ldots\ldots\ldots\ldots\ldots\ldots \quad 4.3$$

or

$$n = \frac{dN}{dt}/\alpha \qquad \ldots\ldots\ldots\ldots\ldots\ldots \quad 4.4$$

Consider now the application of a field so small that this condition is virtually unaltered. By Gauss's law (4.2)

$$dX/dy = 4\pi(n_+ - n_-)e = 0$$

Thus the field is constant, which implies a potential drop proportional to distance, ie.

$$V = V_o + Xy \qquad \ldots\ldots\ldots\ldots\ldots\ldots \quad 4.5$$

The current is given by

$$\begin{aligned} j = enX(k_+ + k_-)n &= eX\left(\frac{dN}{dt}/\alpha\right)^{\frac{1}{2}}(k_+ + k_-) \\ &= \left(e(V - V_o)/y\right)\left(\frac{dN}{dt}/\alpha\right)^{\frac{1}{2}}(k_+ + k_-) \\ &= \text{constant} \times (V - V_o) \qquad \ldots\ldots\ldots \quad 4.6 \end{aligned}$$

Thus, under conditions approaching zero field and zero current, the flame behaves as an ohmic conductor of resistivity $(\alpha/\frac{dN}{dt})^{\frac{1}{2}}/e(k_+ + k_-)$. Since in the flame zone the negative ion appears to be a free electron, k_- is of the order $10^3 k_+$, so that k_+ becomes negligible in the above expressions. If a value of k_- is assumed, the ion concentration under equilibrium conditions (or rather negligible departure from them) can be deduced from resistivity measurements.

Saturation within the reaction zone.

The opposite extreme occurs when the applied potential has just reached a value beyond which the current no longer increases with increasing field. Ion removal by the field

has now become so large as to make recombination negligible by comparison. Thus for positive ions, for instance,

$$\frac{1}{e}\frac{dj_+}{dy} = \frac{dN}{dt} - \alpha n_+ n_- = \frac{dN}{dt} \qquad \ldots\ldots\ldots\ldots \quad 4.7$$

so that j_+ increases linearly across the reaction zone and j_- behaves symmetrically (Fig. 4.1a) because equation 4.7 must apply to either charge. Thus,

$$j_+ = \frac{dN}{dt}ey, \quad j_s = \frac{dN}{dt}eY \quad \text{and} \quad j_- = \frac{dN}{dt}e(Y - y) \qquad \ldots\ldots \quad 4.8$$

However,

$$\left.\begin{aligned} j_+ &= k_+ n_+ Xe \\ \text{and} \qquad j_- &= k_- n_- Xe \end{aligned}\right\} \qquad \ldots\ldots\ldots\ldots\ldots\ldots \quad 4.9$$

so that where j_+ is symmetrical with j_- the two concentration profiles

$$n_+ = \frac{\frac{dN}{dt}y}{Xk_+} \quad \text{and} \quad n_- = \frac{\frac{dN}{dt}(Y - y)}{X k_-} \qquad \ldots\ldots\ldots\ldots \quad 4.10$$

must be entirely different because of the disparity in mobilities. This becomes important in calculating field distribution under the influence of a space charge which is now almost entirely due to positive ions. Thus, substitution into Gauss's law gives

$$\frac{dX}{dy} = \frac{4\pi\frac{dN}{dt}e}{X}\left\{\frac{y}{k_+} - \frac{Y - y}{k_-}\right\}, \qquad \ldots\ldots\ldots\ldots \quad 4.11$$

in which the second term in the brackets is entirely negligible, except where y tends to zero. The contribution of these regions to the integral $X \cdot dX$ is obviously insignificant, so that

$$X^2 = X_o^2 + (4\pi\frac{dN}{dt}e/k_+)y^2 \qquad \ldots\ldots\ldots\ldots\ldots \quad 4.12$$

As long as the field does not exceed saturation conditions,

$$X_o = 0$$

so that

$$X = 2(\pi \frac{dN}{dt} e/k_+)^{\frac{1}{2}} y \qquad \ldots\ldots\ldots\ldots\ldots\ldots \quad 4.13$$

Substitution into equation 4.10 gives the positive ion concentration as

$$n_+ = \tfrac{1}{2}(\frac{dN}{dt}/\pi k_+ e)^{\frac{1}{2}} \qquad \ldots\ldots\ldots\ldots\ldots\ldots \quad 4.14$$

and an electron concentration less than 3% of the above, which has been deemed negligible. The distribution of potential follows from 4.13

$$V = \int_o^y X \, dy = \left(\frac{(\pi \frac{dN}{dt} e}{k_+}\right)^{\frac{1}{2}} y^2 \qquad \ldots\ldots\ldots\ldots\ldots\ldots \quad 4.15$$

the potential drop across the flame being $(\pi \frac{dN}{dt} e/k_+)^{\frac{1}{2}} Y^2$. These results are sketched in Fig. 4.1.

Subsaturation within the reaction zone.

When a field is applied to a flame some ions recombine in the gap while the others are collected at the electrodes. Assuming that the two rates are constant throughout the volume, then

$$(\frac{\partial N}{\partial t})_{\text{generation}} - (\frac{\partial N}{\partial t})_{\text{rec}} - (\frac{\partial N}{\partial t})_j = 0 \ldots. \quad 4.16$$

Now $(\frac{\partial N}{\partial t})_{\text{rec}} = -\alpha n^2$

$j = j_+ + j_- = en(v_+ + v_-) = enX(k_+ + k_-)$

Substituting for n

$$(\frac{\partial N}{\partial t})_{\text{rec}} = -\frac{\alpha j^2}{e^2 X^2 (k_+ + k_-)^2} \qquad \ldots\ldots\ldots\ldots\ldots\ldots \quad 4.17$$

Also $j = ed(\frac{\partial N}{\partial t})_j$ Hence $(\frac{\partial N}{\partial t})_j$

Substituting for $(\frac{\partial N}{\partial t})_j$ and $(\frac{\partial N}{\partial t})_{\text{rec}}$ in 4.16 gives a

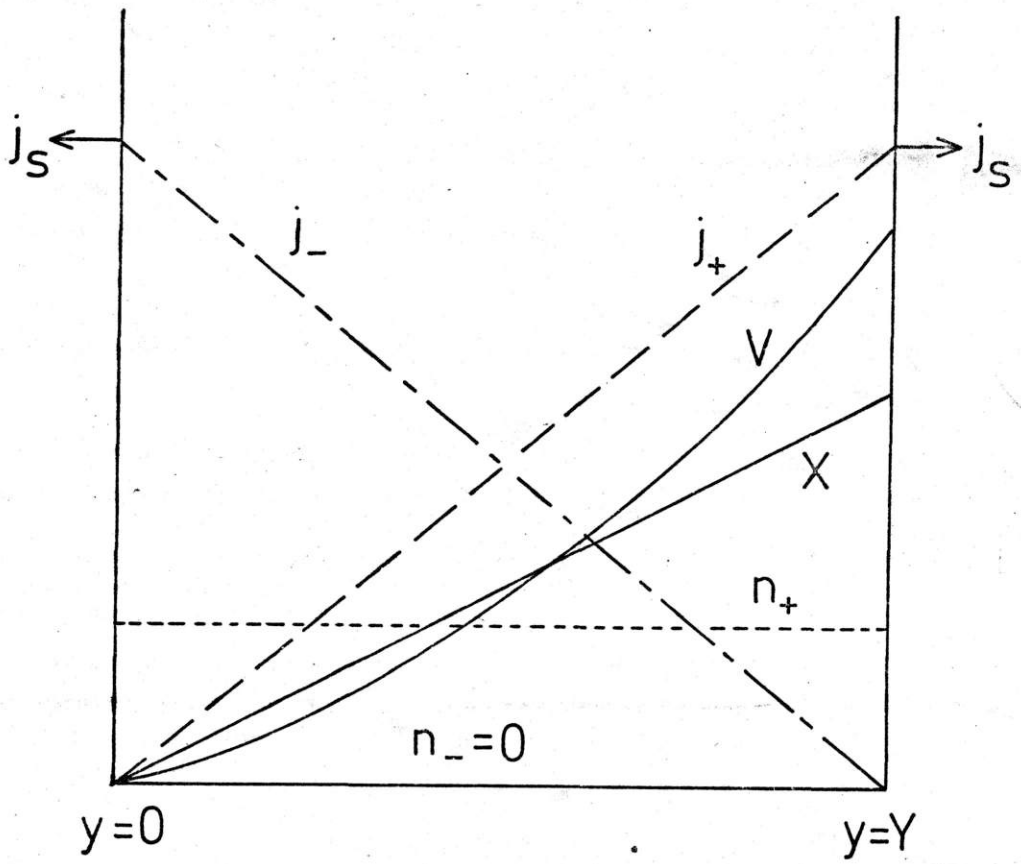

Fig. 4·1 Distribution of electrical parameters within the flame during saturation

quadratic in j the solution of which is:

$$j = \frac{e(k_+ + k_-)^2 X^2}{2\alpha d} \left\{ \left(1 + \frac{4d^2 (\frac{dN}{dt}) \alpha}{(k_+ + k_-)^2 X^2} \right)^{\frac{1}{2}} - 1 \right\} \quad \ldots 4.18$$

Outside the flame.

In the electrode spaces, the same general equations apply, but there is no generation or recombination, ie.

$$\frac{dN}{dt} = 0, \text{ either } n_+ \text{ or } n_- = 0, \text{ and } j_- = j_+ = j = \text{constant}$$

in a one dimensional system. The other major difference is that, provided the electrode spaces are at room temperature, the negative charge carrier is no longer an electron. Electrons associate with neutral molecules during very short path lengths in cold air and k_- will here be of the same order as k_+. This has been confirmed experimentally by comparing Pitot pressures due to ionic winds on either side of the flame and by measurements showing similar potential-current characteristics on both sides[72].

For the general case,

$$j = j_{\pm} = k_{\pm} n_{\pm} eX \quad \ldots\ldots\ldots\ldots\ldots 4.19$$

(the plus or minus sign will henceforth be omitted on the understanding that the argument applies to either side). Substitution into Gauss's law for one dimension gives

$$dX/dy = 4\pi ne = 4\pi j/kX$$

or

$$X^2 = X_o^2 + 8\pi jy/k \quad \ldots\ldots\ldots\ldots\ldots 4.20$$

The potential,

$$V = \int_0^y X\,dy = \pm \frac{k}{12\pi j} \left\{ \left(X_o^2 + \frac{8\pi j y}{k} \right)^{3/2} - X_o^3 \right\} \quad \ldots 4.21$$

Equations 4.20 and 4.21 can be integrated towards each electrode. Once j becomes constant at j_s, equations 4.20 and 4.21 can be written

$$X_y^2 - X_o^2 = \text{const} \times y \quad \ldots\ldots\ldots\ldots\ldots\ldots\ldots \quad 4.22$$

and $$V = \text{const} \times (X_y^3 - X_o^3) \quad \ldots\ldots\ldots\ldots\ldots\ldots \quad 4.23$$

The field in the flame now rises rapidly with applied potential but its variation across the flame zone remains negligible.

The behaviour of the system can be illustrated graphically. Figure 4.2 illustrates a single flame surface which is rather a weak ion source ($j_s = 2 \times 10^{-5}$ A cm^{-2} which is equivalent to $12{\cdot}5 \times 10^{13}$ ion pairs generated per unit area per unit time and corresponds, eg., to a mixture of 8·6% methane in air) placed symmetrically between electrodes 6cm apart. The total potential applied is varied and the corresponding distributions of field (full lines) and potential (dashed lines) are shown.

Figure 4.3 shows the effect on field distribution of varying the position of the same flame between electrodes at the same total separation with conditions maintained at the saturation point.

Conclusions may be drawn concerning the measurement of saturation currents. The field at the electrodes is so much greater than that in the flame that the obvious danger

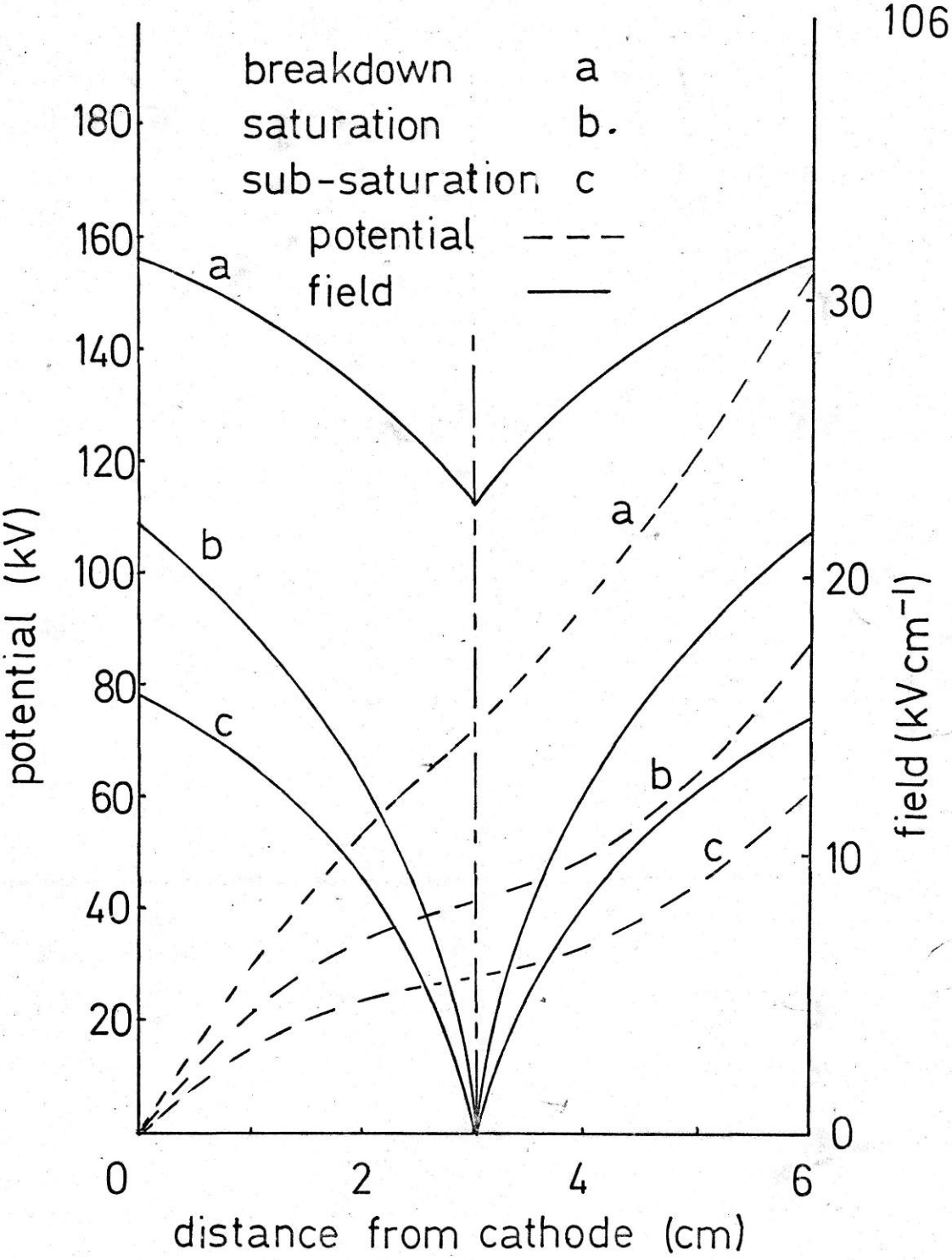

Fig. 4·2 Field and potential distributions for a flame placed midway between electrodes 6 cm apart

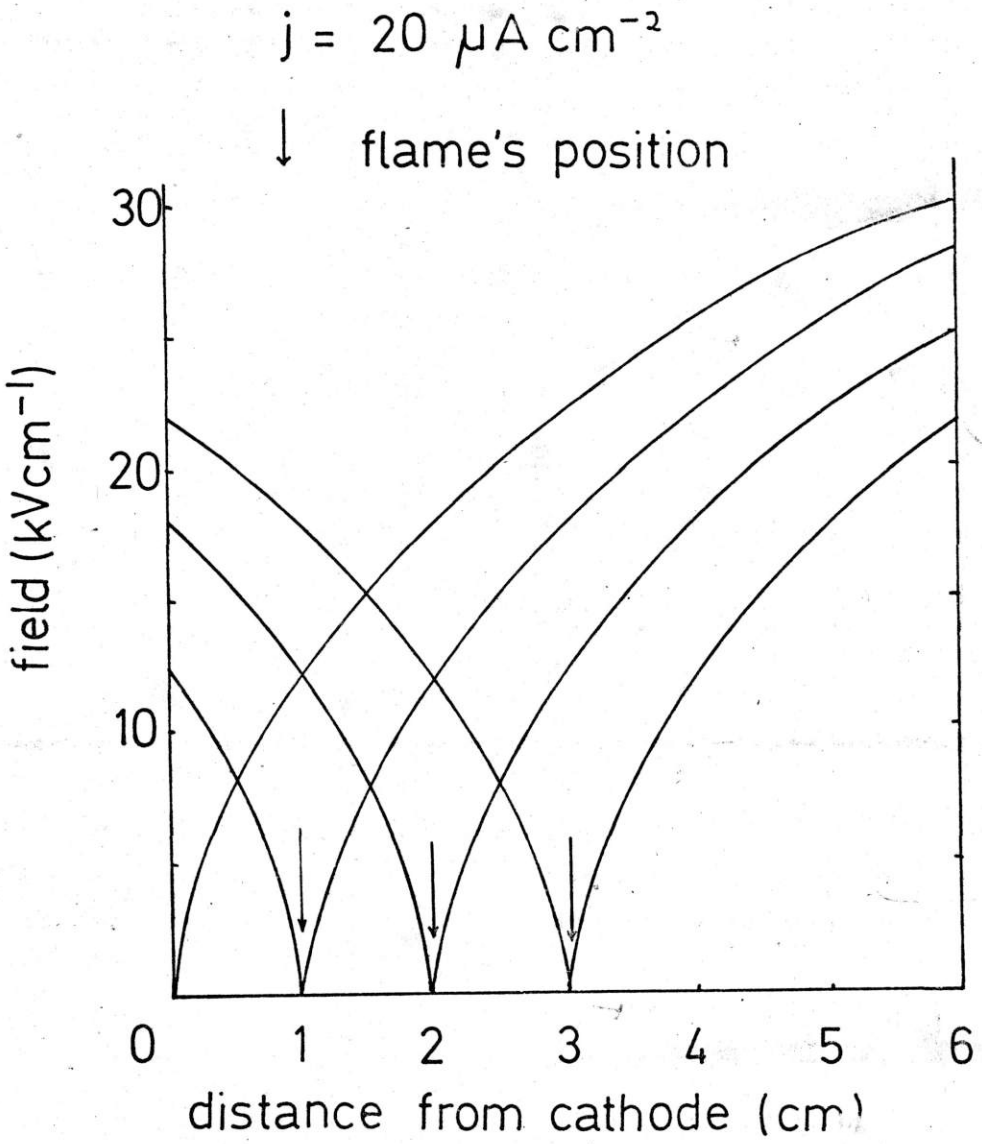

Fig. 4·3 Distribution of field strength for various flame positions

is that it will cause breakdown before the field at the flame reaches the saturation condition. The discrepancy between the two fields increases with j_s (equation 4.20) so that special measures must be adopted for strong ion sources. The graphs show that, in order to extend the range, the flame should be placed symmetrically between the electrodes and the separation between them should be kept as small as considerations of quenching will permit. The condition of symmetry applies because the mobility on either side of the flame has been assumed to be the same.

4.1.4 THE EFFECT OF APPLYING A FIELD TO A WEAK ION SOURCE OVER LARGE DISTANCES

One possibility for removing carbon particles from a flame in a practical system might be to place the electrodes at a large distance from the flame. It will be shown below that this is impossible because of breakdown at the electrodes.

$$X^2 = X_o^2 + \frac{8\pi jy}{k} \qquad \ldots\ldots\ldots\ldots\ldots 4.20$$

When $j \leqslant j_s$ $\quad X_o = 0$

so,

$$X^2 = \frac{8\pi jy}{k} \qquad \ldots\ldots\ldots\ldots\ldots 4.24$$

4.24 is derived with the units in esu - using SI electrical units it becomes,

$$X^2 = \frac{8\pi jy}{k} \times 9 \times 10^{11}$$

The limiting field strength X_b for breakdown in air at STP is 3×10^4 V cm^{-1}.

Rearranging to give y, the distance of the electrode from the ion source -

$$y = \frac{kX_b^2}{8\pi j_b} \times \frac{1}{9 \times 10^{11}} \qquad \ldots\ldots\ldots\ldots\ldots\ldots \quad 4.25$$

The consequences of equation 4.25 are best demonstrated graphically. Fig. 4.4 shows y plotted against j_b (the current at breakdown) for various values of ionic mobility. Values used are 2 $cm^2s^{-1}V^{-1}$ for small ions and 10^{-3} $cm^2s^{-1}V^{-1}$ for carbon particles.

It can be seen that for carbon particles with electrodes at a separation likely in a practical system of 10 - 100 cm. The limiting current before breakdown is 10^{-8} to 10^{-9} A cm^{-2} which would lead to mass deposition rates of around $\cdot 5$ μg cm^{-2} min^{-1} - obviously of no practical use.

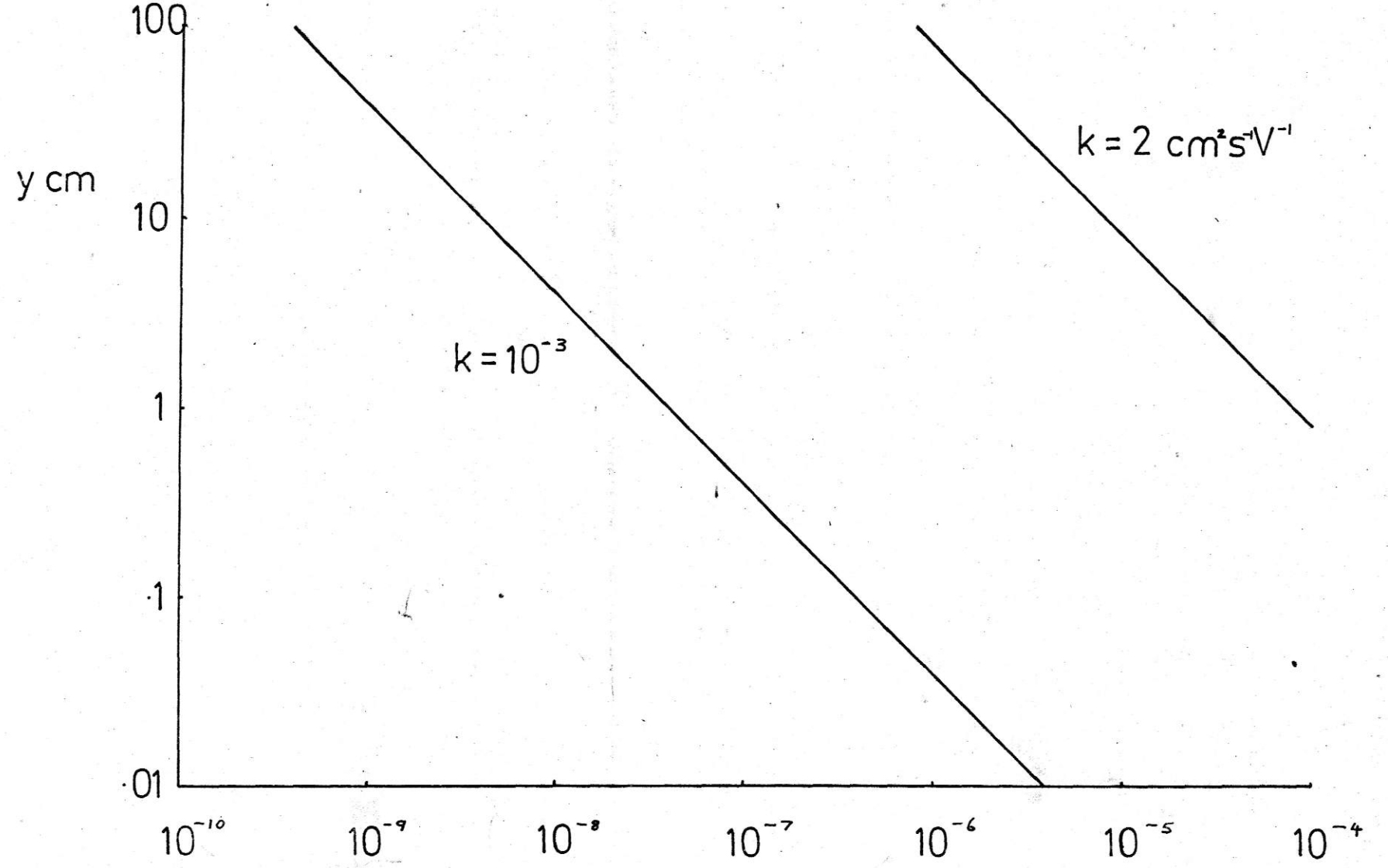

Fig. Electrode - flame separation / breakdown current
4·4

4.2 THE EFFECT OF ELECTRIC FIELDS ON FLAME PRODUCTS

It was demonstrated in section 4.1 that it is impossible to remove carbon from a flame with electrodes placed at a practical distance from the flame. An attempt was then made to collect carbon from the flame products by appying a field to these downstream of the reaction zone. The apparatus used is shown in Fig. 4.5. It consisted of a counterflow diffusion flame using square burner mouths. The flame was vertical and was enclosed in a mica chimney to eliminate convection and entrainment effects. There was a separate set of upper collecting electrodes above the flame.

Using the following gas flow rates a flat flame was obtained which protruded 1cm from the top of the chimney.

Fuel side

Benzene	2·95 $cm^3 s^{-1}$
Ethylene	3.9
Nitrogen	139

Oxygen side

Oxygen	31
Nitrogen	36

These flow rates gave a stable slightly fuel-rich flame, oxygen requirement for stoichiometry is 33.8 $cm^3 s^{-1}$.

Using this flame with no voltage across the bottom electrodes, current was plotted against voltage using the top electrodes at varying heights above the flame, see Fig. 4.6. The experimental points are somewhat scattered because of small fluctuations in the flame and because of the difficulty of

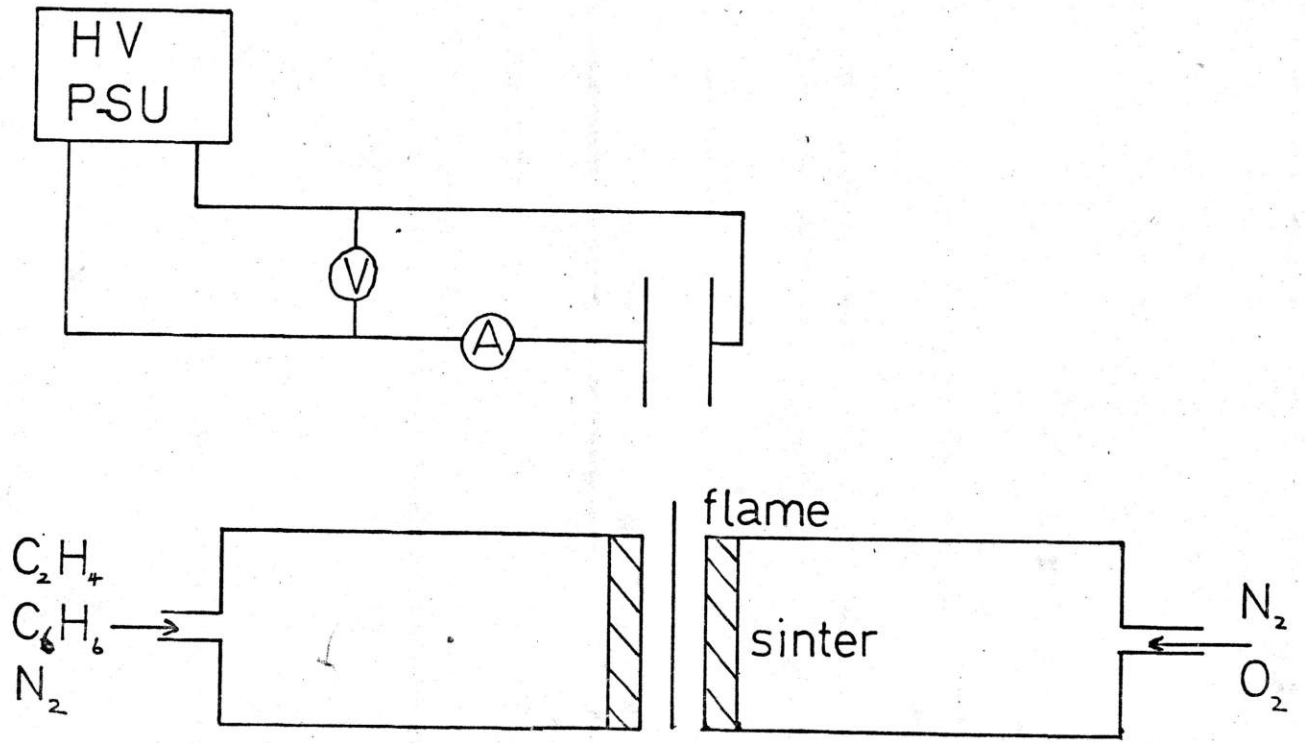

Fig. Apparatus to determine the effect of fields on flame products
4·5

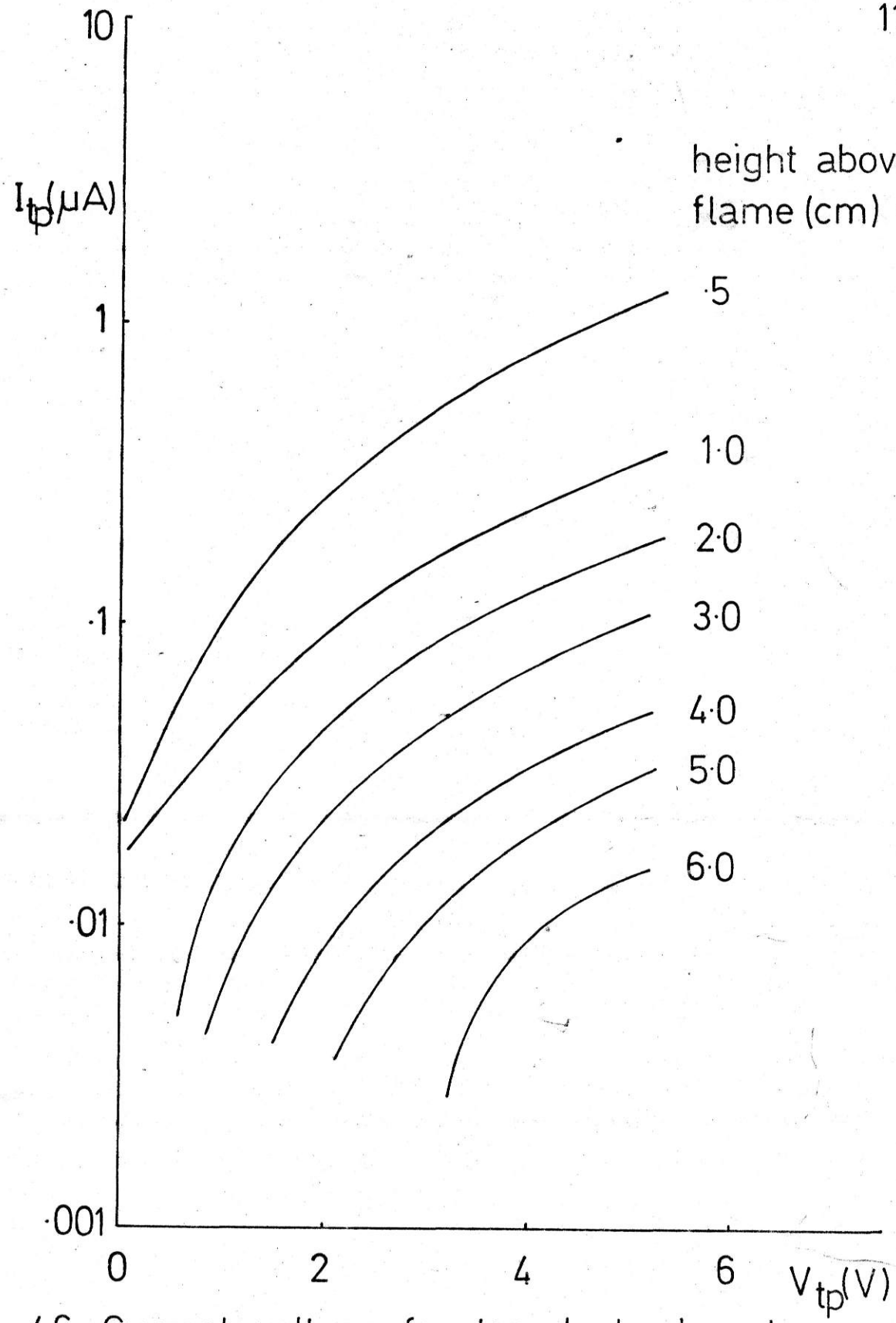

Fig. 4·6 Current-voltage for top electrodes at various heights above the flame

measuring small currents accurately. During the experiments carbon collected on the negative electrode.

A graph of log current against height of electrodes above the flame was plotted for a fixed potential of 5kV, see Fig. 4.7. It is linear and can be used to propose a model on which to discuss the experimental results.

The negative current may be carried by electrons or ions. These may be from either the flame or from the flame products, see Fig. 4.8. The former is more probable as saturated currents were not observed. Assuming that the current arose from the flame the contribution from electrons may be calculated on the basis of published attachment coefficients. Considering attachment of electrons only

$$\frac{dn_e}{dt} = -k_3 n_A n_e$$

The ions are moving with a velocity v_e due to an applied field. Assuming that $v_e \gg v_g$

$$v_e = \frac{dy}{dt} = k_e X = \frac{k_e v}{2y}$$

Hence substituting for dt

$$\frac{dn_e}{n_e} = -\frac{2k_3 n_A}{k_e v} y\, dy \qquad \ldots\ldots\ldots\ldots\ldots\ldots \quad 4.26$$

This relates the electron concentration n_e to the distance y from the flame.

The measured current j with the electrodes at distance y from the flame depends on the electron concentration n_e at the electrodes.

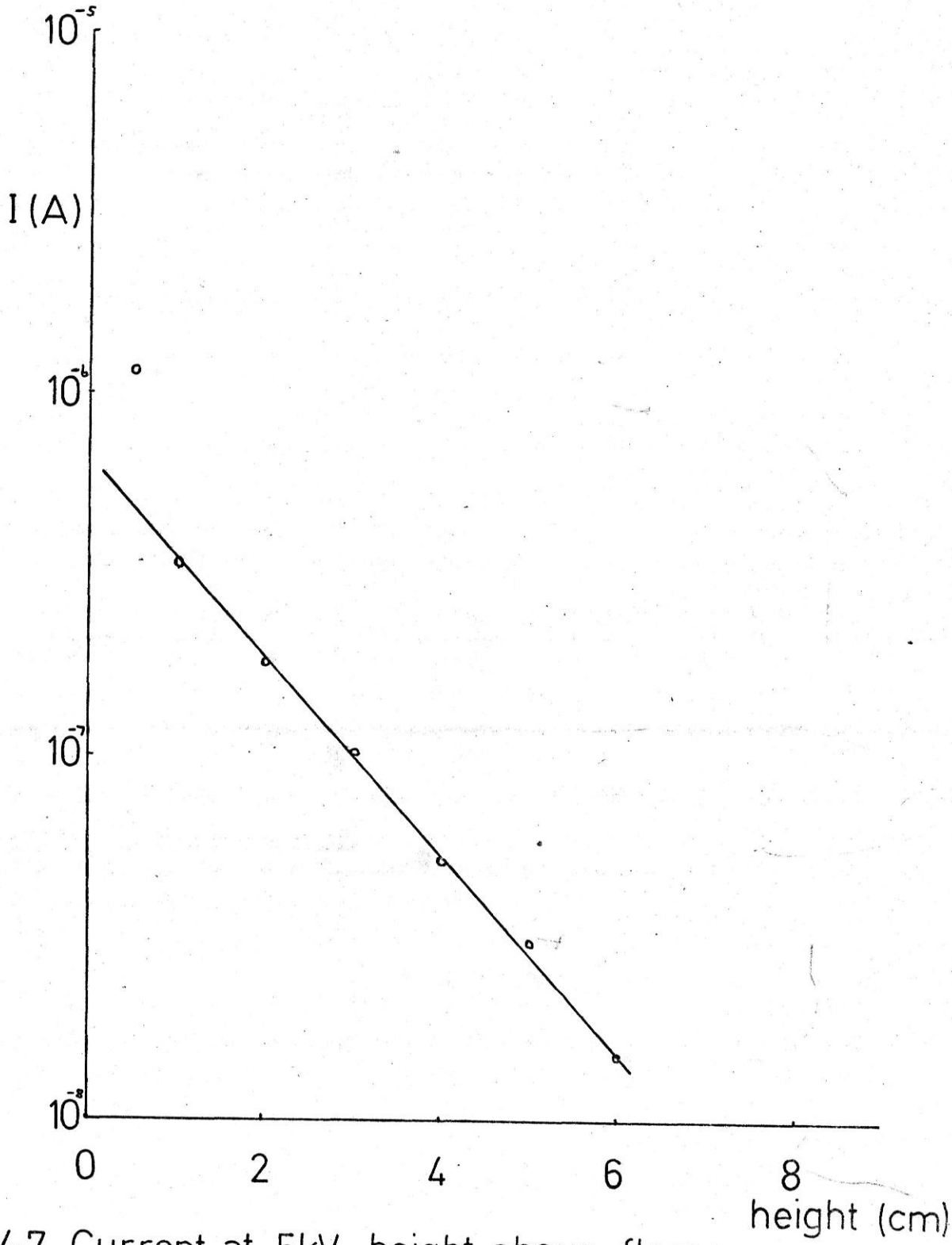

Fig. 4·7 Current at 5kV - height above flame

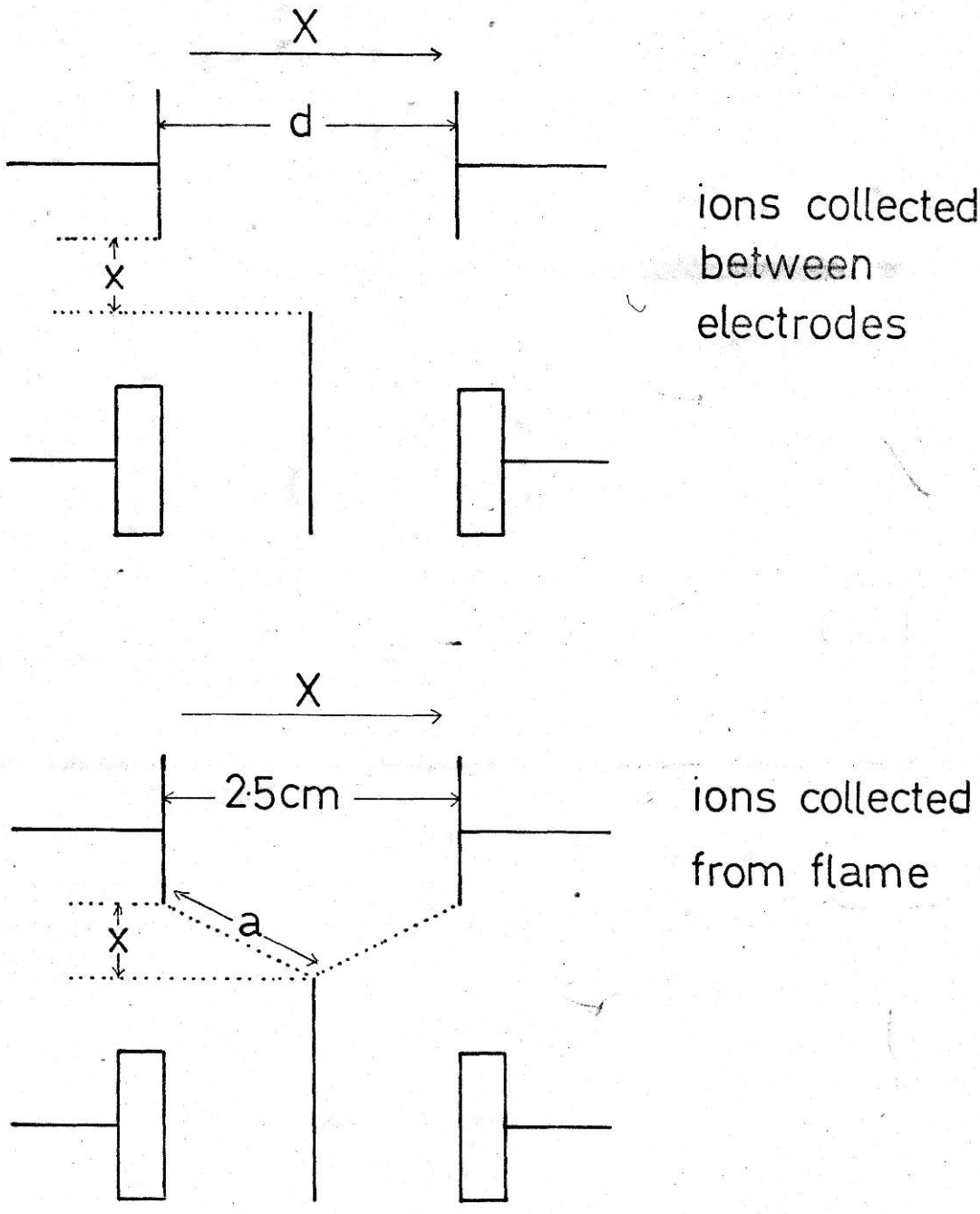

Fig. 4·8 Representation of theoretical models

$$j = n_e e k_e X = \frac{n_e e k_e V}{2y} \qquad \ldots\ldots\ldots\ldots\ldots\ldots \quad 4.27$$

Hence n_e and dn_e can be obtained.

Substituting for these in 4.26

$$\frac{dj}{j} + \frac{dy}{y} = -\frac{2k_3 n_A}{k_e V} y\, dy$$

$$\text{Hence } j = \frac{j_o d}{(d^2 + 4x^2)^{\frac{1}{2}}} \exp -\left\{ \frac{k_3 n_A}{k_e V} x^2 \right\} \qquad \ldots\ldots\ldots \quad 4.28$$

Using:

$j_o = 8 \times 10^{-8}$ A cm^{-2} $\qquad$ $d = 2{\cdot}5$ cm

$k_3 = 3 \times 10^{-12}$ cm^{3}s^{-1} $\qquad$ $n_A \sim 10^{19}$cm^{-3}

$V = 5000$ V $\qquad$ $x = 1$ cm

$k_e = 5 \times 10^5$ cm^{2}mmHg V^{-1}s^{-1} $= 6{\cdot}6 \times 10^2$ at 760 mm [73]

$j \sim 10^{-11}$ A cm^{-2} $\qquad$ cf. $1{\cdot}36 \times 10^{-8}$ A cm^{-2} as measured.

Hence the current must be carried by ions.

Now assuming the current is carried by ions collected from the flame products which are unperturbed until the inter-electrode region and that the current at 5 kV is indicative of the ion concentration between the electrodes.

Using $\frac{dn}{dt} = \alpha n^2$ and $j = n_e v_i$

it can be deduced that

$$j = \frac{j_o e v_i v_g}{j_o \alpha x + e v_i v_g}$$

Using the experimental result that $j = 6 \times 10^{-10}$A cm^{-2} at $x = 6$cm, see Fig. 4.7, a value for α was calculated: giving $\alpha = 5.29 \times 10^{-5}$ cm^3 s^{-1}.

Hence a theoretical curve was plotted for log j against x, see Fig. 4.9. This is not in good agreement with experiment and it therefore seems likely that the ions causing the current are collected from the flame.

The current voltage relationship for a field applied to a flame under sub-saturation conditions is given by equation 4.18.

$$j = \frac{e(k_+ + k_-)^2 X^2}{2\alpha d}\left\{\left\{1 + \frac{4d^2(\frac{dN}{dt})\alpha}{(k_+ + k_-)^2 X^2}\right\}^{\frac{1}{2}} - 1\right\}$$

Using $X = V/d$ where $d = (4x^2 + 6{\cdot}25)^{\frac{1}{2}}$, see Fig. 4.8, then

$$j = \frac{e(k_+ + k_-)^2 V^2}{2\alpha d^3}\left\{\left\{1 + \frac{4d^4\alpha(\frac{dN}{dt})}{(k_+ + k_-)^2 V^2}\right\}^{\frac{1}{2}} - 1\right\} \quad \ldots\ldots 4.29$$

Solving simultaneously for α and $\frac{dN}{dt}$ using two values of j and d gives:-

$$\alpha = \frac{e(k_+ + k_-)^2 V^2 (j_2 d_1 - j_1 d_2)}{d_1 d_2 (d_1^2 j_1^2 - d_2^2 j_2^2)} \quad \ldots\ldots\ldots\ldots\ldots\ldots 4.30$$

$$\frac{dN}{dt} = \frac{d^2 j^2}{e^2 (k_+ + k_-)^2 V^2} + \frac{j}{ed} \quad \ldots\ldots\ldots\ldots\ldots\ldots 4.31$$

Using the following data from Fig. 4.7,

$e = 1{\cdot}6 \times 10^{-19}$ A s $\qquad k_+ = 2$ cm^{2}s^{-1}V^{-1}

$V = 5000$ V $\qquad k_- = 2$

$j_1 = 8 \times 10^{-8}$ A cm^{-2} $\qquad d_1 = 2.5$ cm

$j_2 = 6 \times 10^{-10}$ $\qquad d_2 = (150{\cdot}25)^{\frac{1}{2}}$ cm

the following values of α and $\frac{dN}{dt}$ were calculated,

$\alpha = 5{\cdot}12 \times 10^{-5}$ cm^{3}s^{-1} $\qquad \frac{dN}{dt} = 3{\cdot}55 \times 10^7$ cm^{-3}s^{-1}.

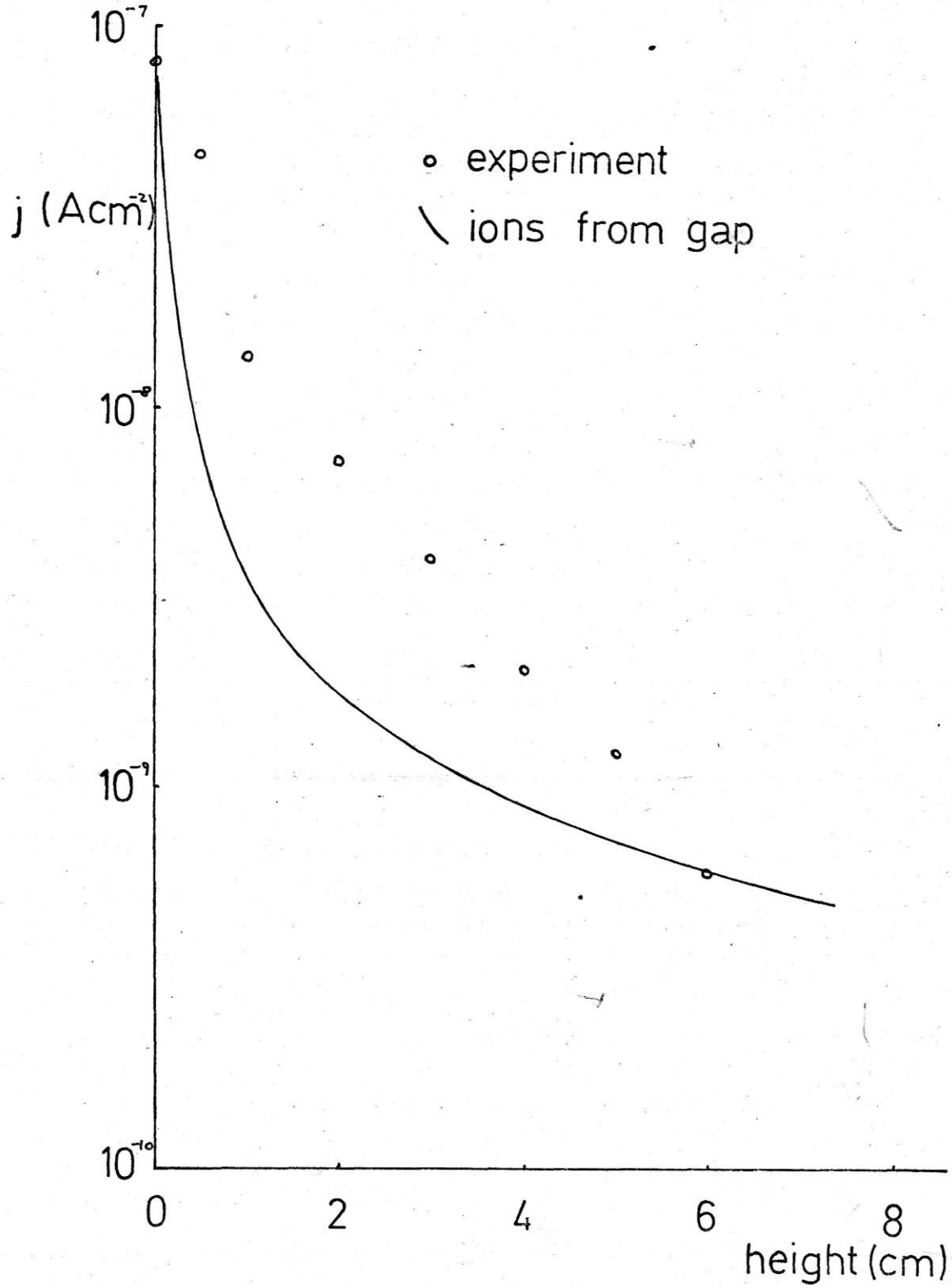

Fig. 4·9 Current density in products - height above flame

Using these figures a characteristic was calculated and plotted, see Fig. 4.10. This is in reasonable agreement with the experimental curve.

Hence the system behaves as if the majority of the current were carried by ions from the flame, so that relatively few would exist between the electrodes at any height above the flame in the absence of a field.

In order to confirm this experimentally a mica sheet was placed between the electrodes with the current flowing. No detectable current change was observed, demonstrating that the ions came from the flame and not between the electrodes.

The deduction that recombination in the products occurs rapidly was tested theoretically. The model chosen was a thin rectangular flow of gas at a uniform temperature containing carbon particles of a constant size, see Fig. 4.11. The temperature profile with height above the orifice was calculated. It was assumed that all the heat loss was by radiation from the carbon particles and that the temperature in a cross section at a given height above the burner was uniform.

$$-\frac{dQ_{out}}{dt} = \varepsilon \sigma T_g^4 A_{rad} \qquad \ldots\ldots\ldots\ldots\ldots\ldots \quad 4.32$$

now $dQ = mc\,dT$

and $m = \rho N_p \frac{4}{3}\pi r^3 A_{rad} y$

$$\therefore \quad \rho N_p \frac{4}{3}\pi r^3 yc \frac{dT}{dt} = -\varepsilon \sigma T_g^4$$

now $\varepsilon \sim C_{abs} N_p y$

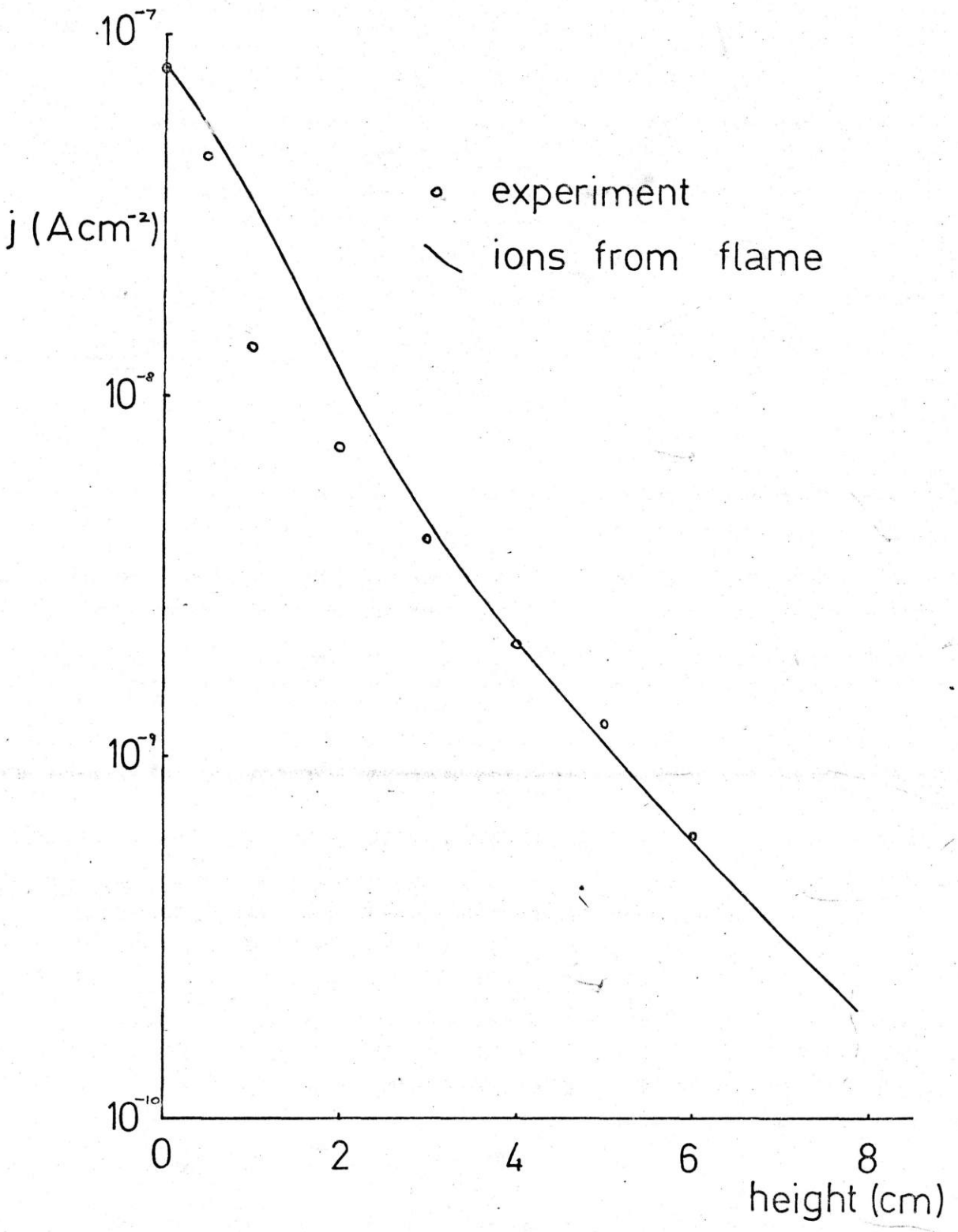

Fig. 4·10 Current density in products - height above flame

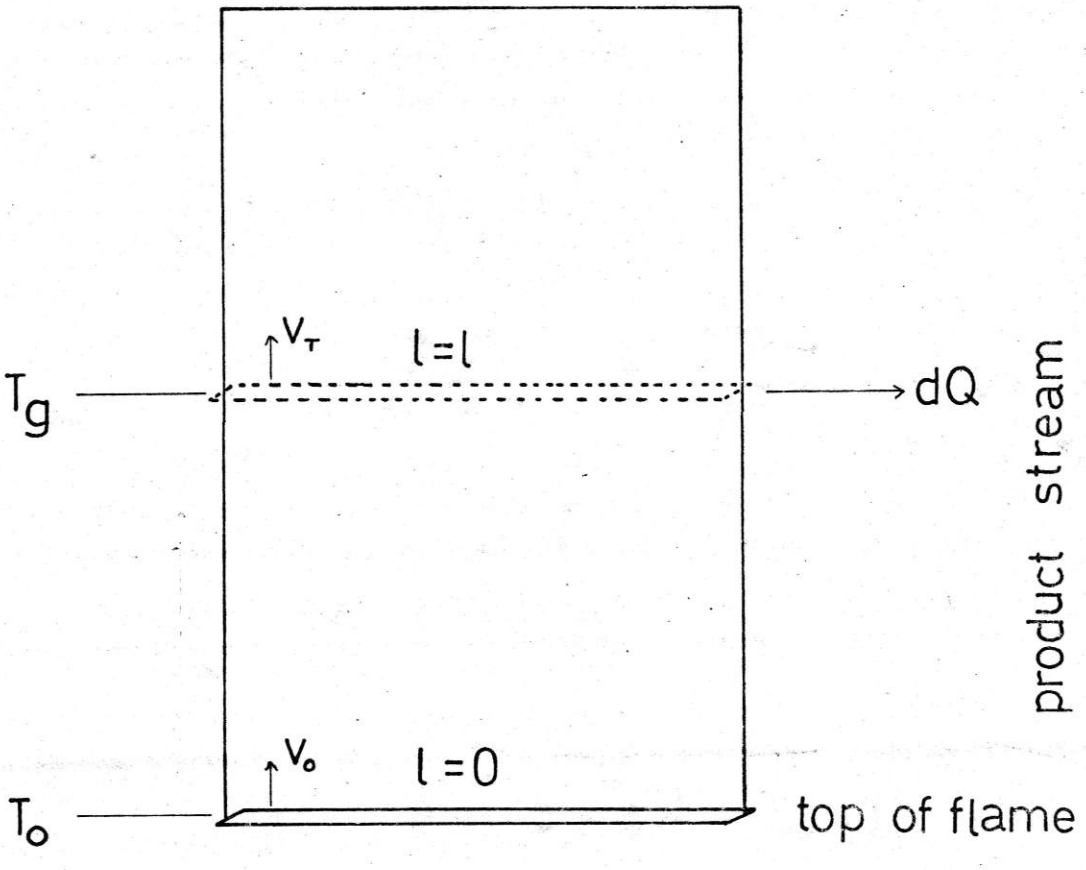

Fig. 4·11 Representation of theoretical model for ion recombination above flame

$$\frac{4}{3}\pi r^3 \rho c \frac{dT_g}{dt} \approx - C_{abs} \sigma T_g^4$$

Hence $$\frac{dT_g}{T_g^4} \approx - \frac{C_{abs}\sigma}{4/3\pi r^3 \rho c} dt \quad \ldots\ldots\ldots\ldots\ldots\ldots \quad 4.33$$

But $\frac{dh}{dt} = v$

and the gas velocity is proportional to gas temperature

so $$\frac{v_T}{v_o} = \frac{T}{T_o}$$

$$dt = \frac{dh T_a}{v_o T_g}$$

Substituting for dt in 4.33 gives

$$\frac{dT_g}{T_g^3} = - \frac{3C_{abs}\sigma T_a}{4\pi r^3 \rho\ cv_o} dh \quad \ldots\ldots\ldots\ldots\ldots\ldots \quad 4.34$$

Integrating and solving for T_g gives:

$$T_g = \left\{ \frac{1}{T_o^2} + \frac{3C_{abs}\sigma T_a}{2\pi r^3 \rho\ cv_o} h \right\}^{-\frac{1}{2}} \quad \ldots\ldots\ldots\ldots\ldots\ldots \quad 4.35$$

Using the following data a temperature profile was calculated, see Fig. 4.12.

T_o	= 2400°K	σ	= $5{\cdot}7 \times 10^{-5}$ erg $cm^2 s^{-1}$ $^oK^{-4}$
T_a	= 300	r	= 20 nm [2]
ρ	= 2 g cm^{-3}	c	= ·17 cal g^{-1}
C_{abs}	= $10^{-12} cm^2$ [74]	v_o	= 100 cm s^{-1}

In order to determine the effect of temperature on the ion concentration and hence the current that may be drawn the temperature dependence of recombination coefficient and mobility must be taken into account.

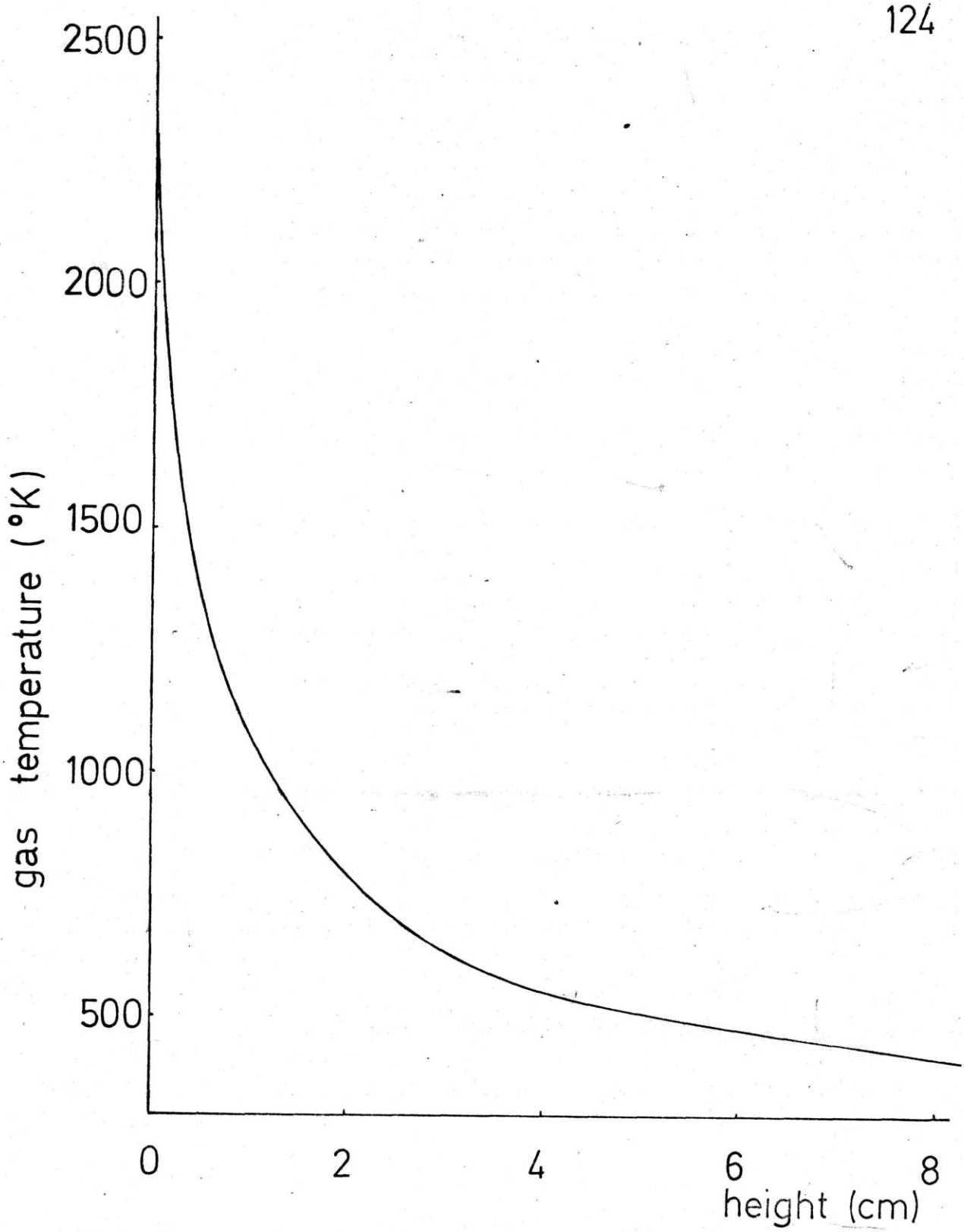

Fig. 4·12 Calculated temperature profile in products

For solid sphere collisions:-

α is proportional to $T^{-7/2}$ [41]

also $k = \text{const}$ [41]

k is proportional to T

Now $$j = \frac{e(k_+ + k_-)^2 X^2}{2\alpha d} \left\{ \left\{ 1 + \frac{4d^2 \frac{dN}{dt} \alpha}{(k_+ + k_-)^2 X^2} \right\}^{\frac{1}{2}} - 1 \right\} \quad \ldots \quad 4.18$$

In the case under consideration

$$\frac{4d^2 \frac{dN}{dt} \alpha}{(k_+ + k_-)^2 X^2} \gg 1$$

so that j is proportional to $k/\alpha^{\frac{1}{2}}$.

Hence j is proportional to $T^{11/4}$

or $j = BT^{2.75}$,

now from Fig. 4.10 $j_o = 8{\cdot}2 \times 10^{-8} A\ cm^{-2}$.

Hence a profile of current versus height was calculated. This is shown in Fig. 4.13.

Comparison of Figs. 4.10 and 4.13 show that the current expected from this model is perhaps not insignificantly smaller than the current measured, though in calculating Fig. 4.13 cooling of the hot products by entrainment was ignored so that this current is probably lower than calculated. However, the experimental result that the ions must come from the flame itself eliminates this possibility of the ions coming from the hot products. Whatever model is used to describe the results, and these are most certainly not attributable to only one model but a hybrid of these, the practical consequences are quite clear. The small currents

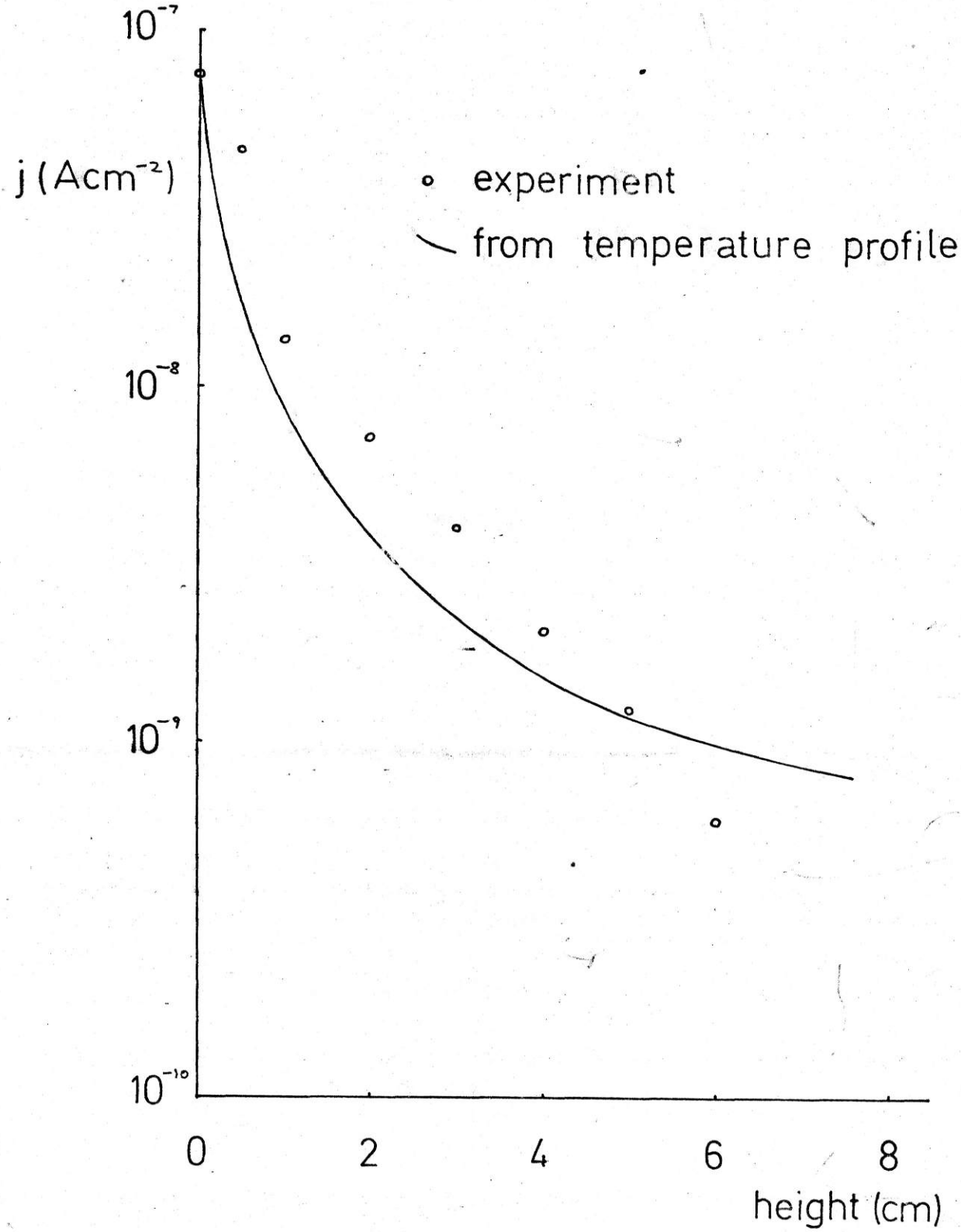

Fig. 4·13 Current density in products - height above flame

measured in this experiment are almost entirely due to small flame ions and not carbon particles and even these currents are two orders of magnitude lower than those produced when the electrodes are applied directly to the flame. Hence the collection of carbon from the products of a sooting flame under these conditions is impractical because the product temperature falls rapidly causing recombination to occur.

4.3 THE EFFECT OF A SMALL PERTURBING FIELD ACROSS THE FLAME

In section 4.2 it was shown that little ionisation existed downstream of the flame in the products. It was decided to try to enhance the product ionisation by applying a small perturbing field directly to the flame, to preseparate the ions and prevent recombination. A larger field was applied to the products to detect any increase in product ionisation.

The burner described in section 4.2 was modified to eliminate the chimney. The gauzes were replaced by brass sinters and the burner mouths were moved closer together. The top electrodes were placed on top of the burner and insulated from it by mica sheets, see Fig. 4.14.

The fuel and oxidant flow rates were adjusted to give a yellow luminous flame equidistant from the electrodes. The flow rates required were:-

Fuel:

Benzene 2·2 $cm^3 s^{-1}$

Nitrogen 54

Oxidant

Oxygen 19

Burner separation: 6 mm

Top electrode separation 34

Top electrode area 1250 mm^2

The current-voltage characteristic of the flame was measured using the burner mouths as electrodes, with the fuel side negative; this is presented in Fig. 4.15.

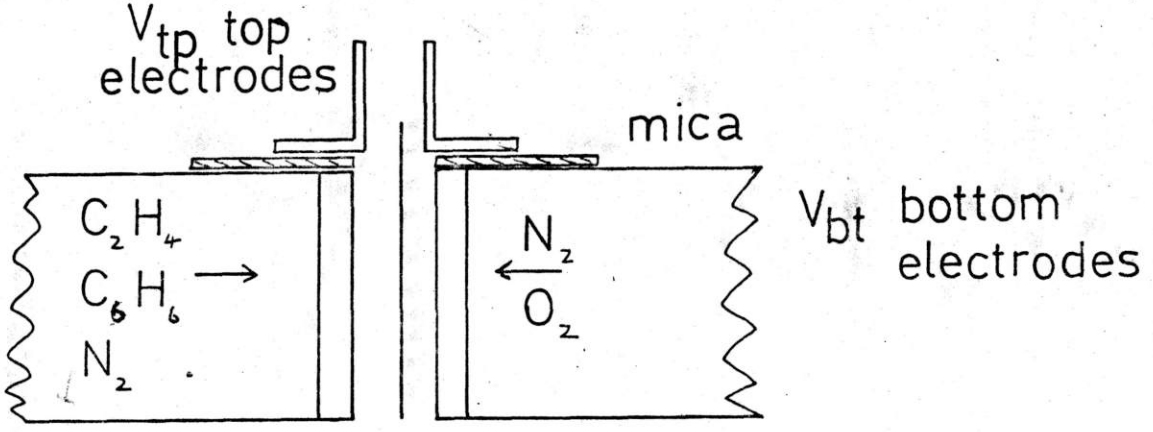

Fig. 4.14 Apparatus for determining the effect of a small perturbing field across the flame

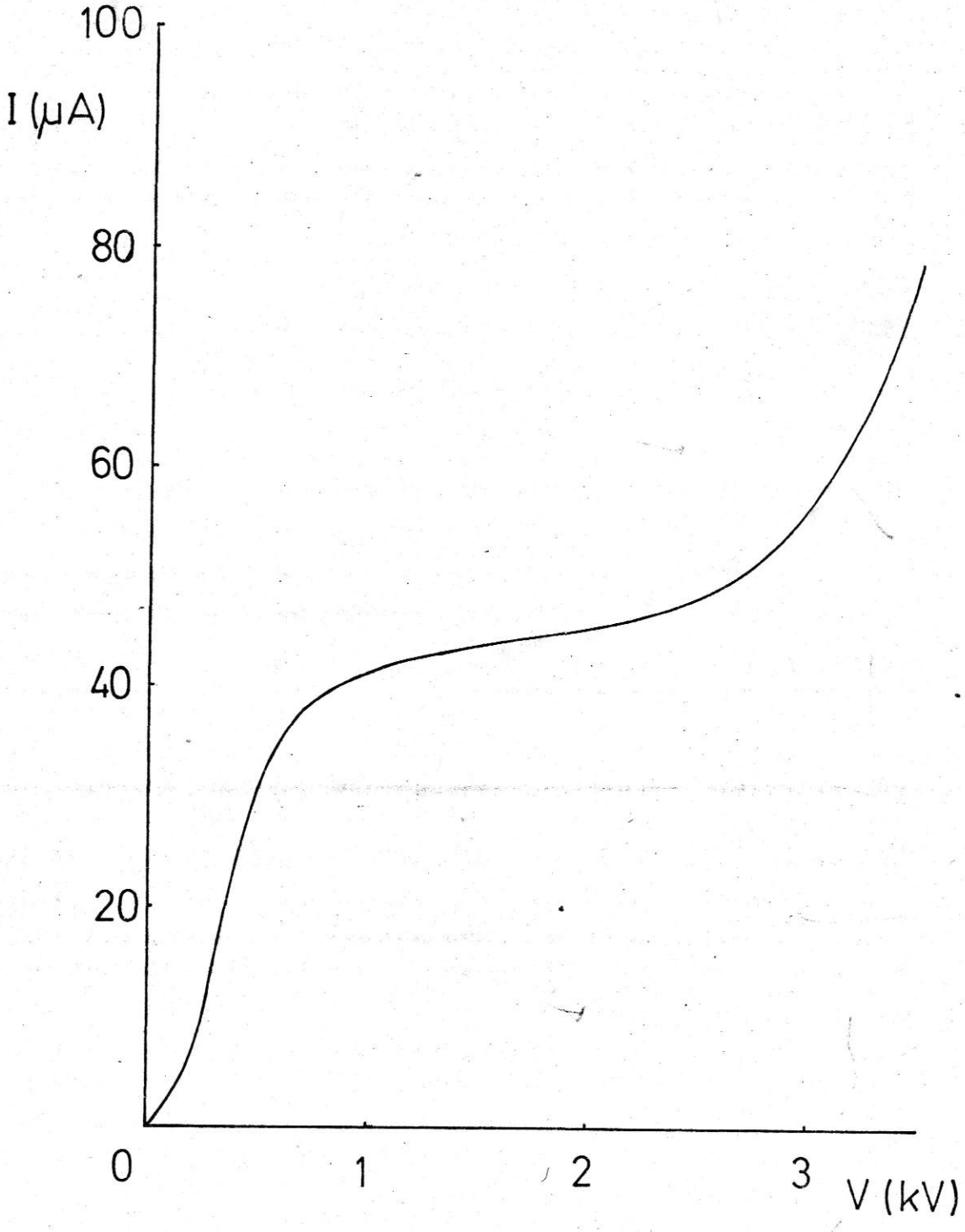

Fig. 4·15 Current-voltage characteristic for flame using bottom electrodes

A series of current-voltage characteristics for the top electrodes were measured using varying potentials between the bottom electrodes. In each case the fuel side electrodes were made negative, see Fig. 4.16. These experiments were repeated several times and the mean top electrode currents at fixed V_{tp} were plotted against V_{bt}, see Fig. 4.17. The current at the top electrodes drops off uniformly with voltage and shows no enhancement at lower voltages.

An attempt was made to account for this by considering the flame as an ion source with fixed rate of production of ions. Some of these were removed by the field across the bottom electrodes thus reducing the effective ion concentration in the flame, from which the current at the top electrodes could be calculated.

The rate of production of ions by the flame and their rate of removal at varying V_{bt} was deduced from Fig. 4.15 assuming each ion bears unit charge. From these figures the remaining concentration of ions in the flame was calculated, see Fig. 4.18.

The flame height and hence the area available to the top electrode also varied with V_{bt}. This area carries at least 90% of the total current at the top electrode, see Fig. 4.10. A series of photographs were taken to measure this, see Fig. 4.19.

Using the equation that,

$$j = \frac{e(k_+ + k_-)^2 V^2}{2\alpha d^3} \left\{ \left\{ 1 + \frac{4d^4 \alpha \frac{dN}{dt}}{(k_+ + k_-)^2 V^2} \right\}^{\frac{1}{2}} - 1 \right\} \quad \ldots\ldots \quad 4.29$$

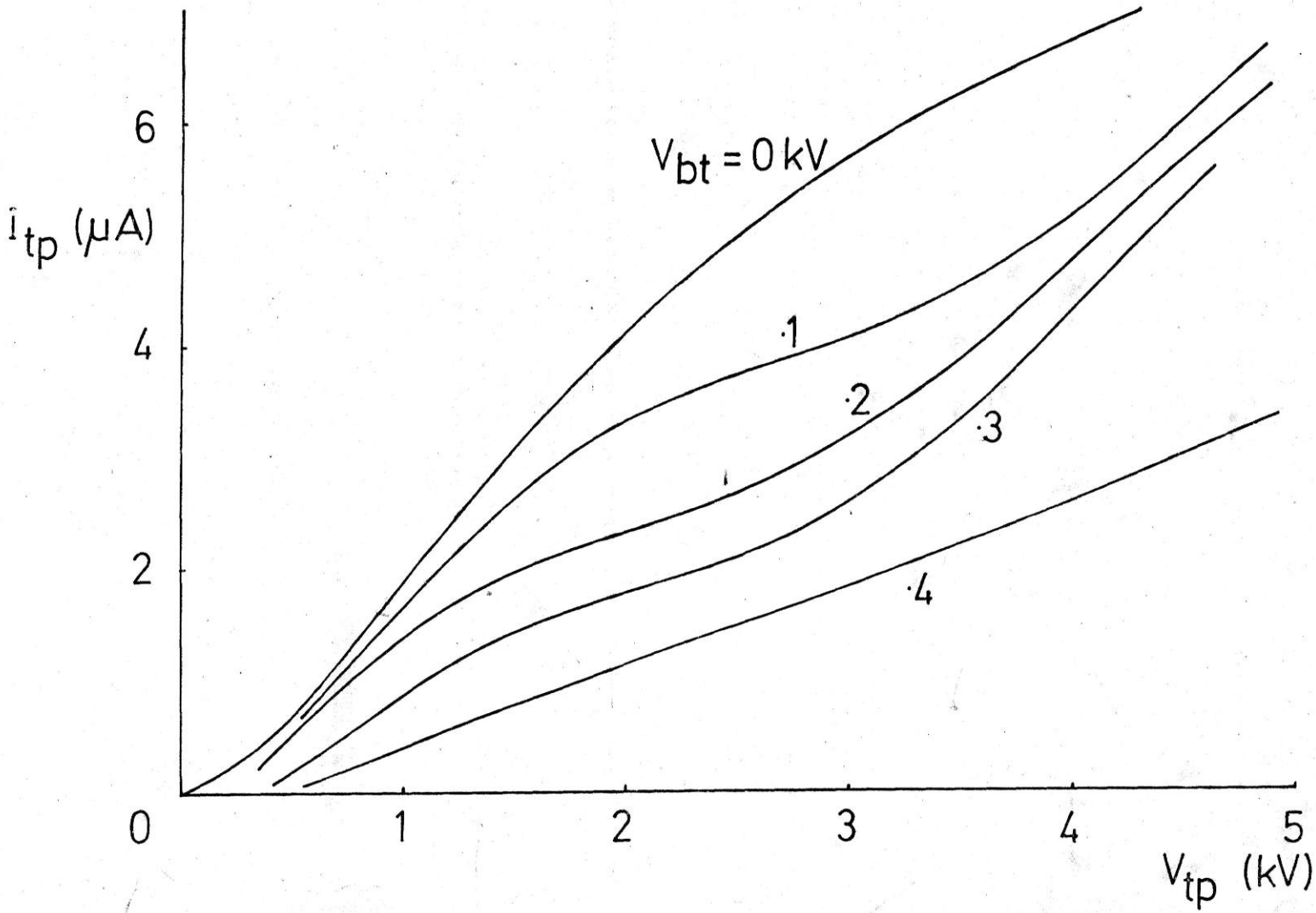

Fig. 4.16 Top electrode characteristics as a function of bottom electrode potential

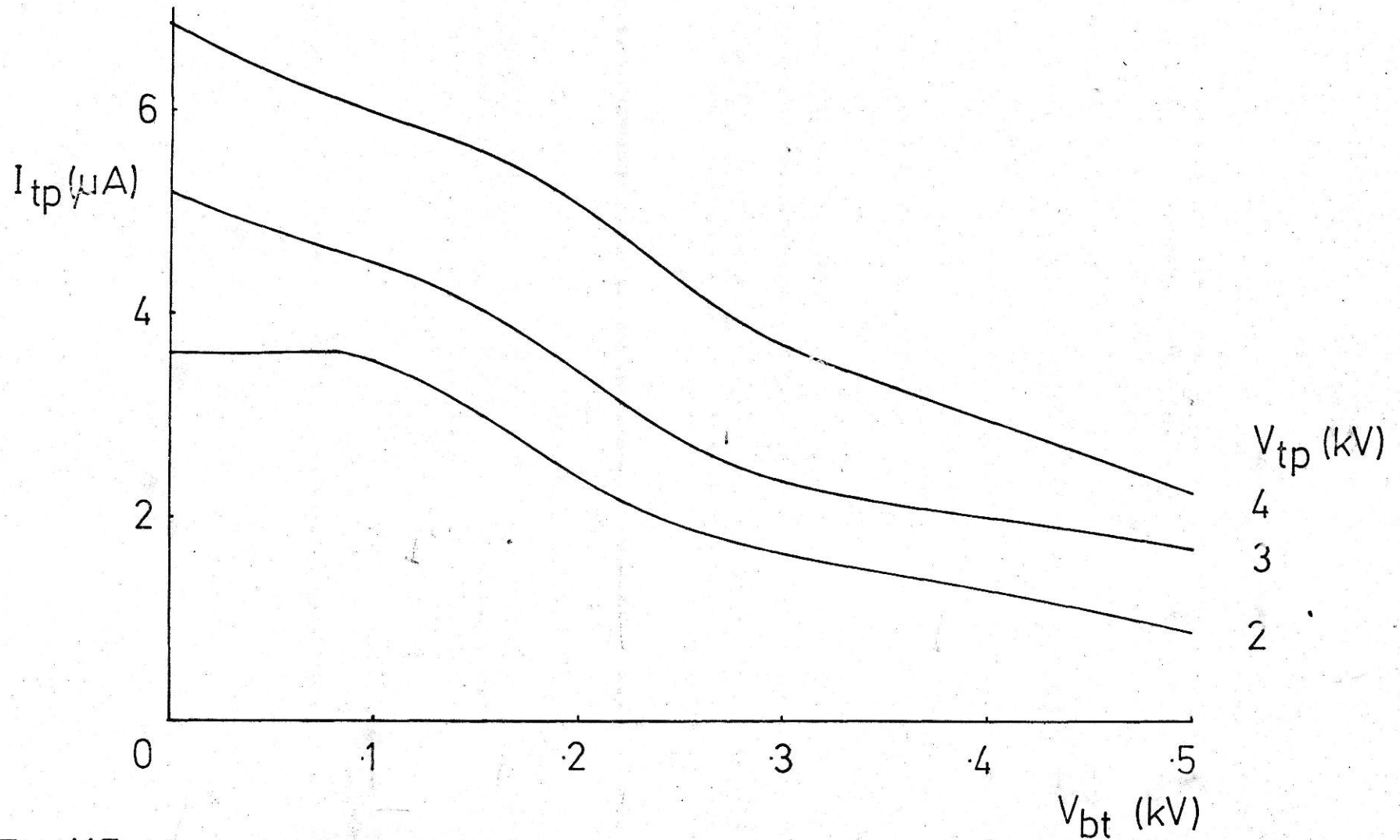

Fig. 417 Mean top electrode current at constant voltage - bottom electrode potential

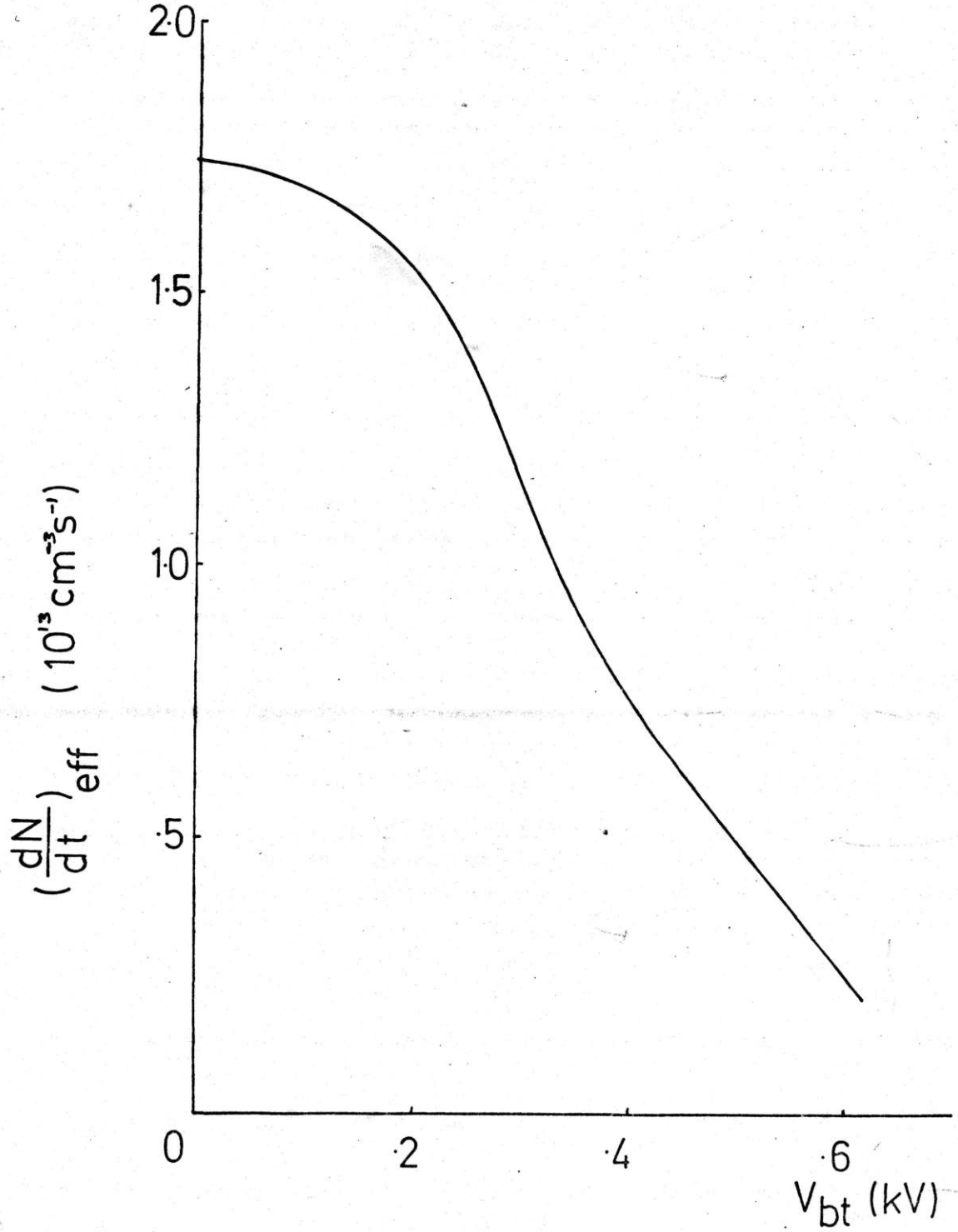

Fig. 4·18 Ion production rate available to top electrodes vs. bottom electrode voltage

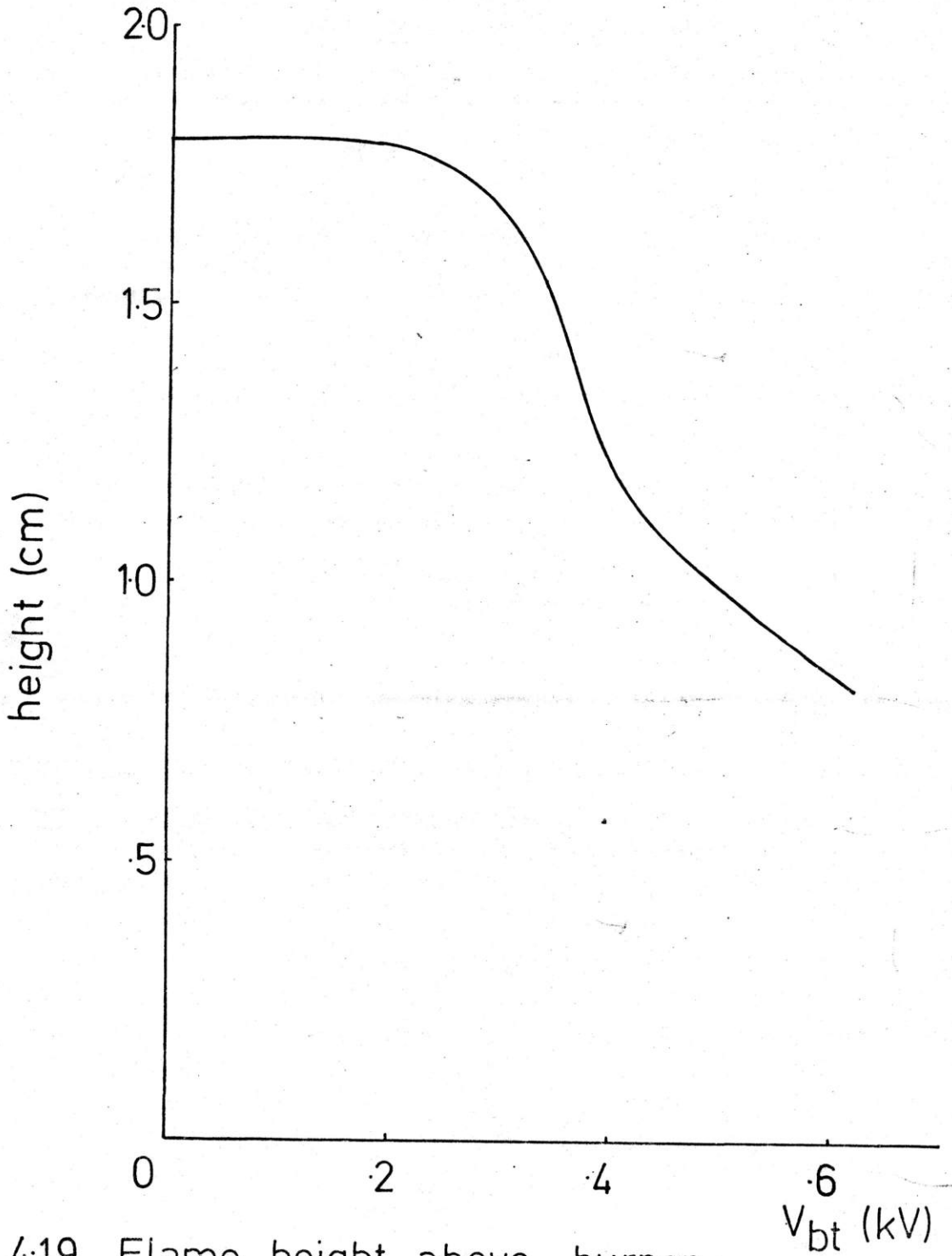

Fig. 4·19 Flame height above burner - bottom electrode voltage

a value for the recombination coefficient was calculated using data at V_{bt}= 0 and V_{tp}= 2 kV giving

$$\alpha = 1{\cdot}18 \times 10^{-5} cm^3 s^{-1}$$

Hence values of current were calculated as a function of V_{bt} for fixed V_{tp}; see Fig. 4.20. The difference between the curves is appreciable especially at intermediate voltages. This could be caused by the current at the bottom electrode being preferentially carried by small ions, leaving lower mobility carbon particles for the top electrodes. However, the proportion of current carried by carbon particles is unlikely to exceed 1% so this effect is probably negligible[2]. The discrepancy could be caused by ionic wind effects and quenching of the flame. At low V_{bt} the flame may be slightly quenched by being brought nearer the electrodes, hence reducing $(\frac{dN}{dt})_{tot.}$. At higher voltages turbulence caused by ionic winds may counteract this returning $(\frac{dN}{dt})_{tot.}$ to its former value.

A series of experiments were carried out at very low V_{bt} varying in steps up to 100V. No change in I_{tp} was observed with any value of V_{tp} hence no value of V_{bt} appears to enhance product ionisation. This can be explained using the following model.

Positive ions and electrons are drawn out from the flame, the latter soon becoming attached to become negative ions. The positive and negative charge carriers then have a similar mobility of ~2 $cm^2 s^{-1} V^{-1}$. These ions drift to their respective electrodes against the gas stream under the influence of a field X V cm^{-1} and their velocity is given by

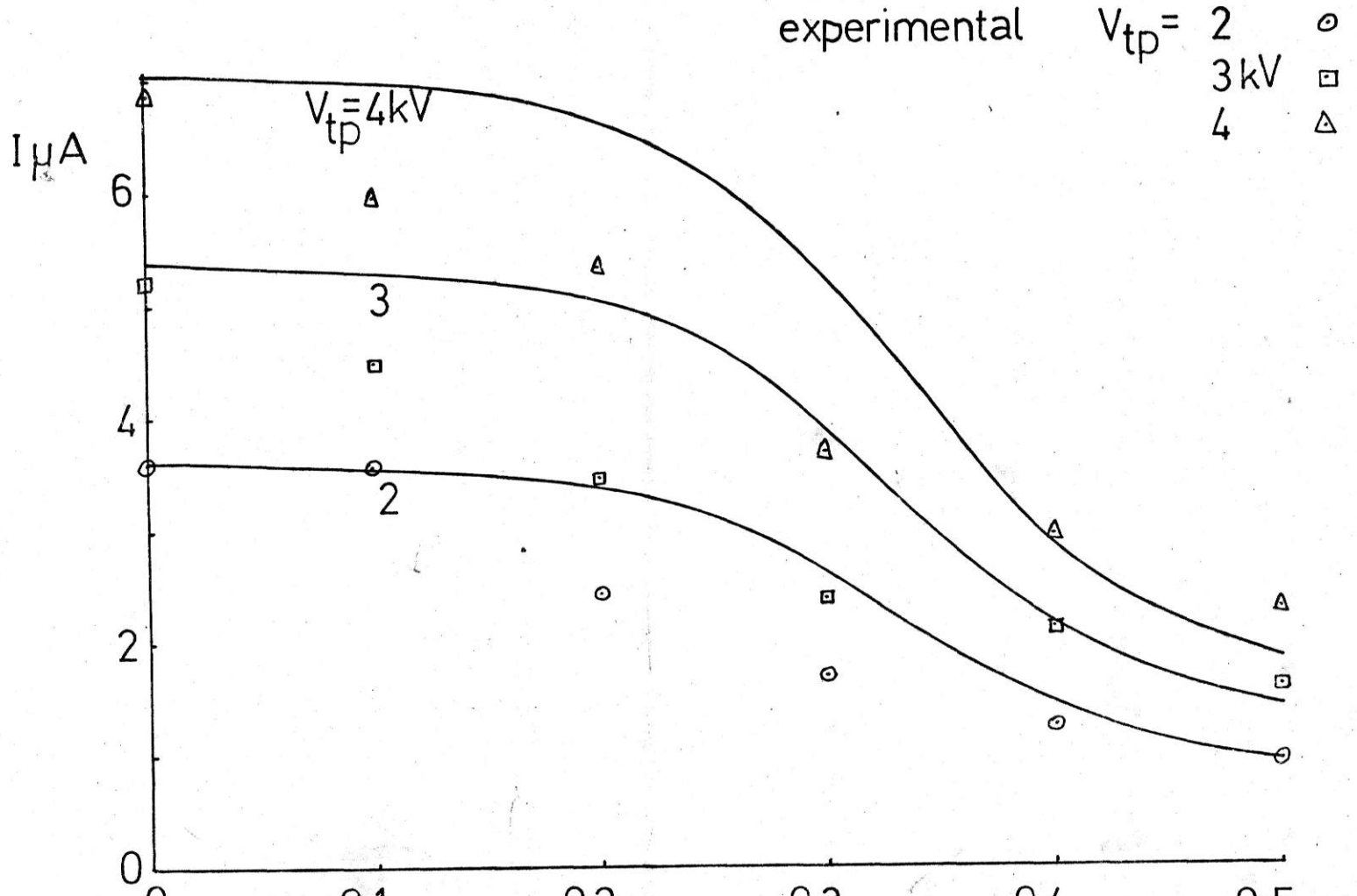

Fig. 4·20 Plots of mean current at fixed V_{tp}/ V_{bt}

$$v_i = \frac{k}{X} \text{ cm s}^{-1}$$

Taking the case of the bottom electrodes the field required to give the ions a comparable velocity to the gas, so that the ions may be carried downstream to the top electrodes, is about 1 V cm^{-1}. This field would cause hardly any separation of charge in the flame because of space charge. As soon as any ion separation occurs this engenders a large field by space charge. So that in order to maintain the charge separation a large field is required. With such fields the ions go to the electrodes and do not remain in the products. Space charge is large because the electrons have a much higher mobility than positive ions and are easily removed from the flame. Hence no enhancement in top electrode current is observed with small voltages across the flame.

Carbon particles, having a much lower mobility, may be separated in this way and collected downstream of the reaction zone, but the amount of carbon collected was found to be insignificant when compared with the amount deposited on the bottom electrodes in the process. No significant amount of carbon ever accumulates on the top electrodes at any value of V_{bt}. This is probably caused by the carbon particles losing their charge before reaching the upper electrode region. It is concluded that product ionisation, downstream of the reaction zone, cannot be appreciably affected by the application of fields to the flame. An effect was observed with carbon particles, but the number collected was small compared with those collected by the perturbing field. These effects may become more significant at much higher flow rates.

4.4 THE TRANSFERENCE OF CARBON INTO A CARRIER STREAM

One of the major problems with the experiment in section 4.3 is that most of the soot was collected on the burner electrodes rather than the collecting electrodes. Hence an attempt was made to separate the carbon from the small flame ions and to collect it at separate electrodes. The method of separation used relies upon the large difference in mobility between the soot and small flame ions.

The apparatus used is shown in Fig. 4.21; the counter-flow diffusion flame was replaced by a sooting premixed flame. Carbon was initially separated by applying a small field to the bottom electrodes. Nitrogen was counterflowed against the ion drift to transfer the slow moving carbon particles into the product stream where it was collected on the top electrodes using another field. The separating field also had the effect of prolonging the life of the charged carbon particles by removing electrons from the product stream and so inhibiting recombination.

The following flow rates were used:

Nitrogen	52 $cm^3 s^{-1}$
Oxygen	16
Benzene	2·2
Ethylene	4·5

The stoichiometry defined as O_2 stoich/ O_2 supplied = 1·88

Electrode separation	1·8 cm
Top electrode area	12·5 cm^2
Bottom electrode area	25·0

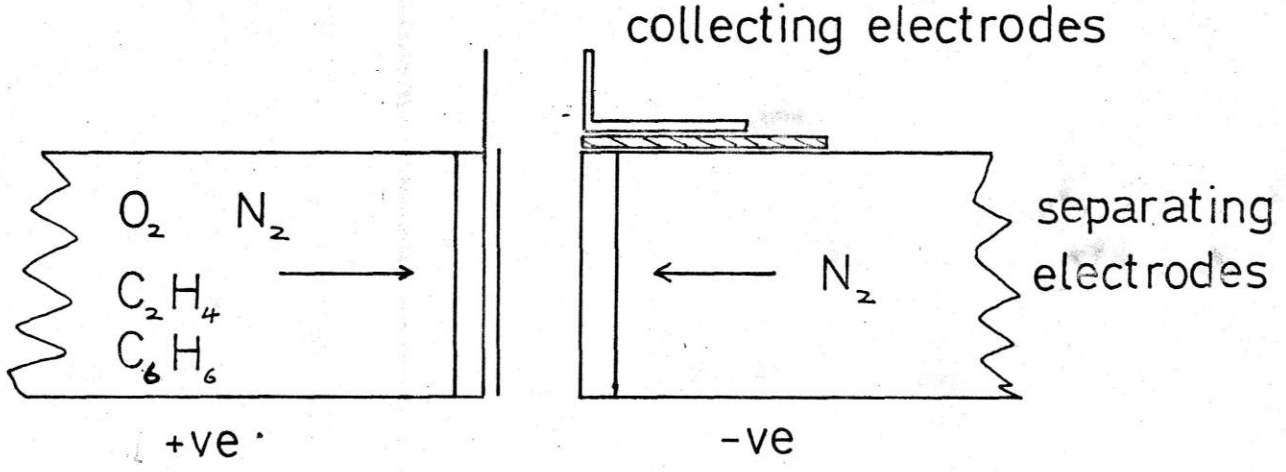

Fig. 4·21 Apparatus for the transfer of carbon into a carrier stream

The flame produced was fuel rich and burnt as a part diffusion flame unless nitrogen was counterflowed, when the excess fuel pyrolysed. The application of a field aerated the flame, the ionic wind entraining air.

A series of current voltage plots were taken for the flame with and without nitrogen flow. These are presented in Fig. 4.22. The curves indicate that the flame becomes aerated at high voltages and hence burns more fuel and increases the saturation current. Thus no saturation current is reached before breakdown. Quenching the flame with nitrogen decreases the ionisation initially but appears to increase the efficiency of aeration at higher potentials.

In order to gather some data on the transfer of carbon to the top electrodes a series of experiments were carried out with V_{tp} fixed at 3 kV. I_{bt} and I_{tp} were measured as a function of V_{bt} at fixed values of v_g. These are presented as two sets of data; Fig. 4.23 shows current voltage plots of I_{bt} and I_{tp} versus V_{bt} at fixed V_{tp} and varying nitrogen flow velocity. Fig. 4.24 shows plots of I_{tp} versus nitrogen flow velocity at fixed V_{bt} and V_{tp}.

During these experiments the majority of carbon was deposited on the top electrodes and very little on the burner mouths.

To estimate the total rate of ion production as a function of nitrogen flow rate the same data was used to plot graphs of I_{tot} versus flow velocity for fixed V_{bt} and V_{tp}, see Fig. 4.25 and I_{tot} versus V_{bt} for fixed v_g and V_{tp}, see Fig. 4.26.

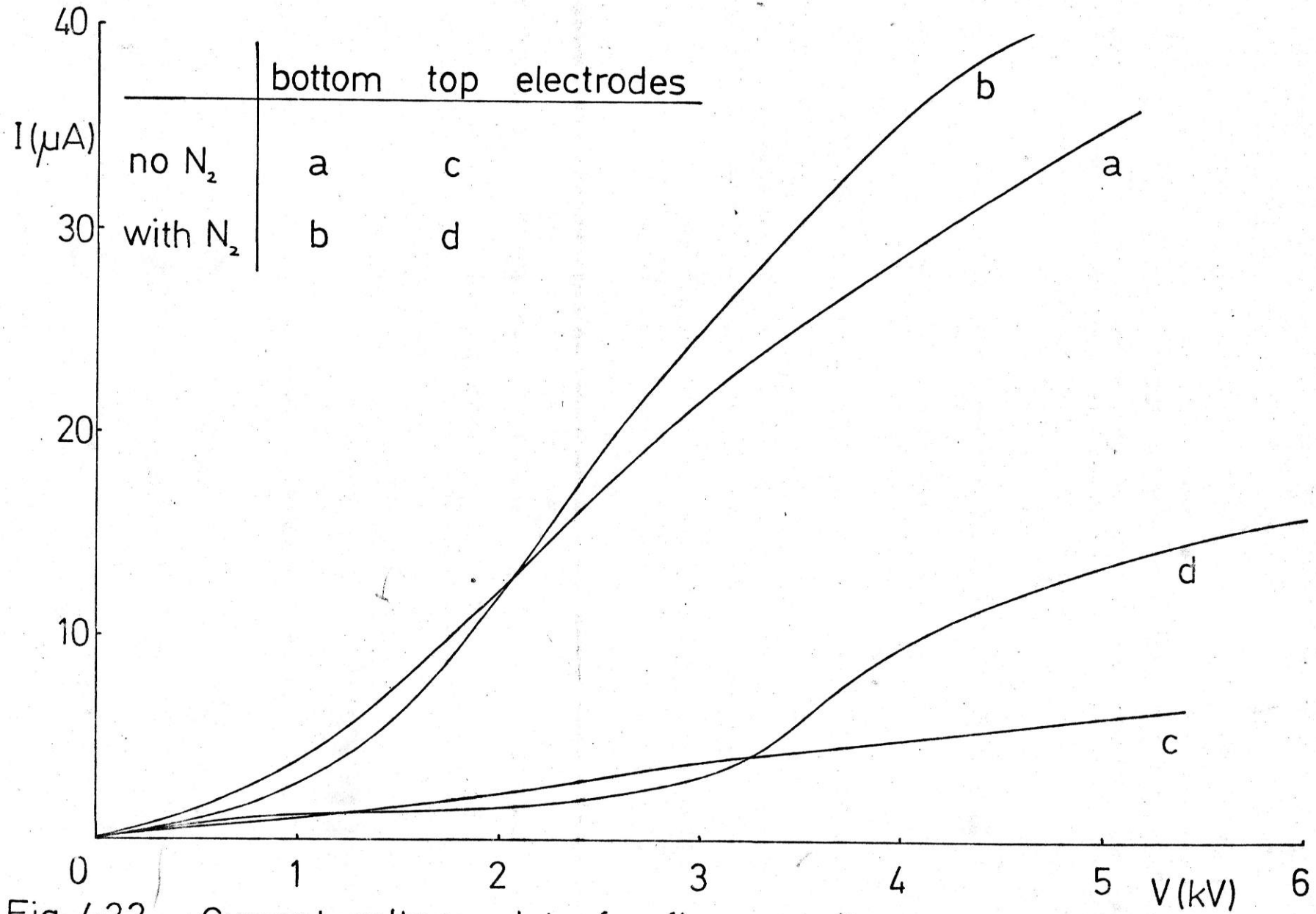

Fig. 4·22 Current-voltage plots for flame ± nitrogen counterflow

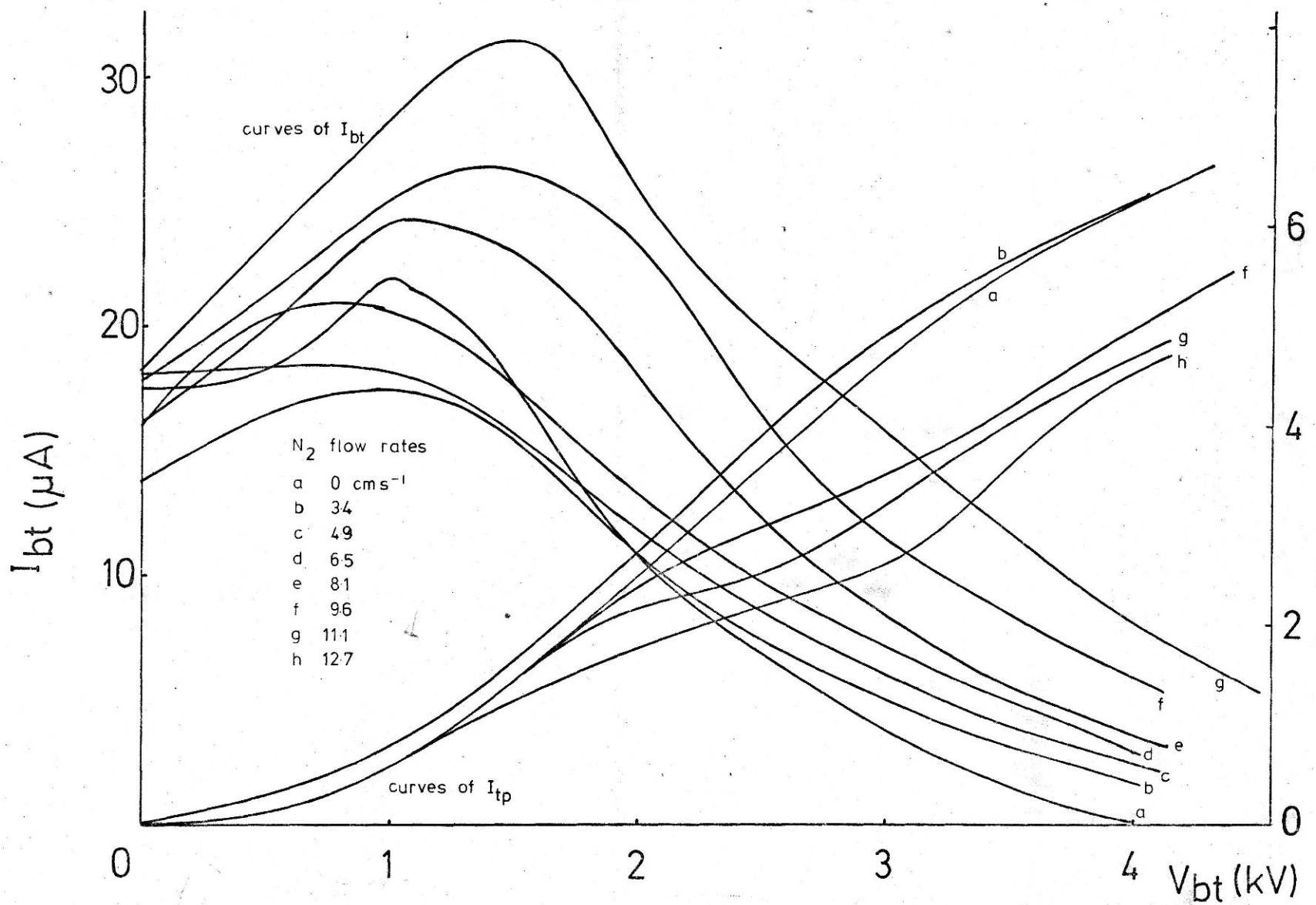

Fig. 4·23 I_{bt} and I_{tp} vs. V_{bt} at fixed V_{tp} and varying N_2 flow rates

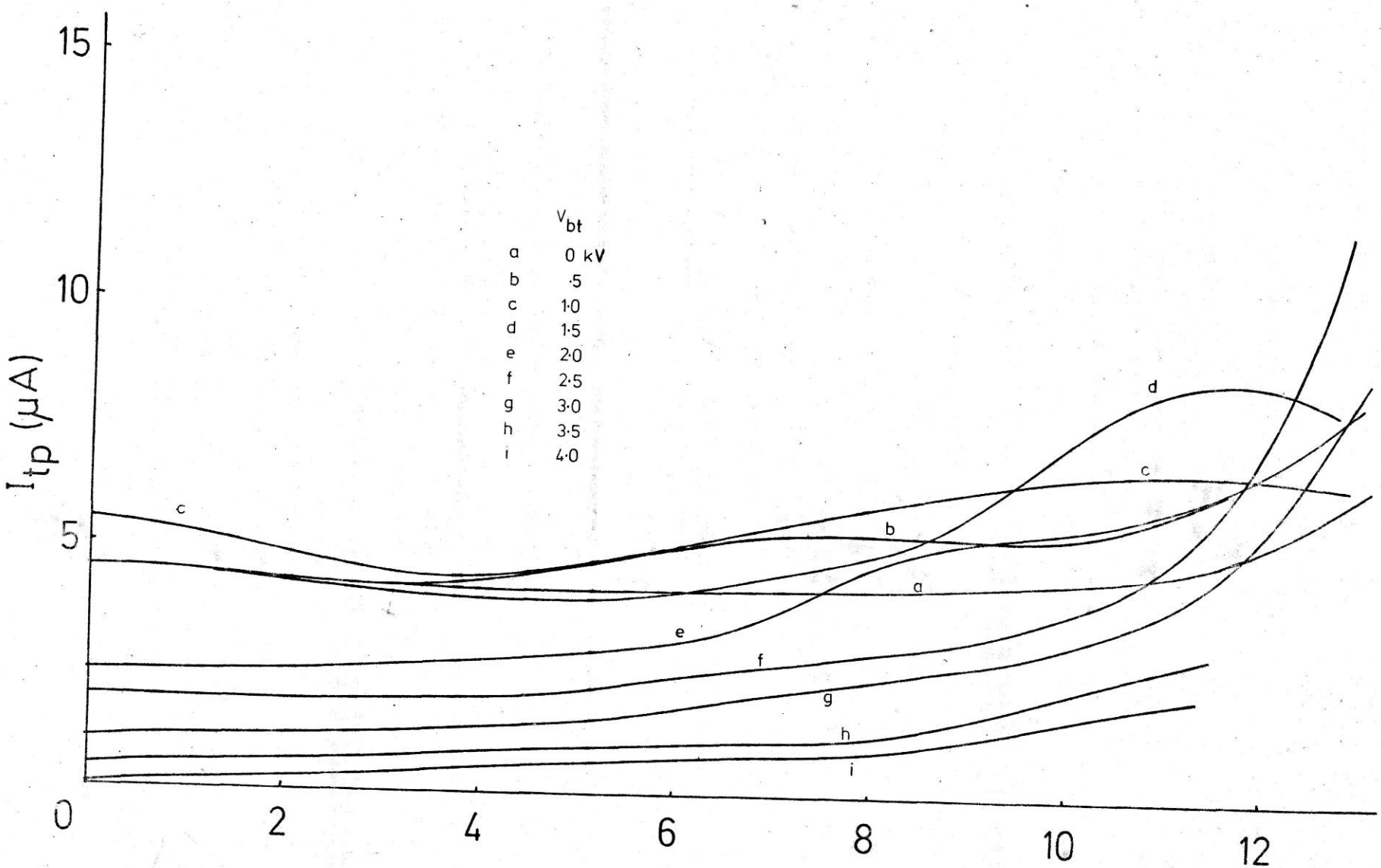

Fig. 4·24 I_{tp} vs. N_2 flow velocity at fixed V_{bt} and V_{tp}

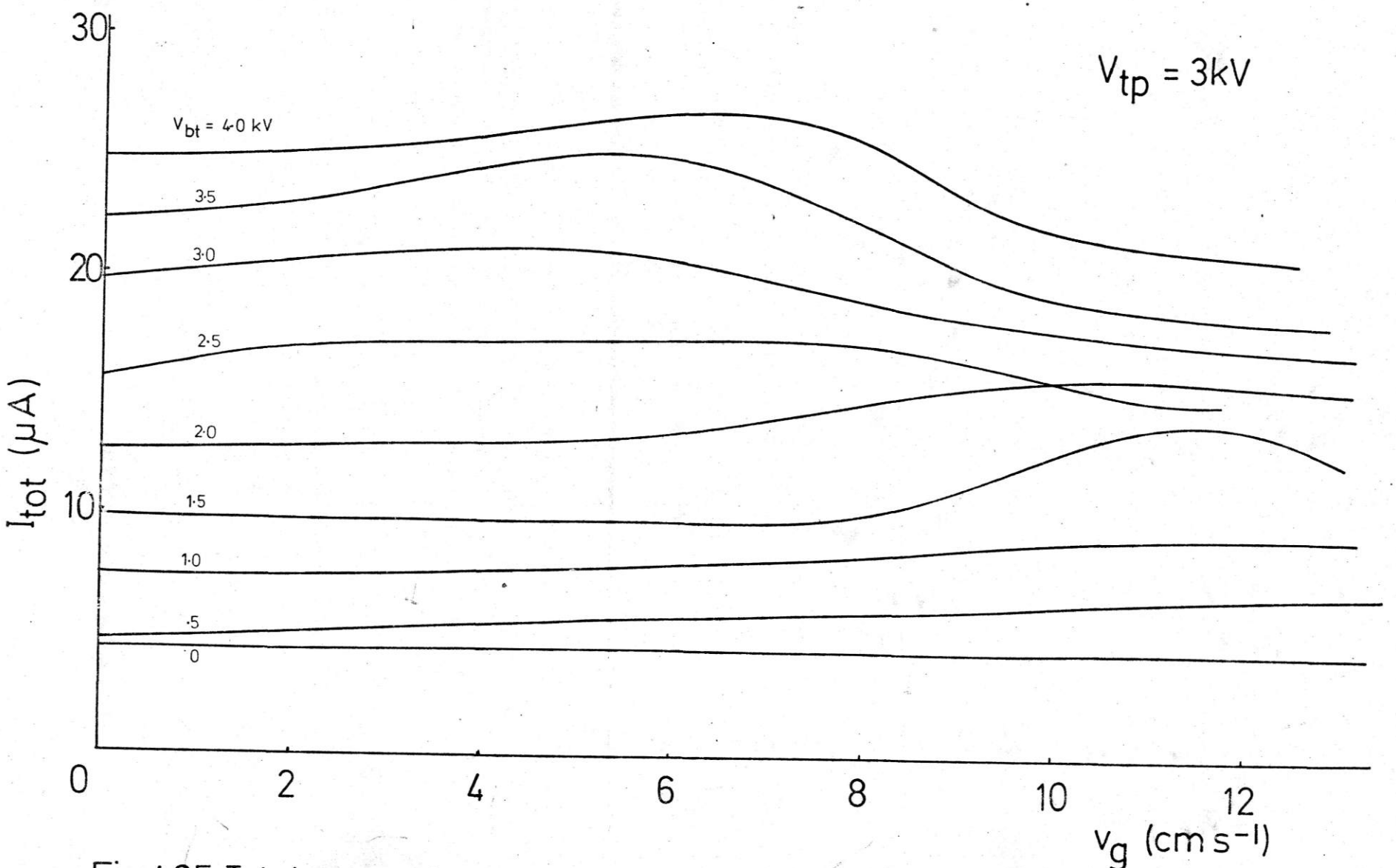

Fig.4·25 Total current vs. N_2 flow at fixed V_{bt} and V_{tp}

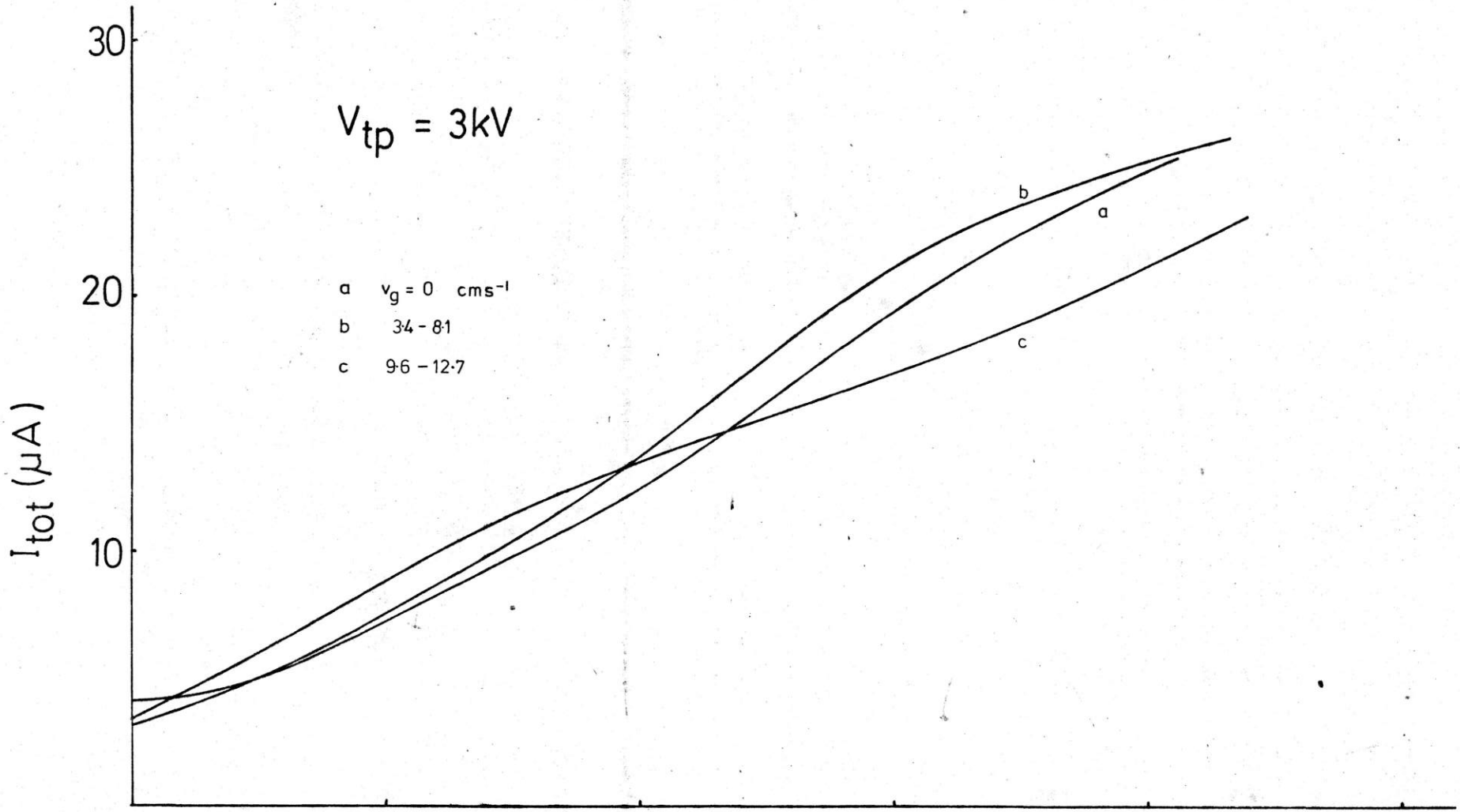

Fig.4·26Total current vs. V_{bt} for fixed N_2 flow and V_{tp}

It is evident from Figs. 4.25 and 4.26 that the rate of production of varies little with nitrogen flow velocity up to 8 cm s^{-1}, at this point it falls off. This only affects the current at high voltages ie. when saturation would normally occur. No plateau occurs because the flame is rich. Increased aeration at high voltages increases the rate of production of ions and hence saturation current. However, the points showing I_{tot} reduced by high nitrogen velocity must be the true saturation current at this degree of aeration and cooling. It can be seen from Fig. 4.26 that the scatter of points starts to occur at V_{bt}= 2.5 kV. This is probably the potential at which saturation sets in and the measured current is representative of total ion production.

The data presented may be used to obtain the mobility and spread of mobilities, and hence data on the particle radii assuming unit charge, of the carbon particles produced during the experiment.

The maxima in the plots of I_{tp} versus V_{bt} at fixed v_g and V_{tp} in Fig. 4.23 are interpreted as being the maximum transference of carbon to the top electrodes, ie. when the ion drift velocity equals the counterflow nitrogen velocity. Mobilities can be worked out from these parameters.

$$k = \frac{v_g}{X_{bt}}$$

The figures obtained are in reasonable agreement at higher nitrogen velocities when transfer would be expected to be more efficient. The mean of 12·1 x $10^{-3} cm^2 s^{-1} V^{-1}$ is also

in good agreement with published figures[2].

Nitrogen veloc.	V_{bt}	X_{bt}	k
3·4 cm s^{-1}	1 kV	·56 kV cm^{-1}	6·1 x 10^{-3} $cm^2 s^{-1} V^{-1}$
4·9	1	·56	8·8
6·5	1	·56	11·7
8·1	1·2	·67	12·1
9·6	1·5	·83	11·6
11·1	1·6	·89	12·4
12·7	1·8	1·0	12·7

Data on the distribution of mobilities may be obtained from Figs. 4.24 and 4.25. The proportion of current transferred to the top electrodes by the counterflow of nitrogen is given by

$$p = \frac{(I_{tp})_{v_g} - (I_{tp})_{v_g=0}}{I_{tp} + I_{bt}} \quad \ldots\ldots\ldots\ldots \quad 4.36$$

The current transferred to the top electrodes is caused by carbon particles having a mobility up to and including that which gives a drift velocity corresponding to the field strength and nitrogen flow velocity.

$$\text{ie. } k = \frac{v_g}{X_{bt}}$$

A plot of the log of equation 4.36 against this highest mobility is shown in Fig. 4.27. Readings were taken up to k = 8·7 and the graph is linear up to this point. Assuming that the graph represents a distribution of mobilities, and that this distribution is symmetrical about the most probable mobility then the line cannot be extrapolated beyond p = 0·5. This point corresponds to a mobility of

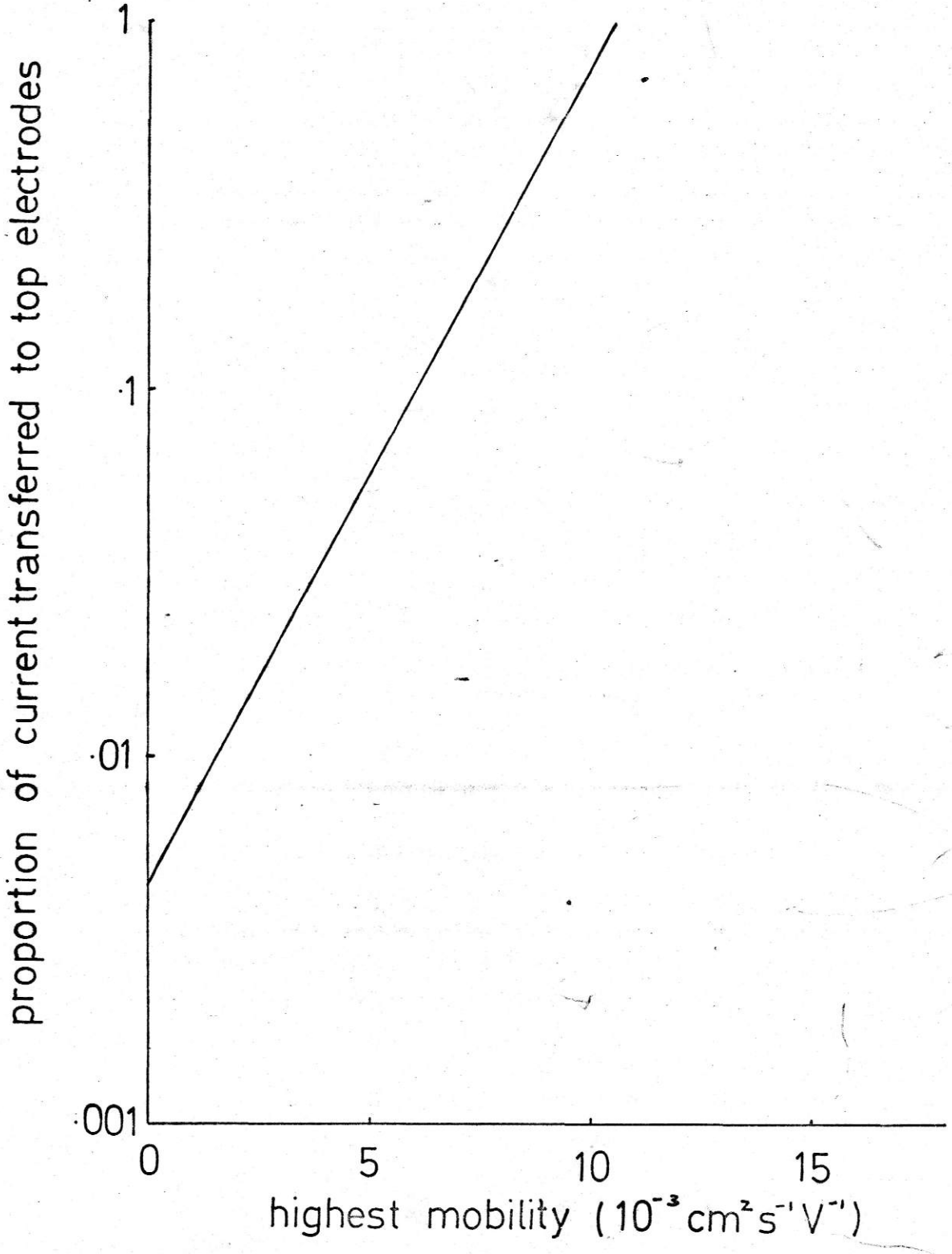

Fig. 4·27 Current transfer - mobility

$9{\cdot}2\ cm^2s^{-1}V^{-1}$.

Now

$$p = \int_0^k n_k\, dk$$

so that $$n_k = \frac{dp}{dk}.$$

From Fig. 4.27:

$$\ln p = h\, k_{max} + b$$

$$\therefore \quad p = \exp(h\, k_{max} + b)$$

hence $$n_k = h \exp(h\, k_{max} + b) \quad \ldots\ldots\ldots\ldots\ldots\ 4.37$$

Values for n_k up to the most probable mobility of 9·2 were calculated using equation 4.37. The probability curve was assumed to be symmetrical and the results are presented in Fig. 4.28. Particle size distribution deduced from the mobility according to Mayo and Weinberg[2] is also shown. This value for the mean mobility obtained here is in reasonable agreement with the mobility obtained from Fig. 4.23 considering the assumptions involved. One of the major assumptions which is almost certainly not valid is that it is assumed in Figs. 4.27 and 4.28 that all the current is carried by carbon particles. This is almost certainly not the case but the general conclusions are perhaps not invalidated if the mechanism of the increase in I_{tp} is considered. During the transfer of carbon particles to the top electrodes under the influence of V_{bt} and v_g the particles have an appreciable momentum and will entrain other parts of the flame and cause the flame to shift generally towards the top electrode.

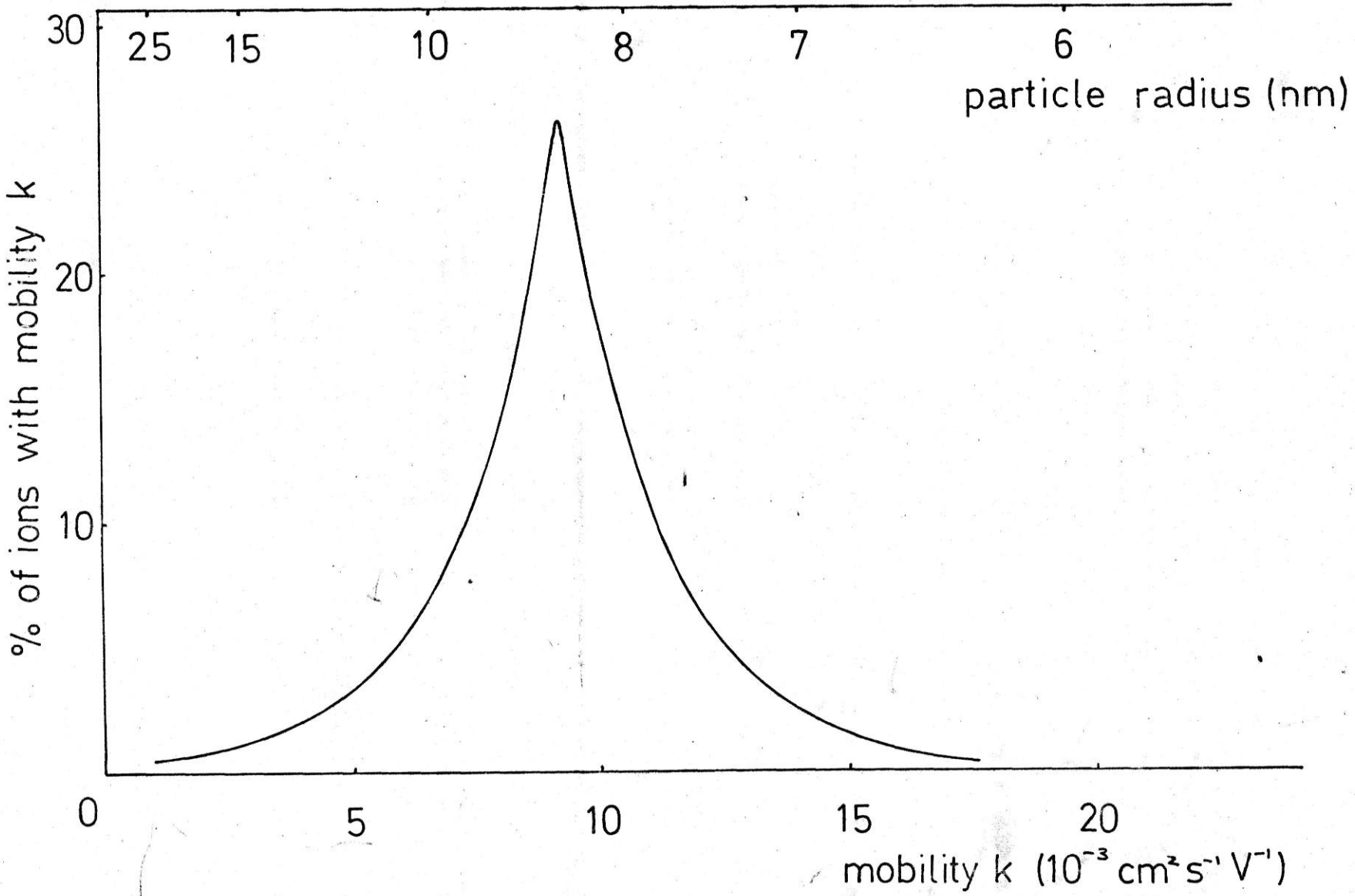

Fig. 4·28 Distribution of mobilities and particle radii

This will have the effect of increasing the current transferred to the top electrodes but this increase will reflect the increase in transfer of carbon to the top electrode.

The counterflow of nitrogen against the drift of carbon particles in an electric field in order to transfer them to collecting electrodes is seen as a possible method for removing soot from flame products. It could, however, only be of practical use under certain circumstances and in cases like the internal combustion engine it could not be used at all.

4.5 CHARGING THE PARTICLES WITHOUT USE OF THE FLAME'S OWN CHEMI-IONISATION

It has been shown in the previous sections that while it may be more efficient to use parent flame ions as a means of manipulating particles it is not always practical or even possible under certain circumstances. These include internal combustion engines and industrial applications where the products have cooled sufficiently to allow recombination to occur and where it is usually not possible to apply electrodes directly to the flame itself.
Hence it was decided to devise a system for charging uncharged carbon particles and then manipulating them.

4.5.1 USE OF A CORONA DISCHARGE

The use of a corona discharge to generate charge for attachment to particles is in common use in 'electrostatic' precipitators. It is, however, very inefficient due to its wastage of the charge generated. A great deal of power is required to ionise the gas in a corona discharge, following which the majority of the free charges created flow to the opposite electrode without attaching, their great velocity being a necessary consequence of the high fields required to reach breakdown; though a limited amount of slowing down can be arranged by causing the field lines to diverge. A quantitative idea of this may be obtained when it is considered that 'electrostatic' precipitators operate at mean field strengths of around 10 kV cm^{-1} whereas other sources of charge will operate at field strengths as low as 400 V cm^{-1} for the same rate of production of charge.

4.5.2 USE OF A SECONDARY FLAME

It has been shown[7] that a small secondary flame will act as an ion source for charging by attachment. The power input required would be considerably smaller than that required for a corona discharge producing a similar number of charges. This apparent efficiency is increased even further when the probabilities of attachment of the ions to carbon particles are considered, also charging in this manner produces one charge per particle[2,7] thus reducing the charging power still further. This can be demonstrated by the following example.

Consider an ethylene/air flame as the source of charge; a stoichiometric ethylene/air flame will give a current of 100 μA cm^{-2} at a burning velocity of 68 cm s^{-1} [75] being equivalent to 14·3 W cm^{-2}. A further ·7 W cm^{-2} would be required to charge and deposit the particles at a rate of 6·3 x 10^{14} particles s^{-1} cm^{-2} assuming unit charge per particle, ie. requiring 2·2 W/10^{14}particles deposited/second. This compares favourably with the figure for 'electrostatic' precipitation of 6 W/10^{14}particles/second[76].

The experimental system for the flame precipitator used by Hardesty and Weinberg[7] is shown in Fig. 4.29. Results obtained together with a discussion on the mechanism of particle charging is also to be found in this reference.

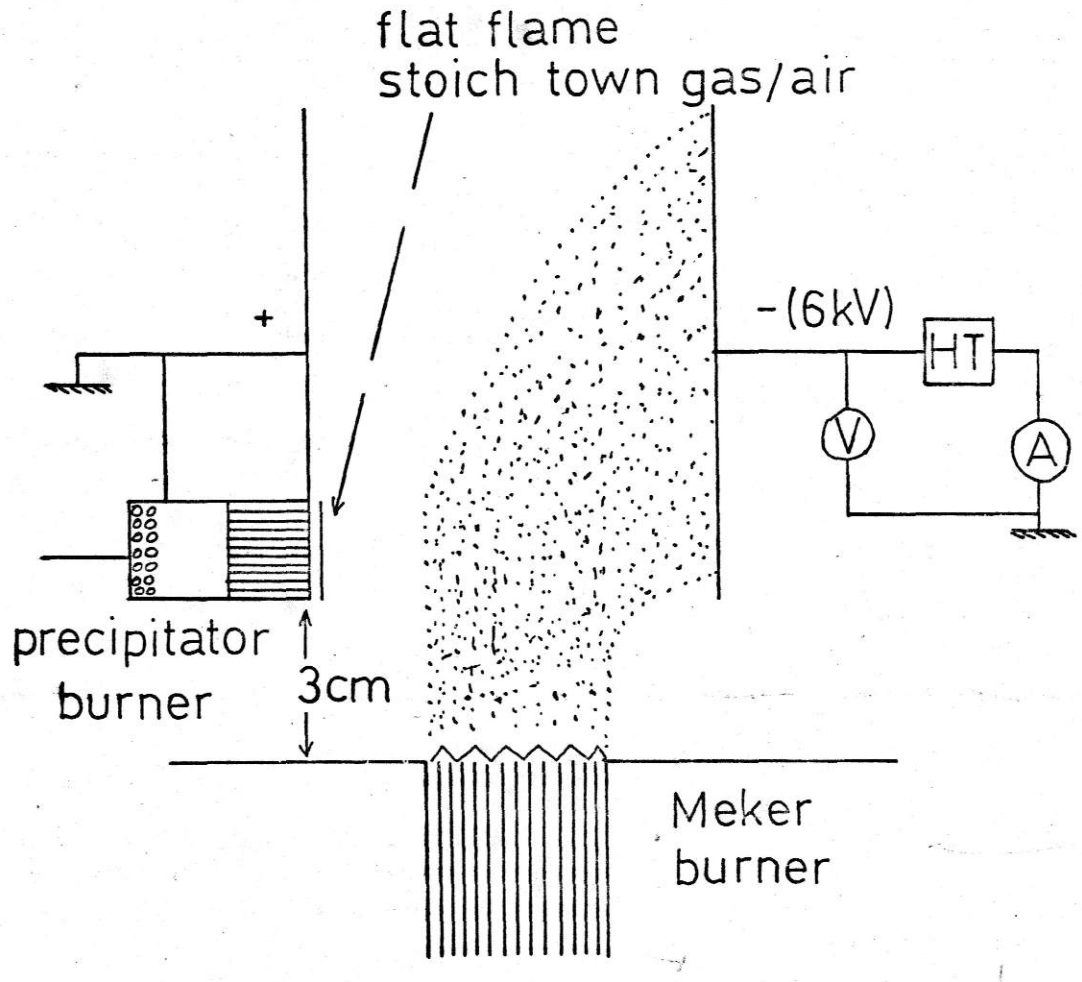

Fig. 4·29 Flame precipitator

4.5.3 USE OF HOT PLATES AS AN ION SOURCE

It was shown in section 2.1 that hot surfaces, particularly those containing alkali metal ions, are good positive ion sources. It was decided to investigate the possible use of these as an ion source for attachment to carbon particles in a precipitator.

Stainless steel plates were used in an attempt to cut down corrosion problems and the plates were coated with a potassium compound, which behaved as the ion source. Some difficulty was experienced in choosing the best compound, the final choice of potassium chromate being a compromise between availability, having a high enough melting point and being non-corrosive. It was applied to the plates by dissolving in water containing a wetting agent and painting the solution on to the plates which were then gently dried over a small flame. The first experiment was to determine the maximum current obtainable from the plates at working temperatures. The apparatus used for this together with the plate configuration used is shown in Fig. 4.30.

The plates were heated with an ethylene-air flame at the following flow rates,

Air 325 $cm^3 s^{-1}$

Ethylene 62.

In order to reduce heat losses by radiation a total of seventeen plates were used with ·5 cm spacing. With this configuration the maximum plate temperature obtained was estimated at 1200°C. With an applied potential of 200V

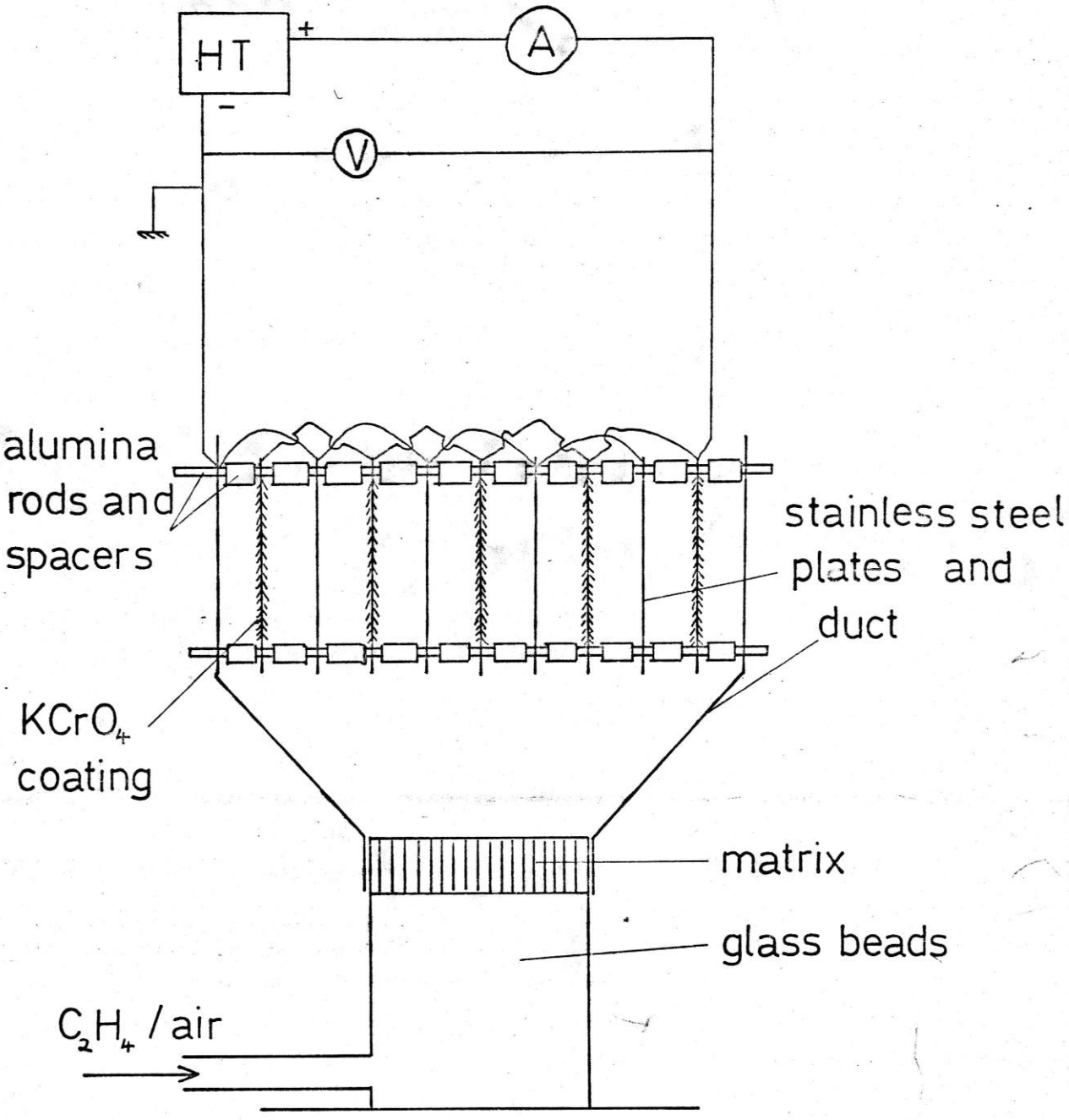

Fig. 4·30 Apparatus to measure the current available from hot plates

(400 V cm^{-1} mean field strength) the measured current was 200 mA. This was the maximum that could be obtained before breakdown. The total conducting area was 800 cm^2 so this current corresponds to the theoretical maximum of ·25 mA cm^{-2} in air[41], although this latter figure is taken at STP so it seems likely that some 'silent' secondary ionisation was occuring at the electrodes. None the less the usefulness of the system can be seen when these large ion currents are obtained at such low potentials.

A simple calculation was performed to determine the best electrode spacing. Assume a stream of carbon particles of mobility k moving in a gas stream with velocity v_p. The electrode separation is d and the length of collecting electrodes parallel to the flow direction is L. Then the minimum field induced ion velocity for 100% particle collection v_{min} is given by:-

$$v_{min} = \frac{v_p d}{L} \qquad \ldots\ldots\ldots\ldots\ldots\ldots \quad 4.38$$

However v_{min} is controlled by the applied voltage V so that:-

$$k = \frac{v_{min} d}{V_{min}} \qquad \ldots\ldots\ldots\ldots\ldots\ldots \quad 4.39$$

combining and rearranging gives:-

$$v_p = \frac{L V_{min} k}{d^2} \qquad \ldots\ldots\ldots\ldots\ldots\ldots \quad 4.40$$

Now the current-voltage-electrode spacing relationship for positive ions produced from hot plates is given by[37]

$$j = \frac{9k\ V^2}{32\pi d^3} \qquad \ldots\ldots\ldots\ldots\ldots\ldots \quad 4.41$$

so that for a given j_{max} V^2/d^3 is constant.

Substituting for V gives:-

$$v_p = \frac{kLB^{\frac{1}{2}}}{d^{\frac{1}{2}}} \qquad \ldots\ldots\ldots\ldots\ldots\ldots\ldots\ldots \quad 4.42$$

where B is a constant.

Hence, the smaller the electrode separation, the more efficient the precipitator. This is also true from the point of view of radiation losses from the plates, however, if the plates are positioned too close together the light fluffy carbon deposit builds up and eventually shorts them out. In view of this a compromise separation of 2 cm was chosen as optimum.

Using this separation the minimum voltage for 100% precipitation may be calculated for a particular flame. Consider a flame with S_u = 30 cm s^{-1}, typical for a sooting flame, see section 3.3. If the products are allowed to undergo a fourfold expansion and their temperature is assumed to be 1700°K after heating the plates, then the particle velocity, v_p, is 45 cm s^{-1}. Assuming L to be 10 cm and the mobility 5 x 10^{-3} $cm^2 s^{-1} V^{-1}$ [2], then using equation 4.40 gives the mimimum potential as 3·6 kV. It was found in practice that 3 kV was the maximum potential that could be applied before breakdown so that 100% efficiency could not be achieved.

The final precipitator arrangement is shown in Fig. 4.31. The plates were heated from one side and the soot introduced from underneath using a benzene in nitrogen diffusion flame (6 $cm^3 s^{-1}$ benzene in 10 $cm^3 s^{-1}$ nitrogen). The effect of applying a field to the plates is shown in the photographs

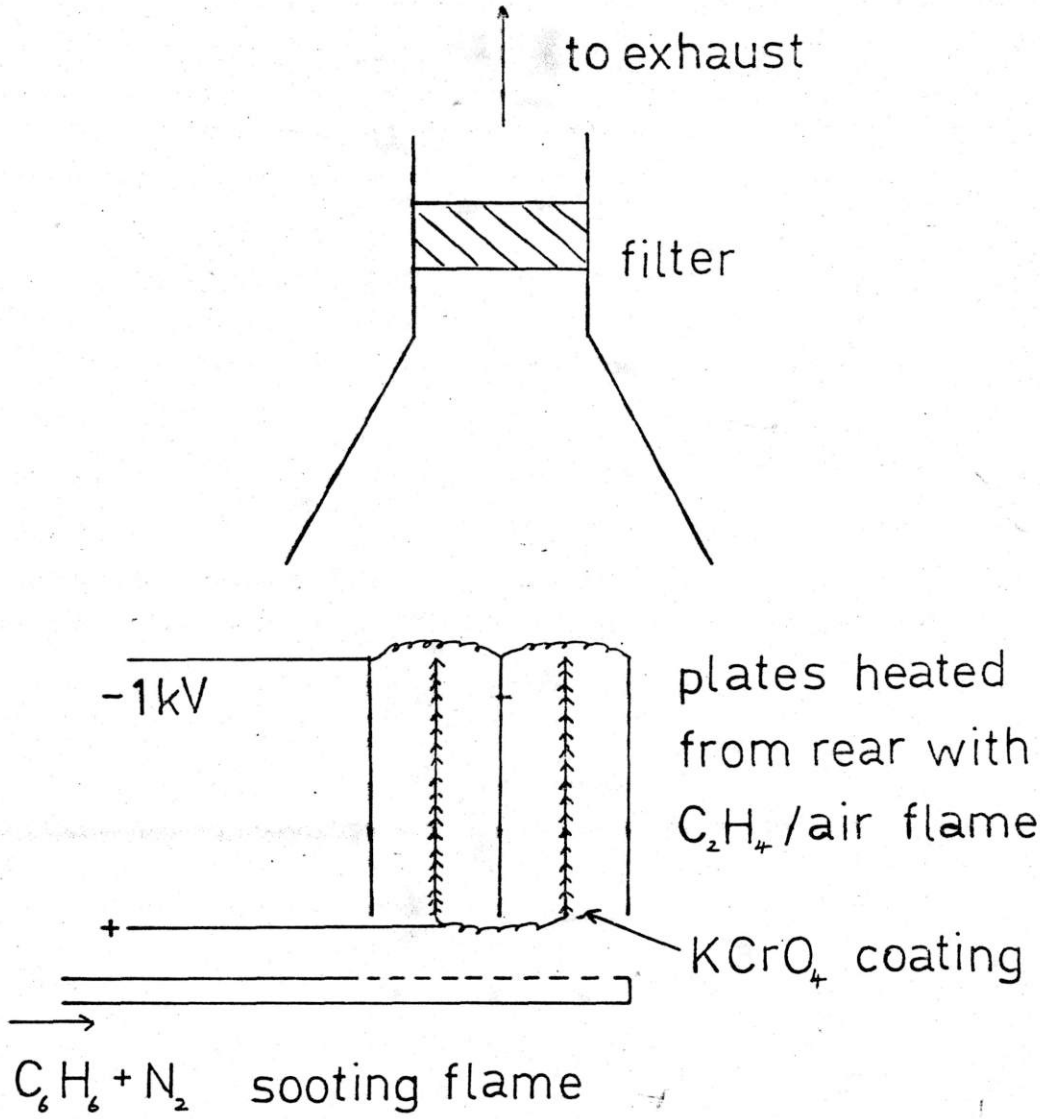

Fig. 4·31 Hot plate precipitator

of Fig. 4.32. To measure the precipitator efficiency a filter was included in the exhaust and the deposit on the plates was weighed. Over a series of runs an average of 7 mg min^{-1} was collected in the exhaust with no applied field and 5 mg min^{-1} on the plates with 2·1 in the exhaust with a field applied, giving an efficiency of 71%. This can be considered reasonable when it is taken into account that the configuration used made 100% efficiency an impossibility. Also the plates were hotter in the centre than the edges and some soot may have escaped this way.

4.5.4 DISCUSSION OF METHODS OF PRECIPITATION

The three methods of precipitation described above are perhaps not as distinct as it may seem and in practice a combination of these may be found to be more suitable. The most efficient method of precipitation would be to use plates in the hot products to be cleaned so that they provide the heating for the plates. It may be necessary to use a separate collecting field or probably longer path lengths within the plates to achieve 100% efficiency.

However, under most circumstances it may not be possible to heat the plates sufficiently in this way eg. for precipitating acid smut in a power station exhaust. Here the exhaust temperature is only of the order of 200°C so that an external heating source would be required. Heating the plates electrically would probably make it more expensive than using a corona discharge but if fuel was used only a small flame would be needed and it could be fairly cheap. If this

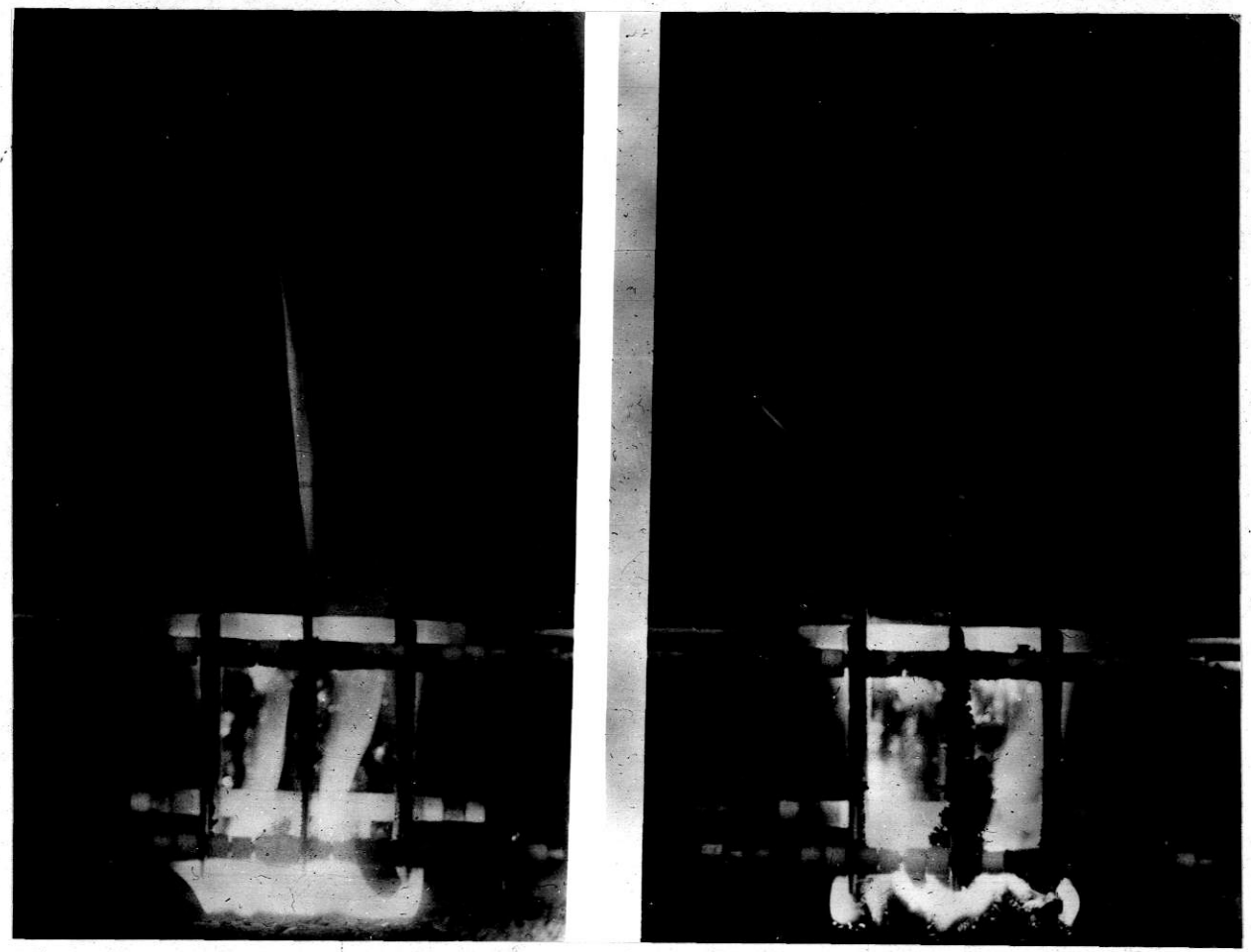

a b

Fig. 4.32 Hot plate precipitator a) no field b) with applied field.

second flame were used it could be done in one of two ways. The flame could be made to sit on the electrodes and so heat them to provide ions or it could be used as an ion source itself, thus only heating the gas, which would be more efficient. If it heated the electrodes it would be a combination of these. If the flame is stabilised on a porous burner which is also the emitting electrode then the distiction merely becomes a difference in gas flow velocities.

By using hot electrodes breakdown would occur at lower voltages so that in some cases secondary ionisation might be used as an alternative source of charge. In this system a combination of all three methods could operate.

Whatever method of precipitation is used there always remains the problem of removing the collected soot from the electrodes. This is done mechanically in industrial precipitators by rapping the electrodes. In some cases where a cycle of fuel rich - air rich operations is envisaged, eg. an internal combustion engine it would be possible to burn the carbon off the plates. The soot deposits in the fuel rich cycle and burns off in the air rich cycle. In other applications the injection of excess air into the exhaust could be made to burn off the deposited carbon.

4.6 GENERAL CONCLUSIONS

There is no difficulty in manipulating charged particles, the field, mobility and charge acquisition are all parameters which can be calculated and are well known[41]. The only limitation to practical effects is the breakdown strength of air. This is related to current density and electrode spacing by equation 4.24

$$x_b^2 = \frac{8\pi jy}{k} \qquad \ldots\ldots\ldots\ldots\ldots\ldots \quad 4.24$$

From this other maxima may be calculated, if the mass and mobility of the particles are known then the maximum mass deposition rate can be calculated as can the maximum ionic wind velocity[41].

The practical problem, in the work discussed in this chapter, has been to discover the most efficient way of producing the charged particles in a position where they may be collected on electrodes.

The most efficient way of doing this would be to make use of the parent flame ions. These are a necessary consequence of combustion of hydrocarbons and would merely recombine if not perturbed. It was shown in section 4.1.4 that it is impractical to collect soot on electrodes at large distances from the flame due to breakdown at the electrodes. Section 4.2 dealt with the application of a field directly to the flame products; this proved impractical because the soot particles recombined rapidly before the collecting electrode space was reached. Section 4.3 described an attempt to apply a small perturbing field to the flame to initiate the

separation of charge in order to prevent early recombination. This was found to be impractical because of space charge, the separated ions just going to the perturbing electrodes.

Section 4.4 described the transference of the charged carbon from the flame into a carrier stream for later deposition. This was found to be a practical solution, but one with few possible applications because of the complexity of the design and the need to apply a field directly to the flame.

In section 4.5 various methods of particle charging and precipitation were considered. These methods seem to offer the best solution. The most efficient way would be to use the hot products to heat plates which could then be used as an ion source, some plate materials contain alkali metal impurities anyway thus obliviating the necessity to maintain a coating on them. If this becomes impractical because the device can only be positioned in the cold product region then a separate flame could be used as the ion source, or less efficiently to heat emitting plates. Alternatively the least efficient method would be to use a corona discharge. This could be done at hot electrodes, giving a lower breakdown field and so a combination of all three methods could be an effective way of charging particles for precipitation. The efficiency of the various methods may be compared numerically. For a corona precipitator the power requirement is 6 W/10^{14}particles/second compared to 2·2 W for a flame precipitator and ·11 W for plates heated by the product stream.

CHAPTER 5

THE EFFECT OF ELECTRONS ON THE EMISSION OF SOOT FROM FLAMES

The effects of additives on soot formation in flames has been studied by several workers[14-16,18,19,67]; the most effective additives have generally proved to be substances which have low ionisation potentials or form particles of low work functions. Thus it has been known for a long time in the carbon black industry that the alkali metals, when introduced in parts per million, alter the 'structure' of the black and that the effectiveness of the additive in breaking long chains is in the inverse order of its ionisation potential. It has been found that, although the order of effectiveness within each group of elements is determinded by the ionisation potential, this does not apply across groups, the alkaline earths, for example, differing from the alkali metals, barium additives which produce $BaOH^+$ as the positive ion being the most effective. It has also been found that the same additive can produce suppression of soot formation, or its promotion, depending on the amount and the position in which it is introduced. Where the position of addition is not localised, the pattern is that small amounts of additive produce promotion whilst large amounts produce suppression with a cross-over point of zero effect inbetween. When the additive is introduced locally - e.g. on a wire - insertion at the base of the flame produces suppression while introduction higher up results in an increase of soot produced[19].

Chemical as an alternative to electrical effects have been considered responsible for these observations[18]. Since electronic structure is inevitably related to chemistry, the issue is most likely to be resolved by the application of electric fields. Different groups of workers, however, have used either additives, or applied fields - not both simultaneously. In what follows a hypothesis is proposed based on free electrons and then tested by the combination of the two techniques. Although the results bear out the hypothesis and, furthermore, offer a novel practical method for controlling soot emission, this does not, of course, constitute a proof that chemical effects could not also be important.

5.1 HYPOTHESIS

The great majority of this work has been carried out in diffusion flames, ie. flames in which the reactants are initially separate, the maximum temperature and the main reaction zone occuring close to the stoichiometric contour. Now this is also close to the surface along which ionisation will peak, being a strong function of temperature. It is not, however, the region of carbon formation, since conditions for pyrolysis are most favourable on the fuel side, where there is a lack of oxygen. Thus if ionisation is to play a major part in soot formation, the diffusion coefficient of the charge carrier must be a most important parameter. Of the particles involved, it is the electron that has by far the largest diffusion coefficient and it is known that the negative charge carrier in the high temperature zones

of flames is an electron[41]. It is therefore supposed, as an initial hypothesis, that the effect of additives is entirely due to the free electrons which they produce. An attempt is then made to account for all previous experimental observations in terms of such a hypothesis and, if that is successful, some further crucial experiments are designed.

Although the chief role of an influx of additional electrons into the pyrolysis zone is likely to be that of neutralising positive charges, this can have two diametrically opposed end results. Where all or most of the particles[2,5,41], or chains of particles, are positively charged, neutralisation of positive charges at their extremities would stop them repelling one another and thereby remove the obstacle to agglomeration. Agglomerates of appreciable size are much less likely to burn away during their subsequent passage through the high temperature zones in the presence of oxygen. When only a fraction of the chains is charged, on the other hand, agglomeration occurs by dipole action, the rate reaching a maximum when the fraction charged is a half. For smaller proportions of charged particles, electrons will therefore decrease agglomeration rates.

This proposition actually accords extremely well with the observed facts. These are best discussed in terms of the results presented in Fig. 5.1[67]. The fundamental parameters are the particle radius and number; the mass is a consequence of these. The facts requiring explanation are:-

1) particle radius always decreases with amount of additive
2) a peak in particle number occurs
3) additive reduces the length of chains.

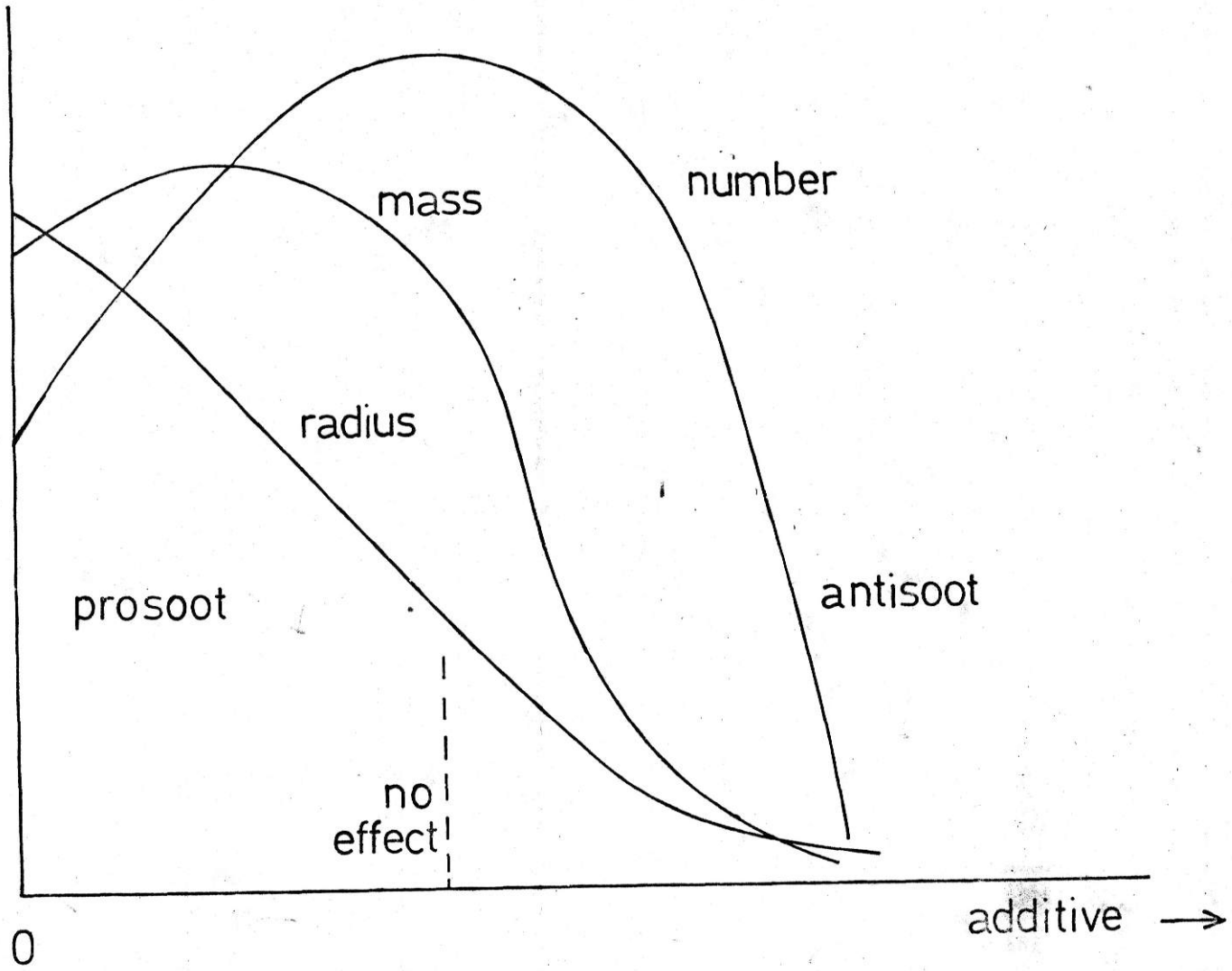

Fig. 5-1 Particle parameters - additive concentration

The rate of nucleation of particles is assumed to be constant and unaffected by the additive and the particles are all assumed to bear an initial positive charge - this being lost through recombination. Particles continue to grow on the surface, regardless of charge, thus increasing their diameter until agglomeration and chaining occur. The rate of agglomeration and chaining depends on the proportion of charged particles present and is at a maximum when this equals a half.

The introduction of large electron concentrations neutralises all particles and prevents agglomeration. The particles grow no further than the limiting size before agglomeration occurs and so most burn up giving a small number of small particles.

The peak in particle number must occur because fewer particles are being burnt up. This must be caused by an increase in chain size - if the chains are shorter then they must be composed of larger units caused by increased agglomeration before chaining.

The introduction of small electron concentrations reduces the charge on particles and promotes agglomeration and chaining. Because this now occurs more quickly particles grow to a larger size by agglomeration before forming chains - also the number of chains growing will be increased. Once a chain has started growing there is little likelihood of it combining with another chain, irrespective of whether its growth has been terminated by an electron. The maximum number of

particles must correspond to the maximum rate of agglomeration and chaining.

With no additive agglomeration and chaining occur more slowly, the rate being controlled by 'natural' recombination of particles. The chains formed are longer and thinner made from particles with the largest fundamental radius. Some chains burn up.

Reduction of particle size is explained by the earlier onset of agglomeration and chaining and by increased burning rate when agglomeration and chaining does not occur.

Large electron concentrations will eventually always inhibit agglomeration and thereby suppress soot formation. Electron concentrations insufficient to neutralise a very large proportion of particles under conditions where the majority of particles is charged will act mostly as a 'glue' in encouraging small particles to aggregate and thereby increase the mass of soot escaping.

The dependence on the mobility of the positive ion also falls into place, although the role attributed to it is diametrically opposed to what has been supposed hitherto. In terms of the above hypothesis, the positive ion act chiefly through recombining with the electrons it meets away from the high temperature zone (it is of course much more likely to encounter an electron than a carbon particle). The larger the ion the smaller its excursion.

Although this tentative hypothesis thus accounts for all the experimental observations, a much more direct test would be one in which the additive would be discouraged from migrating by being held on a wire at a relatively low temperature, whilst the charges emanating from it could be controlled by an electric potential applied to the wire.

5.2 SUPPLEMENTARY EXPERIMENTS

Nichrome wires coated with barium oxide and uncoated wires of 0·2 mm diameter were inserted at various heights into diffusion flames of propane diluted with argon, burning with air. The flames consisted of single, approximately flat, faces, which were contrived very simply by attaching a 'fish-tail' nozzle to the fuel burner tube and blowing off the second flame face by an adjacent argon stream emerging from a similar nozzle, see Fig. 5.2. The results are shown in the photographs of Fig. 5.3 and the current-voltage characteristics of Fig. 5.4.

It will be apparent from the photographs that the results are in exact accord with the predictions of the hypothesis in that it is the electron which produces effects characteristic of the additive. At heights where the additive promotes soot formation (Fig. 5.3b as compared with 5.3a) application of a negative potential, encouraging the emission of electrons, greatly increases the effect (Fig. 5.3c) by neutralising charges on already formed agglomerates and chains allowing further agglomeration. (The theory predicts that all chains when fully grown end up charged.) Application of sufficient

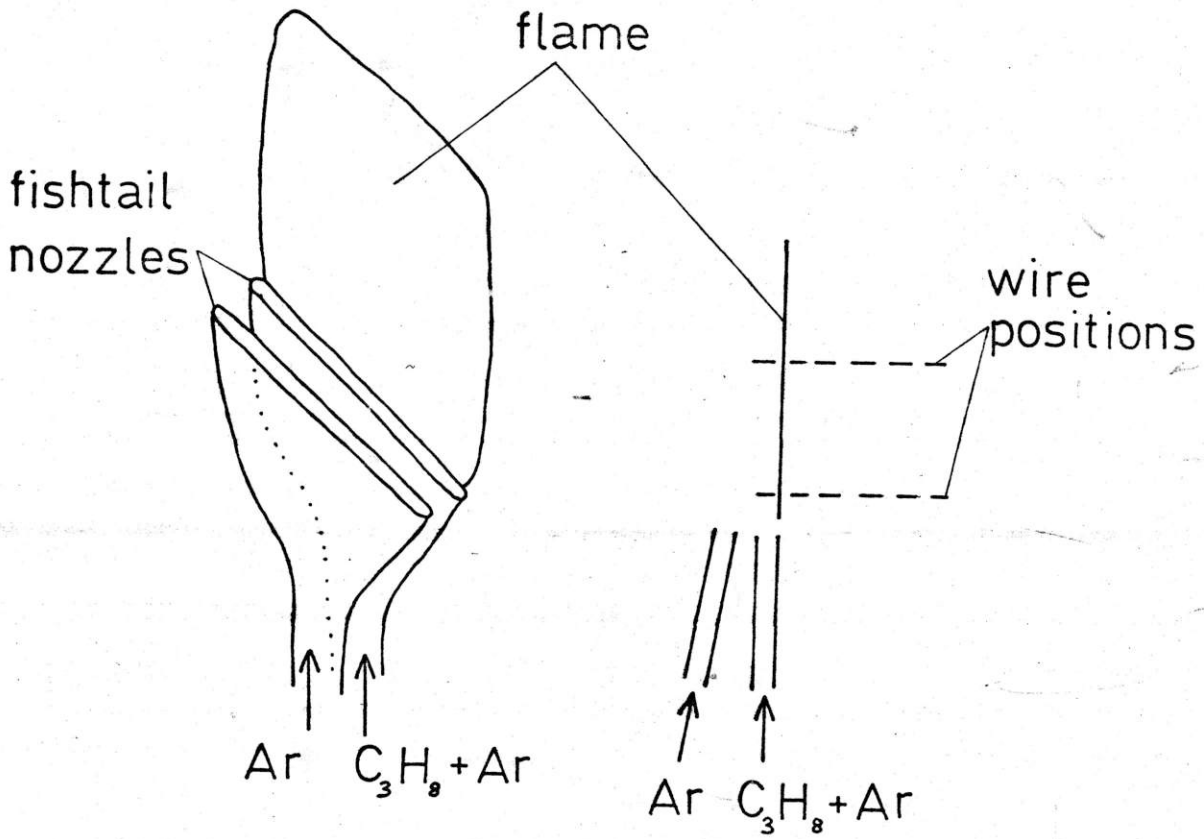

Fig. 5·2 Apparatus to determine the effect of electrons on the emission of soot from flames

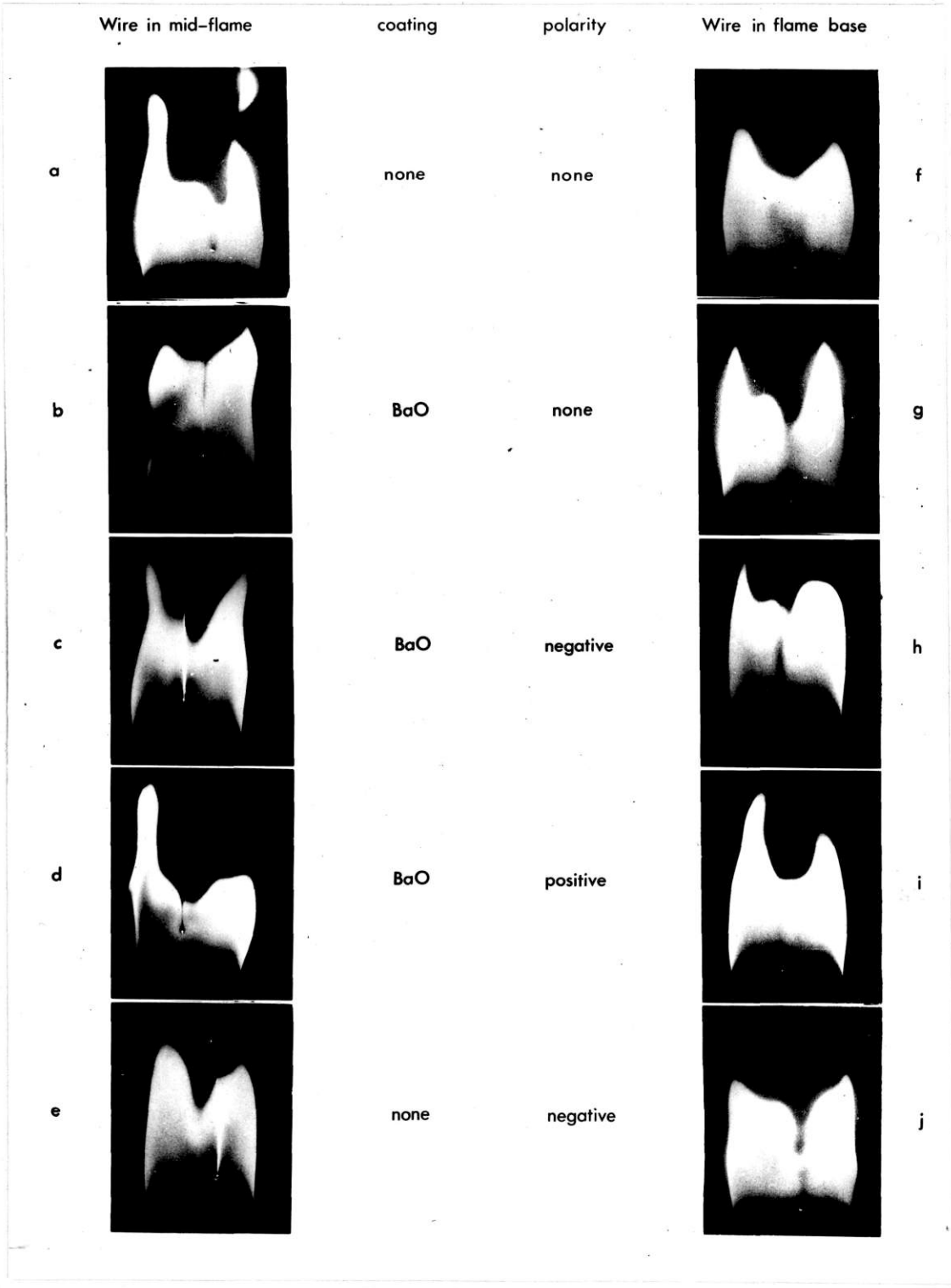

Fig. 5.3 The effect of coating and polarity on soot formation above wires.

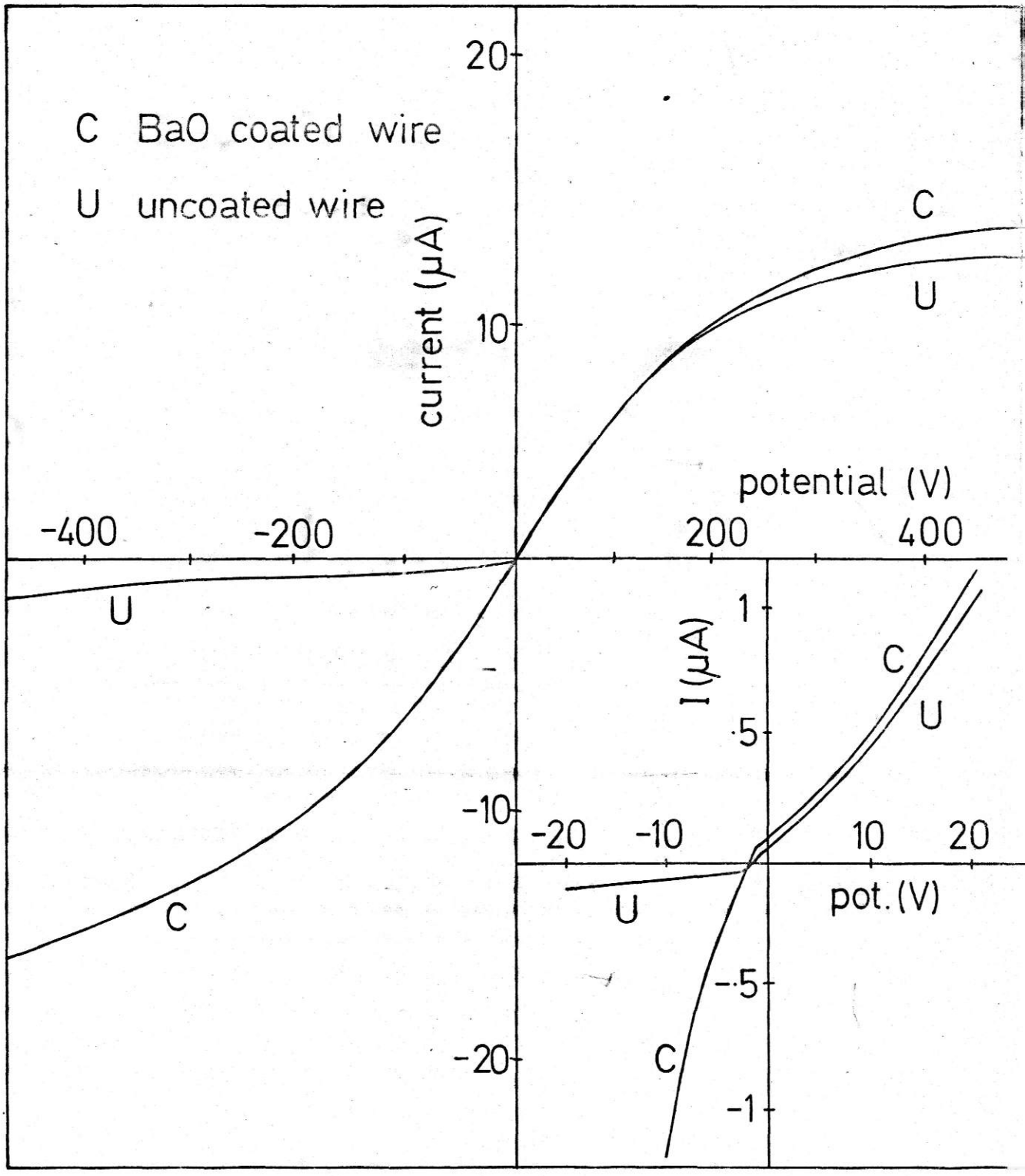

Fig. 5·4 Current/potential characteristics of wires in mid-flame, w.r.t. the burner

positive potential prevents the effect altogether (Fig. 5.3d); removal of electrons causes all particles to end up charged earlier, thus terminating chain development.

It transpired from the voltage-current characteristics that positive potentials not only prevented electron emission but led to the emission of positive ions (Fig. 5.4) and some ionic wind effects came into evidence at higher currents. The absence of soot formation in the case of positive ion emission casts doubt on previous suppositions that positive inorganic ions themselves act as nuclei; they do of course mop up electrons.

It was tried, unsuccessfully, to explain these effects in terms of what is already known about the effects of electric fields on carbon formation. According to this, the negatively charged wire would be expected to collect the positively charged carbon particles - and this is indeed precisely what happens in the case of the uncoated wire (Fig. 5.3e) - rather than to increase soot formation. Once a layer of carbon is built up on the wire, of course, electron emission sets in.

Figure 5.3 (f-j) illustrates the effects observed when wires are inserted into zones in which suppression is produced by the additive in the absence of an applied potential (Fig. 5.3g). Although these are the reverse of the pattern of Fig. 5.3 (a-e) they can also be summarised by the observation that the behaviour associated with additives is manifested by free electrons. Addition of electrons at the base of

the flame reduces the positive particle concentration, preventing agglomeration and chaining and the particles burn up. Removal of electrons from the base of the flame has the opposite effect.

5.3 CONCLUSIONS

It is not intended to suggest that the entire subject of sooting in flames could be accounted for in terms of free electrons and it is thought very likely that the underlying chemical processes retain the importance that has been attributed to them. However, it does appear possible to account for the behaviour of ionising additives entirely in terms of the electrons they produce as regards both suppression and promotion, the effect of the amount of additive, the site of its introduction and the effect of ion size. What is probably much more important is all the observed effects can be produced by controlling the emission of free charges electrically, using coated surfaces maintained hot by the flame, and connected to a source of electrical potential - without introducing additives into the fuel and, thereafter, into the atmosphere by way of exhaust gases. The power that would be involved in injecting electrons in this manner would, of course, be quite small, one milli-amp being sufficient to provide 6×10^{15} particles per second.

CHAPTER 6

CONCLUSIONS AND RECOMMENDATIONS

6.1 CONCLUSIONS

The carbon particles produced, during the pyrolysis of ethylene on hot surfaces, are charged and would be amenable to control by electric fields. Charged particles are also produced during the low temperature pyrolysis of ethylene in a shock tube, suggesting the formation of $C_3H_3^+$. In any event charged particles are produced during pyrolysis of ethylene with and without hot surfaces present and so are amenable to electrical control.

The effect of electric fields on the propagation reaction in sooting flames is less than 10% and so the effect of electric fields on carbon formation is not a manifestation of this. In the case of non-sooting flames the effect of fields on the burning velocity is less than 4%.

Fast electrons have no effect on the burning velocity of hydrogen-oxygen-argon mixtures though this may be because their concentration in the reaction zone is reduced almost to zero.

It is of no practical use to apply fields to flames with large electrode-flame spacings in order to remove particulates. In such a system breakdown is a limitation and the maximum mass collection rate with electrode-flame spacings of 10-100 cm would be $\cdot 5\ \mu g\ cm^{-2}\ min^{-1}$. Application of a field direct to the flame products is also not practical as the soot

particles lose their charge rapidly before the inter-electrode space is reached and attempts to prolong the life of these charged particles failed because of space charge effects.

It was possible to transfer charged carbon particles into a carrier stream and to collect them but this had little practical importance and the principle of having to charge the particles separately was accepted. The most efficient way of charging them would be to use hot coated plates in the product stream maintained hot by the products themselves. A second flame could also be used either to heat the plates or as a source of charge. The least efficient method is to use a corona to charge the particles. These methods are compared numerically; for a corona precipitator the total power requirement is 6 W/10^{14} particles/second compared to 2·2 W for a flame precipitator and ·11 W for plates heated by the product stream.

Electrons were shown to affect soot formation in diffusion flames and it is possible to account for the behaviour of additives in terms of the electrons they produce. The observed effects can be reproduced by controlling the emission of free charges electrically, using coated surfaces maintained hot by the flame, and connected to a source of electrical potential - without introducing additives into the fuel and hence into the atmosphere.

The investigation was instigated to look for methods of controlling flame carbon in a way that would be applicable to practical systems. Two solutions were found based on

different theories but using similar apparatus having coated surfaces heated by the flame. In the first case emitting positive ions using high potentials and in the second electrons using low potentials.

6.2 RECOMMENDATIONS FOR FURTHER WORK

1. Further work should be carried out on the shock tube pyrolysis of ethylene to try to elucidate the ion forming mechanism. This might include work on systems containing no oxygen and following the C_2 and CH concentrations spectroscopically during pyrolysis as well as the ion concentration. On line mass spectroscopic analysis using molecular beam sampling would also be useful.

2. An attempt should be made to perturb the burning velocity of non-sooting flames using electrons excited by an HF field. A DC component added to this field could be used to ensure that the excited electrons had their maximum concentration in the pre-reaction zone.

3. Work should be done on applying the effects of electrons on soot formation to more practical systems. This could take the form of a wire matrix, possibly electrically heated, inserted into the flame base. The possibility of producing enhanced yields of uniform sized soot particles could also be examined.

4. A practical precipitator for use in a furnace exhaust or a car exhaust should be built. An attempt to develop

a suitable plate material should be made; this could be a potassium doped conducting ceramic. The life of such a material should be investigated.

REFERENCES

1. Lawton,J. & Weinberg,F.J., Proc. Roy. Soc. A277 468 (1964).
2. Mayo,P.J. & Weinberg,F.J., ibid A319 351 (1970).
3. Payne,K.G. & Weinberg,F.J. ibid A250 316 (1959).
4. Place,E.R. & Weinberg,F.J., Aeron. Res. Counc. 25560 C.F.C.K. 648 (1964).
5. Place,E.R. & Weinberg,F.J., Proc. Roy. Soc. A289 192 (1965).
6. Place,E.R. & Weinberg,F.J., 11th Symp (Internat) on Comb. 245 (1967).
7. Hardesty,D.R. & Weinberg,F.J., 14th Symp. (Internat.) on Comb. 907 (1973).
8. Howard,J.B., 12th Symp. (Internat.) on Comb. 877 (1969).
9. Homann,K.H. & Wagner,H.Gg., 11th Symp. (Internat.) on Comb. 371 (1967).
10. Bonne,U., Homann,K.H. & Wagner,H.Gg., 10th Symp. (Internat.) on Comb. 503 (1965).
11. Homann,K.H. & Wagner,H.Gg., Proc. Roy. Soc. A307 141 (1968).
12. Tesner,P.A., Faraday Symposium of the Chem. Soc. 7 (1973).
13. Howard,J.B., Wersborg,B.L. & Williams,G.C., ibid.
14. Addecott,K.S.B. & Nutt,C.W., Amer. Chem. Soc. Div. Petrochem. 14 (4) A69-80 (1969).
15. Salooja,K.C., Combustion Inst. European Symp. (Weinberg,F.J. Ed.) 400, Academic Press, London 1973.
16. Feugier,A., ibid 406.
17. Homann,K.H., Mochizuki,M. & Wagner,H.Gg., Z. Physik. Chem. N.F. 37 299 (1963).
18. Cotton,D.H., Friswell,N.J. & Jenkins,D.R., Combustion and Flame 17 87 (1971).

19. Salooja,K.C., Nature 240 350 (1972).

20. Peeters,J., Comb. Inst. Euorpean Symp. (Weinberg,F.J. Ed.) 245, Academic Press London 1973.

21. Kinbara,T. & Noda,K., 12th Symp. (Internat.) on Comb. 395 (1969).

22. Kinbara,T. & Noda,K., 13th Symp. (Internat.) on Comb. 333 (1971).

23. Kinbara,T. & Noda,K., 14th Symp. (Internat.) on Comb. 321 (1973).

24. Calcote,H.F., 8th Symp. (Internat.) on Comb. 184 (1962).

25. Peeters,J. & van Tiggelen,A., 12th Symp. (Internat.) on Comb. 437 (1969).

26. Green,S.A. & Sugden,T.M., 9th Symp. (Internat.) on Comb. 607 (1963).

27. Calcote,H.F., ibid 622.

28. Calcote,H.F., Kurzius,S.C. & Miller,W.J., 10th Symp. (Internat.) on Comb. 605 (1965).

29. Matsuda,S. & Gutmann,D., J. Chem. Phys. 53 3324 (1970).

30. Matsuda,S. & Gutmann,D, ibid, 54 453 (1971).

31. Kistiakowsky,G.B. & Michael,J.V., ibid, 40 1447 (1964).

32. Calcote,H.F., Combustion and Flame 1 385 (1957).

33. Deckers,J. & van Tiggelen,A., 7th Symp. (Internat.) on Comb. 254 (1959).

34. Knewstubb,P.F. & Sugden,T.M., ibid, 247.

35. Boothman,D., Lawton,J., Melinek,S.J. & Weinberg,F.J., 12th Symp. (Internat.) on Comb. 969 (1969).

36. Von Engel,A., Ionised Gases, Oxford 1965 p. 90.

37. ibid, p. 13.

38. Gaydon,A.G. & Hurle,I.R., The Shock Tube in High Temperature Chemical Physics, Chapman & Hall 1963.

39. Joffe,J. & Delaney,E.G., Chemical Engineering 65 139 (1958).

40. Matsch,L.W., Capacitors, Magnetic Circuits & Transformers, Prentice Hall Inc. 1964 p. 55.

41. Lawton,J. & Weinberg,F.J., Electrical Aspects of Combustion, Clarendon Press, Oxford 1969.

42. Gaydon,A.G., The Spectroscopy of Flames, Chapman & Hall 1957, p. 197.

43. Lyon,R.K. & Kidd,P.H., J. Chem. Phys., 34 1069 (1961).

44. Kunugi,T., Sakai,T., Soma,K. & Sasaki,Y., Ind. & Eng. Chem. Fundamen. 8 (3) 374 (1969).

45. Thomson,J.J., Report of the Brit. Assoc., 501 (1910).

46. Malinowski,A.E., J. Chim. Phys. 21 496 (1924).

47. Lewis,B.J., J. Am. Chem. Soc., 53 1304 (1931).

48. Calcote,H.F. & Pease,R.N., Ind. Eng. Chem. Ind. Edn. 43 2726 (1951).

49. Fox,J.S., Combustion and Flame, 9 422 (1965).

50. Heinsohn,R.J., Wulfhorst,D.E. & Becker,P.M., ibid 11 288 (1967).

51. Guenault,E.M. & Wheeler,R.V., J. Chem. Soc 195 (1931) & 2788 (1932).

52. Nakamura,J., Combustion and Flame 3 277 (1959).

53. Popov,V.A. & Sheklein,A.V., Combustion, Explosions and Shock Waves 1 58 (1966).

54. Heinsohn,R.J., Thillard,S.V. & Becker,P.M., Combustion and Flame 13 442 (1969).

55. Bone,W.A., Fraser,R.P. & Wheeler,W.H., Proc. Roy. Soc. A132 1 (1931).

56. Calcote,H.F., 3rd Symp. (Internat.) on Comb. 245 (1953).

57. Fowler,R.G. & Corrigan,S.J.B., Phys. Fluids 9 2073 (1966).

58. Becker,P.M., discussion following Fox,M.D. & Weinberg,F.J., 13th Symp. (Internat.) on Comb. 641 (1971).

59. Jaggers,H.C. & von Engel,A., Combustion and Flame 16 275 (1971).

60. Botha,J.P. & Spalding,D.B., Proc. Roy. Soc. A225 71 (1954).

61. Van Tiggelen,P.J., contribution following Ref. 63 and private communication.

62. Dussart,B., Utilisation des Proprietes Electriques des Flammes pour la Mesure des Vitesses de Propagation. Memoire de Licence 1971. Universite Catholique de Louvain, Laboratoire de Physico-Chemie de la Combustion.

63. Fox,M.D. & Weinberg,F.J. 13th Symp. (Internat.) on Comb. 641 (1971).

64. Lawton,J., Mayo,P.J. & Weinberg,F.J., Proc. Roy. Soc. A303 275 (1968).

65. Jones,A.R., Schwar,M.J.R. & Weinberg,F.J., ibid A322 119 (1971)

66. Bradley,D. & Ibrahim,S.M.A., Comb. Inst. European Symp. (Weinberg,F.J. Ed.) 291, Academic Press, London 1973.

67. Bulewicz,E.M., Evans,D.G. & Padley,P.J., personal communication.

68. Poncelet,J., Berendsen,R. & van Tiggelen,A., 7th Symp. (Internat.) on Comb. 256 (1959).

69. Kinbara,T., Nakamura,J. & Ikegami,H., ibid 263.

70. Padley,P.J. & Sugden,T.M., 8th Symp. (Internat.) on Comb. 207 (1962).

71. Bulewicz,E.M. & Padley,P.J., 9th Symp. (Internat.) on Comb. 638 (1963).

72. Payne,K.G. & Weinberg,F.J., 8th Symp. (Internat.) on Comb. 207 (1962).

73. Von Engel,A., Ionised Gases, Oxford 1965 p. 127.

74. Kracella,N.L., J. Quant. Spectr. Radiative Transfer 5 245 (1965).

75. Bowser,R.J. & Weinberg,F.J., Combustion and Flame 18 296 (1972).

76. White,H.J., Industrial Electrostatic Precipitation, Pergammon Press 1963.

77. Weinberg,F.J. & Wilson,J., Proc. Roy. Soc., A314 175 (1970).

78. Gosling,A.J., Lampard,D. & Fussey,D.E., Comb. Inst. European Symp. (Weinberg,F.J. Ed.) 388, Academic Press, London 1973.

79. Hooker,W.J., 7th Symp. (Internat.) on Comb. 949 (1959).

80. Peeters,J., personal communication.

81. Tsang,W., Bauer,S.H. & Waelbroeck,F., J. Phys. Chem. 66 282 (1962).

82. Fairbairn,A.R. & Gaydon,A.G., Proc. Roy. Soc. A239 464 (1957).

83. Ferguson,R.E., J. Chem. Phys. 23 2085 (1955).

84. Fairbairn,A.R., 8th Symp. (Internat.) on Comb. 304 (1961).

85. Wiberg,K.B. & Bartley,W.J., J. Am. Chem. Soc. 84 3980 (1962).

86. Smith,F.A., Chem. Rev. 21 389 (1937).

87. Lawton,J., Mayo,P.J., Thong,K.C. & Weinberg,F.J., Electrochem. Eng. Symp. Newcastle Univ., The Inst. of Chemical Engineers, London 1971.

88. Haber,F., Sber Preuss Akad. Wiss. 11 1962 (1929).

LIST OF SYMBOLS

a	=	flame electrode spacing.
b	=	constant, as subscript refers to breakdown.
bt	=	as subscript refers to bottom electrodes.
c	=	specific heat.
d	=	electrode separation.
e	=	electronic charge, as subscript refers to electron.
f	=	speed of sound.
g	=	as subscript refers to gas phase.
h	=	gradient.
i	=	as subscript refers to ions.
j	=	current density.
k	=	ionic mobility.
$k_{1,2}$	=	rate constants.
k_3	=	attachment coefficient.
k_r	=	relative dielectric constant.
k_{th}	=	thermal conductivity.
k_z	=	Bolzmann constant.
l	=	height above ion source, length.
m	=	mass.
n	=	particle concentration.
p	=	proportion of current transferred to top electrodes.
q	=	charge.
r	=	radius.
s	=	as subscript refers to saturation or to solid phase.
t	=	time.
tp	=	as subscript refers to top electrodes.
v	=	velocity.
x	=	height of electrodes above flame.

y = space co-ordinate.

z = distance from burner.

A = area, as subscript refers to neutral molecules.

A_r = Arhennius frequency factor.

B = constant.

C = capacity.

C_{abs} = absorbtion cross section.

D = constant.

E = activation energy.

F = ionic body force/ unit volume.

G = work function.

H, H_f = enthalpy, enthalpy of formation.

I = current.

L = length of collecting electrodes.

M_1 = incident shock Mach No.

N = Avagadro number.

N_p = concentration of particles.

Nu = Nusselt No.

$(\frac{dN}{dt})$ = rate of ion generation.

P = pressure.

Q = heat content.

R = gas constant.

Re = Reynolds No.

S = flame area.

S_u = burning velocity.

T = absolute temperature.

V = potential.

V_f = volume flow.

X = field strength.

Y = reaction zone thickness.

α = recombination coefficient.

γ = ratio of specific heats.

η = viscosity.

ρ = density.

ε_o = dielectric constant of free space.

σ = Stephans constant.

ε = emissivity.

1 = as subscript refers to initial conditions.

2 = as subscript refers to incident shock.

4 = as subscript refers to initial conditions in the driver gas.

5 = as subscript refers to reflected shock.

$\pm$ = as subscript refers to sign of ion.